Heat-Affected Zone Studies of Thermally Cut Structural Steels
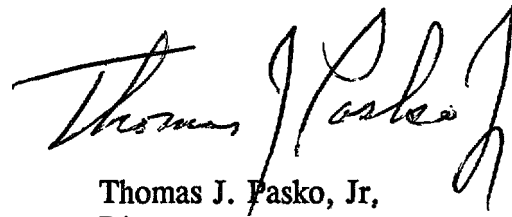
U.S. Department of Transportation
Federal Highway Administration

Research and Development
Turner-Fairbank Highway Research Center
6300 Georgetown Pike
McLean, Virginia 22101-2296

DOT/FHWA

101660

FOREWORD

The influence of the heat-affected zone generated by thermal cutting on structural steel has been investigated with respect to heat-affected zone ductility and impact toughness. Due to the localized nature of the heat-affected zone, special test specimens and practices were utilized. This report considers the influence of oxy-fuel cutting conditions on the heat-affected zone properties of structural steel.

Thomas J. Pasko, Jr,
Director
Office of Advanced Research

NOTICE

This document is disseminated under the sponsorship of the Department of Transportation in the interest of information exchange. The United States Government assumes no liability for its contents or use thereof. This report does not constitute a standard, specification, or regulation.

The United States Government does not endorse products or manufacturers. Trade and manufacturers' names appear herein only because they are considered essential to the object of this document.

1. Report No. FHWA-RD-93-O 15	2. Government Accession No.	3. Recipients Catalog No.
4. Title and Subtitle HEAT-AFFECTED ZONE STUDIES OF THERMALLY CUT STRUCTURAL STEELS		5. Report Date **December 1994**
		6. Performing Organization Code
7. Author(s) W. E. Wood		8. Performing Organization Report No.
3. Performing Organization Name and Address Oregon Graduate Institute of Science & Technology 19600 N.W. von Neumann Drive Beaverton, OR 97006-1999		IO. Work Unit No. (TRAIS) D1B
		11. Contract or Grant No. DTFH61-86-X-00119
12. Sponsoring Agency Name and Address Office of Advanced Research Federal Highway Administration 6300 Georgetown Pike McLean, VA 22101-2296		13. Type of Report and Period Covered Final Report Aug. 1986 - Sept. 1992
		14. Sponsoring Agency Code

15. Supplementary Notes
Contracting Officer's Technical Representative (COTR): Charles McGogney, HAR-20

16. Abstract

Thermal cutting is a procedure that is integral to the manufacture and fabrication of steel. Thermal cutting is particularly important in the production of plate steels, where it is commonly used for trimming the as-rolled plate to the required rectangular dimensions.

The influence of the heat-affected zone generated by thermal cutting on structural steel has been investigated with respect to heat-affected zone ductility and impact toughness. Due to the localized nature of the heat-affected zone, special test specimens and practices were utilized. This report considers the influence of oxy-fuel cutting conditions on the heat-affected zone properties of structural steel.

17. Key Words Structural steel, oxy-fuel, heat-affected zone, thermal cutting, mechanical property.		18. Distribution Statement No restrictions. This document is available to the public through the National Technical Information Service, Springfield, Virginia 22 16 1.	
19. Security Classif. (of this report) Unclassified	20. Security Classif. (of this page) Unclassified	21. No. of Pages 92	22. Price

Form DOT f 1700.7 (8-72) Reproduction of completed page authorized

<center>**METRIC/ENGLISH CONVERSION FACTORS**</center>

ENGLISH TO METRIC	**METRIC TO ENGLISH**

LENGTH (APPROXIMATE)

1 inch (in) = 2.5 centimeters (cm)

1 foot (ft) = 30 centimeters (cm)

1 yard (yd □ 0.9 meter (m)

1 mile (mi) = 1.6 kilometers (km)

LENGTH (APPROXIMATE)

1 millimeter (mm) = 0.04 inch (in)

1 centimeter (cm) = 0.4 inch (in)

1 meter (m) = 3.3 feet (ft)

1 meter (m) = 1.1 yards (yd)

1 kilometer (km) = 0.6 mile (mi)

AREA (APPROXIMATE)

1 square inch (sq in, in^2 = 6.5 square centimeters (cm^2)

1 square foot (sq ft, ft^2 = 0.09 square meter (m^2)

1 square yard (sq yd, yd^2) = 0.8 square meter (m^2)

1 square mile (sq mi, mi^2) = 2.6 square kilometers (km^2)

1 acre = 0.4 hectares (he) = 4,000 square meters (m^2)

AREA (APPROXIMATE)

1 square centimeter (cm^2) = 0.16 square inch (sq in, in^2)

1 square meter (m^2) = 1.2 square yards (sq yd, yd^2)

1 square kilometer (km^2) = 0.4 square mile (sq mi, mi^2)

1 hectare (he) = 10,000 square meters (m^2) = 2.5 acres

MASS · WEIGHT (APPROXIMATE)

1 ounce (oz) = 28 grams (gr)

1 pound (lb) = .45 kilogram (kg)

1 short ton = 2,000 pounds (Lb) = 0.9 tonne (t)

MASS · WEIGHT (APPROXIMATE)

1 gram (gr) = 0.036 ounce (oz)

1 kilogram (kg) = 2.2 pounds (lb)

1 tonne (t) = 1,000 kilograms (kg) = 1.1 short tons

VOLUME (APPROXIMATE)

1 teaspoon (tsp) = 5 milliliters (ml)

1 tablespoon (tbsp □ 15 milliliters (ml)

1 fluid ounce (fl oz) = 30 milliliters (ml)

1 cup (c) = 0.24 liter (l)

1 pint (pt) = 0.47 liter (l)

1 quart (qt) = 0.96 liter (l)

1 gallon (gal) = 3.8 liters (l)

1 cubic foot (cu ft, ft^3) = 0.03 cubic meter (m^3)

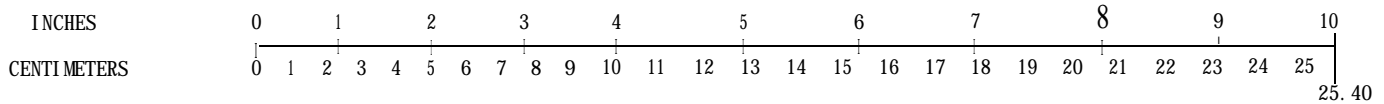1 cubic yard (cu yd, yd^3) = 0.76 cubic meter (m^3)

VOLUME (APPROXIMATE)

1 milliliters (ml) □ 0.03 fluid ounce (fl oz)

1 liter (l) = 2.1 pints (pt)

1 liter (l) = 1.06 quarts (qt)

1 liter (l) = 0.26 gallon (gal)

1 cubic meter (m^3) = 36 cubic feet (cu ft, ft^3)
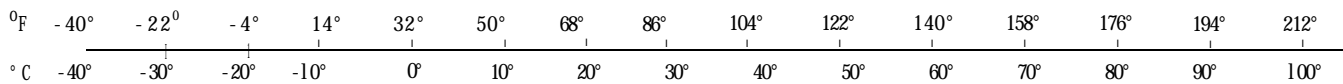
1 cubic meter (m^3) = 1.3 cubic yards (cu yd, yd^3)

TEMPERATURE (EXACT)

$[(x-32)(5/9)]$ ^oF □ y ^oC

TEMPERATURE (EXACT)

$[(9/5)$ y + 32] ^oC □ x ^oF

<center>**QUICK INCH-CENTIMETER LENGTH CONVERSION**</center>

INCHES	0	1	2	3	4	5	6	7	8	9	10
CENTIMETERS	0 1 2 3 4 5	6 7 8	9 10 11	12 13	14 15 16	17 18	19 20	21 22	23	24 25	25.40

<center>**QUICK FAHRENHEIT-CELSIUS TEMPERATURE CONVERSION**</center>

^oF	-40°	-22°	-4°	14°	32°	50°	68°	86°	104°	122°	140°	158°	176°	194°	212°
°C	-40°	-30°	-20°	-10°	0°	10°	20°	30°	40°	50°	60°	70°	80°	90°	100°

For more exact and or other conversion factors, see NBS Miscellaneous Publication 286, Units of Weights and Measures. Price $2.50. SD Catalog No. C13 10286.

TABLE OF CONTENTS

TABLE OF CONTENTS (Continued)

LIST OF FIGURES

LIST OF FIGURES (Continued)

LIST OF TABLES

INTRODUCTION

THERMAL CUTTING

Thermal cutting is a procedure that has been used in the manufacture and fabrication of steel for decades.(') Thermal cutting is particularly important in the production of plate steels, where it is commonly used for trimming the as-rolled plate to the required rectangular dimensions.

Thermal cutting encompasses the entire range of electric arc and flame-initiated cutting processes. Different types of thermal cutting processes are discussed briefly before turning to oxy-fuel gas cutting (OFC).[2]

Metal Powder Cutting

Finely divided iron-rich powder suspended in a jet of moving air or dispensed by a vibratory device is directed into the gas flame in metal powder cutting (POC). The iron powder passes through and is heated by the preheat flame so that it burns in the oxygen stream. Heat generated by the burning iron particles improves cutting action. Cuts can be made in stainless steel and cast iron at speeds only slightly lower than those for equal thicknesses of carbon steel. By adding a small amount of aluminum powder, cuts can be made through copper and brass. Typical POC applications include removal of risers; cutting of bars, plates, and slabs to size; and scrapping.

Chemical Flux Cutting

Chemical flux cutting processes are well suited to materials that form refractory oxides. Finely pulverized flux is injected into the cutting oxygen before it enters the cutting torch. The torch has separate ducts for the preheat oxygen, fuel gas, and cutting oxygen. When the flux strikes the material, the refractory oxides that are formed on the material surface when the cutting oxygen is turned on reacts with the flux to form a slag of lower melting temperature compounds than the material. This slag is driven out by the cutting oxygen, enabling oxidation of the metal to proceed. Chemical fluxing methods are used to cut stainless steel.

Oxy-Fuel Gas Gouging

The oxy-fuel gas gouging process makes grooves or surface cuts in material instead of cutting through the material in a single pass. This process uses special cutting torches and/or special tips. Tips for gouging vary to suit the size and shape of the desired groove or surface cut. Torches may include an attachment for dispensing iron powder to increase the speed of cutting or to permit the scarring of stainless steel. Gas consumption, especially of oxygen, is much greater than in ordinary OFC.[2]

Plasma Arc Cutting

Plasma arc cutting (PAC) uses a high-velocity jet of high-temperature ionized gas to cut carbon steel, aluminum, copper, and other metals. At temperatures above $5500\ ^0C$ (as in a welding arc), gases partially ionize and exist as a plasma (a mixture of free electrons, positively charged ions, and neutral atoms). The plasma jet melts and displaces the workpiece material in its path. Since PAC does not depend on a chemical reaction between the gas and the work metal because the process relies on heat generated from an arc between the torch electrode and the workpiece, and because it generates very high temperatures (28,000 ^0C compared to 3000 ^0C for oxy-fuel), it can be used on almost any material that conducts electricity, including those that are resistant to OFC. The process increases the productivity of cutting machines over OFC without increasing space or machinery requirements.[2]

Air Carbon Arc Cutting and Gouging

Air carbon arc cutting (AAC) and gouging severs or removes metal by melting with the heat of an arc struck between a carbon-graphite electrode and the base metal. A stream of compressed air blows the molten metal from the kerf or groove. Its most common uses are: (1) weld joint preparation; (2) removal of weld defects; (3) removal of welds and attachments when dismantling tanks and steels structures; and (4) removal of gates, risers, and defects from castings. The process cuts almost any metal because it does not depend on oxidation to keep the process going. The low heat input of air carbon arc gouging makes this process ideal for weld joint preparation and for weld removal of high-strength steels.[2]

Oxygen Arc Cutting

Oxygen arc cutting uses a flux-covered tubular steel electrode. The covering insulates the electrode from arcing with the sides of the cut. The arc raises the work material to kindling temperature (minimum temperature needed for oxygen to react with the material), and the oxygen stream oxidizes and removes the material. Oxidation, or combustion, liberates additional heat to support continuing combustion of sidewall material as the cut progresses. The electric arc supplies the preheat necessary to obtain and maintain ignition at the point where the oxygen jet strikes the work surface. The process finds greatest use in underwater cutting. When cutting oxidation-resistant metals, a melting action occurs. The covering on the electrode acts as a flux. The electrode covering functions in a manner similar to that of powdered flux or powdered metal injected into the gas flames in the flux-injection method of OFC of stainless steel.[2]

Oxy-Fuel Gas Cutting

For oxidizable metal such as ferritic steel, OFC is the process of choice for manufacturers and fabricators. In comparison with other cutting methods, OFC offers low initial equipment cost, high productivity and versatility, and little required operator training.[']

Oxy-fuel gas cutting includes a group of cutting processes that use controlled chemical reactions to remove preheated metal by rapid oxidation in a stream of pure oxygen. A fuel gas/oxygen flame heats the workpiece to ignition temperature, and a stream of pure oxygen feeds the cutting (oxidizing) action. The OFC process, which is also referred to as burning or flame cutting, can cut carbon and low-alloy plates of virtually any thickness.

Tool and Workpiece Characteristics of Oxy-Fuel Gas Cutting

The classic conditions that must be fulfilled to permit oxy-fuel flame cutting of steel materials are as follows:[3]

1. The material must be oxidizable.

2. The ignition temperature of the material must be below its melting temperature.

3. The melting point of the oxides must be below the melting temperature of the workpiece.

4. The combustion heat must be high.

5. The thermal conductivity must be low.

These requirements are met by plain carbon steels and low-alloy steels. In addition, it is also possible to flame cut a number of higher alloyed steels without the need for special measures.

Since it is well known that titanium can be flame cut, the classic conditions need to be modified. The melting temperature of titanium is in the order of 1670 ^{0}C; the melting temperature of the oxide (TiO_2), however, is around 300 ^{0}C higher. Further, the ignition temperature is not a chemical constant and therefore cannot be precisely determined.

Physical and Chemical Phenomena of the Process

In the OFC process, the cutting oxygen is not in immediate contact with the parent metal, but is constantly enveloped by a shroud of liquid iron oxide (figure 1). Between this slag jacket and the solid parent metal there is a layer of partially molten iron. The iron atoms diffuse through the slag, and are largely combusted by the cutting oxygen to form FeO. Therefore, the cutting oxygen jet fulfills a dual function. On one hand, its purpose is to further a chemical reaction by forming a compound with the iron atoms. On the other hand, it has the task of ejecting the slag, which is formed continuously during the cutting process, out of the cutting kerf.

The combustion of iron to form Fe0 is a highly exothermic reaction, which, in conjunction with the heating flame, provides the heat necessary to maintain the process of progressively melting the parent metal during a continuous cut. Recent research has shown that the parent material is not completely combusted as the oxides are interspersed with

Parent metal

Crystallized molten layer

Cutting oxygen jet

Oxide film from primary iron combustion

Oxide film from secondary iron combustion

(a) Top View.

Cutting direction

Nozzle

Heating flame

Molten parent metal

Cutting oxygen

Slag jacket
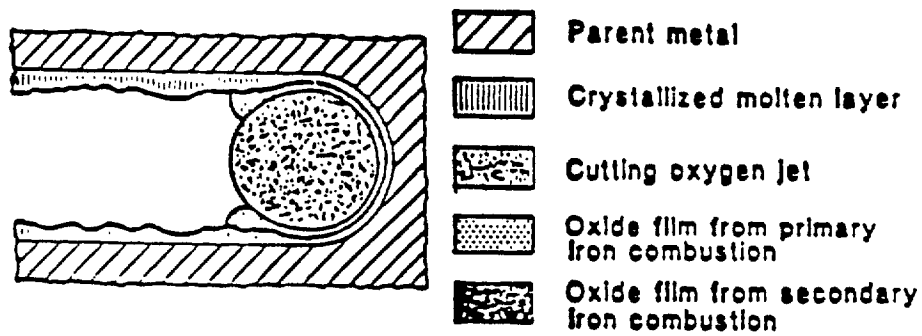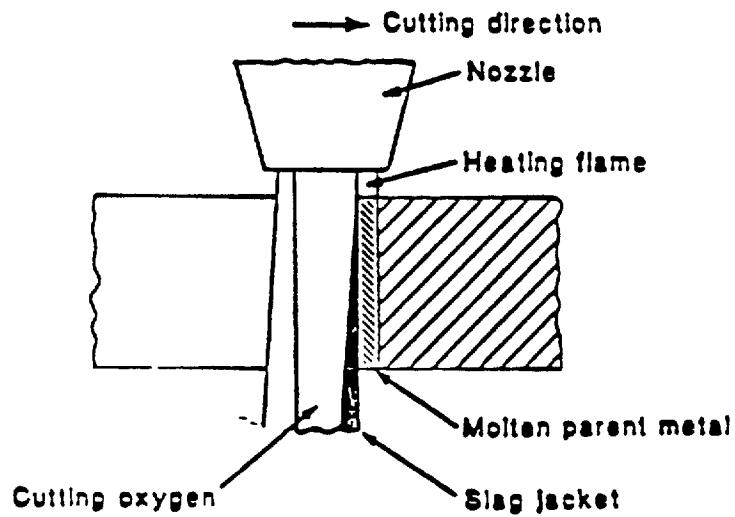
(b) Cross-section.

Figure 1.   Flame-cutting process (schematic).

4

uncombusted iron.   This indicates that the oxide layer in the cutting kerf is diluted with molten iron on account of turbulence.

The amount of liquid iron oxide removed increases towards the bottom edge of the cut.   In other words, the layer of iron oxide becomes progressively thicker (figure 2).   This reduces the diffusion rate of the iron atoms released from the molten layer.   However, the diffusion rate is a determining factor with regard to cutting speed. Therefore, the thicker the plate, the lower the cutting speed.

Figure 2 also shows that the heating flame can only be effective near the surface of the plate.   This is because the heat that it introduces cannot, in the case of thicker materials, make its way immediately to the bottom edge of the plate.   The parent metal at the bottom of the plate is heated and melted by the hot slag.

BACKGROUND LITERATURE

Most research programs have studied the flame-cut steel's properties rather than the HAZ properties.   It is important to study the HAZ produced by thermal cutting to understand the variations in the edge-related properties induced by thermal cutting. As the flame-cut HAZ is a few millimeters wide, it is necessary to use subsize specimens for Charpy V-notch (CVN) tests to study the HAZ's CVN impact properties exclusively.   Some of the earlier works on subsize CVN tests are also discussed here.

Thermal Cutting

There are many works that describe the standard methods of thermal-cutting steel plates.[3-8] Parameters like oxygen purity and fuel gas selection in OFC are discussed along with other related cutting processes.[8]   Also, the procedure for cutting high-alloyed steels and thicker plates are outlined.

It is well known that the flame-cut surfaces are not as smooth as machine-cut surfaces.[6, 9-11] The recommendation for constructional steel components that are subjected to fatigue loading is that the roughness of the cut surface should not exceed 150 um.[11] This is valid only for steels that are weldable without preheat, have a yield strength below 420 N/mm^2, and a thickness below 40 mm. The effect of cutting variables (including oxygen pressure, cutting speed, nozzle type, and preheat flame) on the quality of the cut surface has been considered.[8, 12]

For steels, the cutting operation requires sufficient heating to bring a small portion of the piece to be cut to a high (kindling) temperature (around 1350 ^{O}C).[13] During cooling, the cut edges undergo metallurgical transformations that may result in hardening near the cut edge. Generally, the HAZ consists of one of the two series of structures shown in figure 3, depending on whether the cutting operation was performed with or without preheating.[14] In

With preheating   Without preheating

0.07   0.05

35 (mm)   35 (mm)

29   29

2   2

___⌄___ – Ledeburite   ☰☰☰ – Martensite /Troosite

▦ – Martensite   ▨ – Ferrite

▨ – Troosite II   ☰☰☰ – Low carbon martensite or
                                    ferrite Widmanstatten
▩ – Troosite I   (fine grain)
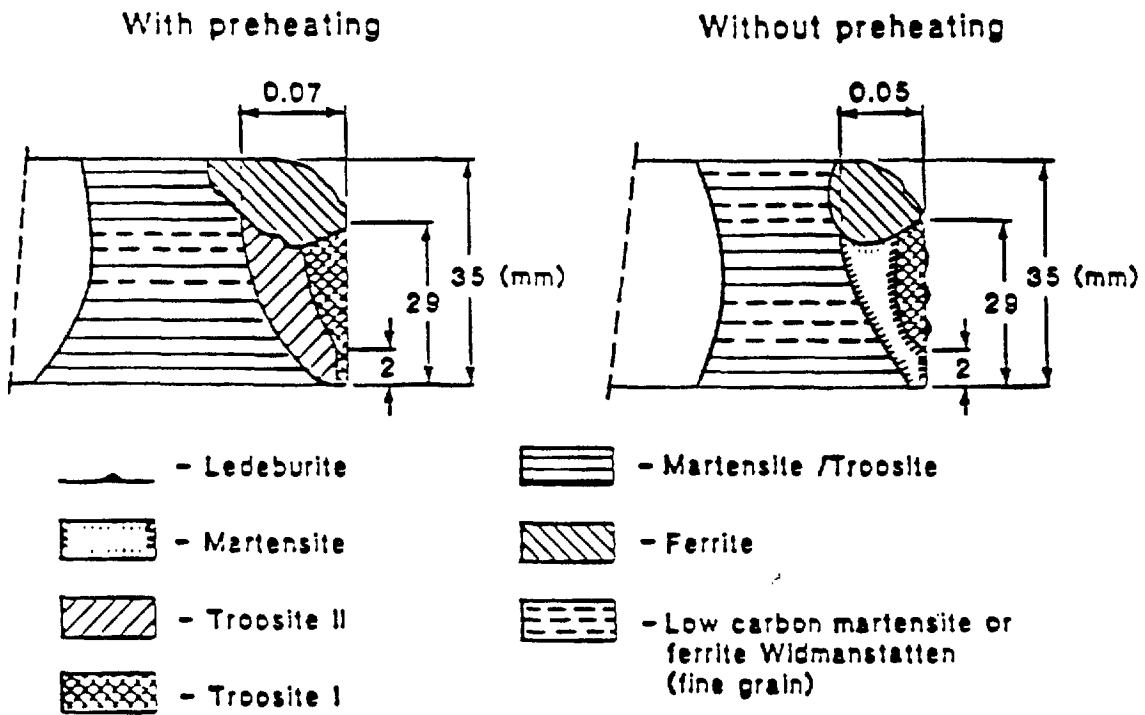
Figure 2.   Structure of the heat-affected zone (HAZ) after oxygen cutting.

Rolling direction
———→

X
↓

| Flame-cut surface |

↑
X'

(a)

A

Heat-affected zone
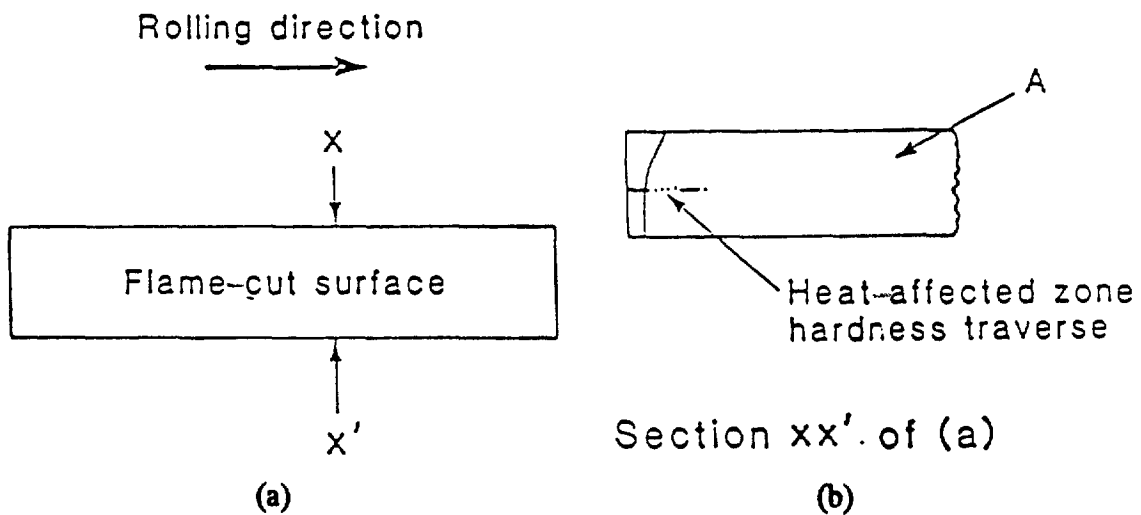hardness traverse

Section xx'. of (a)

(b)

Figure 3.   Orientation of hardness profiles across HAZ.

6

fatigue strength studies of flame-cut AE355 steel, Piraprez observed the following characteristics of oxygen-cut edges:[15]

1. The carbon concentration is increased along the cut edge in a very thin layer about 0.l-mm-deep. As hardness is a direct function of carbon content, the thin region along the cut edge is very hard. According to Piraprez, this increased carbon content does not come from the cutting flame nor from the diffusion of carbon towards the cut edges, but from the material that was melted during the cutting. It is only at depths of 1.5 mm (and not 0.1 mm) that the hardness begins to decrease to reach the value for the base material about 3 mm from the surface.

2. The heat distribution, due to the oxygen-cutting, produces a field of residual stresses in the cut pieces. The distribution of these stresses along the edge has not yet been defined, neither in sign nor in value. Studies to date are not conclusive as some authors speak of compression stresses, while others speak of tensile stresses.[14, 16-18]

3. The cut surfaces develop grooves oriented in the direction of the cutting flame. In most cases, these grooves are perpendicular to the service-induced stress fields, which is very unfavorable for fatigue resistance. Moreover, the fatigue resistance may be further reduced by additional imperfections. Additionally, grooves may also affect the resistance to brittle fracture that depends mostly on the depth and the sharpness of the grooves.[15] When cutting with preheat, the hardness of the thin high-carbon martensite layer is reduced. If the material and the cut surface is of good quality, the fatigue strength is then reduced by 10 percent. The same reduction is obtained if the cut surface receives a heat-treatment after cutting to reduce hardness. These are valid only for constructional steels with a yield strength below 420 N/mm^2 and a thickness below 40 mm.[11]

Nibbering, Thomas, and Bos studied the properties of plasma-cut structural steel Fe5 10, thickness 25 mm.[19] They found a maximum hardness of 450 Hardness-Vickers (HV) located at a depth of 0.1 to 0.3 mm under the surface of the cut. The hardness of the plasma-cut edge was much lower than the hardness of oxy-acetylene cut edges (non-preheated), cut with the same cutting speed. The surface contained a layer of low-carbon martensite with a thickness of about 50 um. This layer was followed by a transition zone consisting of bainite and very fine ferrite-pearlite. The white (non-etching) high-carbon martensite, such as was found at the surface of an oxy-acetylene cut, was not present. Other investigators have reported similar trends in their results regarding the HAZ hardness and microstructure produced by oxy-fuel cutting and PAC.[20-22]

The effect of thermal cutting on mechanical properties has been studied by relatively few investigators. Ho, Lawrence, and Alstetter evaluated the effect of oxygen-cutting on the fatigue resistance of A572 and quenched and tempered A514 steels.[21] For the A572 steel, the differences in the fatigue resistance resulting from different cutting methods (flame cut and plasma arc cut) were very small. For the A514 steel with a fatigue life greater than 1.5 x 10^4 cycles, a machined surface has greater fatigue resistance than flame-cut and quenched, and tempered (after cutting) surfaces. Heat treatment of the flame-cut surface did not improve fatigue resistance much. All flame-cut surface failures initiated at the roots of serrations (valleys of the surface). It seems that the geometry of flame-cut surface defects is more

important than microstructure in determining the fatigue crack initiation site. For the plasma arc cut A572 specimens, the fatigue crack initiation point was mainly at the upper edge of the flame-cut surface, as Goldberg reported.[23]   Surface residual stresses alter the mean stress that, in turn, greatly influences the fatigue crack initiation life.   Compressive residual stresses reduce the mean stress level so that the fatigue life is longer and the fatigue strength is higher. Tensile residual stresses shorten the fatigue life. The Netherlands group showed this effect for flame-cut surfaces of A572 steel.[14]

The fatigue properties of oxygen-cut surfaces may be altered as a result of changes in chemical composition, microstructure, residual stresses, and geometrical features such as roughness, gouges (pits due to lateral torch instability), drag lines (curved lines brought about by insufficient oxygen flow), and melted edges.   The differences in the fatigue resistance between flame-cut and small gouged surfaces is negligibly small for both A572 and A5 14 steels. Deep surface gouges have a negative influence on the fatigue resistance. Neither grinding nor repairing gouges by welding increases the fatigue resistance compared with the gouged surface for both steels. At lives greater than 2×10^5 cycles, A572 flame-cut surfaces have greater fatigue resistance than A5 14, but at lives less than 10^5 cycles, the fatigue resistance of the A514 flame-cut surface is greater than that of A572.[21]

Honda, Kitamura, and Yamada conducted fatigue tests for HT80 steel racks.[20] They found during fatigue testing that cracks were first initiated on the surface of a compressive fillet, but ultimately stopped growing. Cracks were then initiated on the surface of a tensile fillet, resulting in rack failure. Defects resulting from torch-cutting were observed on the surfaces and the surface roughness for the torch-cut specimens were remarkably higher than that for the machined specimens. The fatigue strength of the torch-cut racks were of lower value compared to the machined racks.

Several investigators have shown that the fatigue resistance and other properties of flame-cut surfaces are quite variable due to the use of different materials and cutting conditions.[14, 19, 23-26]

Recently A588, A572, and A36 steels have been studied for their performance in bend tests.(') Based on the results, bend rating of these thermally cut steels were formulated. It is found that the average thermal-cut edge hardness is the primary variable in predicting bend rating, followed generally by carbon content, plate temperature, cutting speed, and CVN toughness.

Subsize Charpy Specimen Impact Tests

Several investigators have studied the effect of specimen thickness on the CVN toughness values of ferritic steels.[27-35]   Some of them tested lo-mm-thick laminated specimens made up of subsize specimens bonded together.   It is usual to extract a specimen of reduced thickness for small section thickness or inconveniently shaped components, if a standard Charpy specimen of cross-sectional dimensions of 10 x 10 mm and a length of 55 mm cannot be extracted.[36] The most commonly specified subsize specimen thicknesses are 7.5, 5, and 2.5 mm, but specimens of two-thirds and one-third the normal lo-mm-thickness (i.e., 6.7 and

3.3 mm) have also been tested. There is no simple relationship between results obtained using subsize specimens and results from full-size, lo-mm-thick specimens. The loss of through-thickness constraint is subsize specimens causing a shift in the ductile-to-brittle transition temperature in ferritic steels. It can also influence upper-shelf, or fully ductile, specimen behavior. The influence of reduced CVN specimen thickness on ferritic steels that display a transition from ductile to brittle behavior with temperature, is a reduced transition temperature, unless splitting occurs. A reduction in transition temperature of $0.7(10\text{-}t)^2$ ^{0}C, where t = the specimen thickness in mm, appears to fit the data reasonably well for ferritic steels of room temperature, being defined at a constant absorbed energy per unit ligament area.[36]

For ferritic steels:[37] (1) when a subsize specimen is used because the section is too thin, the reduced thickness of the test specimen must be used to model the benefits of a reduced section thickness with regard to the risk of brittle fracture rather than attempting to correlate back to the result that would have been obtained in a full-size specimen, and (2) where a subsize specimen is used because a component has an inconvenient configuration, an empirically derived correlation may be required to deduce the result that would have been obtained in a full-size specimen or at least a larger specimen. Hence, it is recommended for ferritic steels that the test temperature for the subsize specimen should be reduced from that which would otherwise have been required for the full-size specimen, to model the effect of thickness on the transition temperature.[37] The decreasing transition temperature with decreasing CVN specimen thickness has also been observed.[38, 39]

PRESENT WORK OBJECTIVE

The aim of the present work is to characterize the HAZ in thermally cut A514, A572, and A588 steels and to study its fracture behavior under tension and impact test conditions.

PRESENT WORK APPROACH

In the present work, the HAZ's of thermally cut A514, A572, and A588 steels were studied, The effect of cutting speed on HAZ appearance and microstructure was studied by thermally cutting these steels with oxy-acetylene flame at two different cutting speeds (12.7 and 38.1 cm/min). The effect of the cutting speed on HAZ mechanical properties was evaluated by microhardness tests across HAZ, by tension tests, and by impact tests. Both the effects of temperature and strain rate on tensile properties were studied. Also, limited tests on tensile specimens of different thickness were done to find the effect of specimen size when tested at a low temperature and at a high strain rate. Subsize Charpy specimens with different notch orientations with respect to flame-cut surface and HAZ were used for impact tests. Both flame-cut surfaces and fractured tension and impact test surfaces were subjected to scanning electron microscopy analysis.

EXPERIMENTAL PROCEDURE

MATERIALS

The steels chosen for this work were 25-mm-thick ASTM A514, A572, and A588 plate steel. Their chemical composition and physical properties are given in table 1. All steels are low-carbon, low-alloy steels with 1 percent Mn content. Both A572 and A588 steels were in the hot-rolled condition, whereas the A514 was in quenched and tempered condition. Hence, the yield strength (YS) and ultimate tensile strength (UTS) values of A514 steel were higher than A572 and A588 steels. The top of the plates and rolling direction were marked for identification purposes in thermal cutting experiments.

THERMAL CUTTING

The thermal cutting process employed throughout this work was the OFC process. The fuel gas used was acetylene and the various cutting parameters used are listed in table 2.

Tip Size and Tolerance Between Plate and Tip

There are lists available from torch-tip manufacturers for the tip sizes to be used for the range of metal thickness values for fuel gas.   The tip dimensions increase with the thickness of the steel to be cut.   These lists can be referred to if the plate to be cut is not painted or rusty and the flame to be used is a neutral flame.   The tip size used for the present work was #2 and, as the thickness was more than 12.7 mm, the torch tip was held straight up and down, perpendicular to the face of the horizontal surface.   The distance between tip and plate was kept in the range of 3.2 to 4.8 mm in order to hold the part of the preheat flame with the highest amount of heat close to the surface of the plate.   If the tip is too far off, then it won't preheat fast enough and the cutting speed will slow down.   If it is too close, then the cutting tip will overheat, start to melt the plate, and the tip will start backfiring.   (Backfiring is the momentary recession of the flame into the torch tip followed by immediate reappearance or complete extinguishment of the flame.)   This leads to delay in the cutting process as the torch needs to be relighted to start the cutting process again.

O_2/C_2H_2 Pressure and Flow Rate

The acetylene pressure is adjusted until sufficient acetylene emerges to form a gap of about 3.2 mm between the tip and the flame.   Then the oxygen pressure is adjusted until the flame burns with the desired balance or neutral characteristic. The neutral flame is produced with a mixing ratio of approximately one volume of oxygen to one volume of acetylene. When the flame is on the carburizing side, whitish streamers of unburned acetylene are seen leaving the blue inner cone and entering the sheath flame. As the acetylene supply is decreased, these streamers decrease in length until there remains only the sharply defined blue inner cone and the sheath flame. At that instant, the neutral oxy-acetylene flame has been

11

Table 1.   Steels studied.

1. A51 4   Rolled and austenized at 898.9°C for 1 hr, water-quenched and tempered at 648.9°C for 1 hr and aircooled.
2. A572 Rolled and aircooled.
3. A588 Rooled and aircooled.

Physical properties

Steel	Yield strength MPa	UTS MPa	Percentage elongation(5.1cm)	CVN Joules (J)
A514	834.3	889.5	27	42 at -34.4°C
A572	427.5	561.9	22	104.4 at -12.2°C
A588	355.1	520.6	17	195.3 at -12.2°C

Chemical composition

Steel	C	Mn	P	S	Si	Cu	Ni	V	Al	Cr	Mo	Ti	B
					Percent by weight								
A514	.19	.92	.009	.009	.26	.23	.1	.04	.059	.46	.18	.034	.0019
A572	.15	1.3	.009	.009	.29	-	-	.02	.037	-	-	-	-
A568	.14	.95	.007	.007	.39	.27	.06	.02	.04	.45	.03	-	-

Table 2.   Flame-cutting parameters.

Torch tip	Clearance between tip & plate (mm)	Presure x 10^3Pa		Cutting speed cm/min	
		O_2	C_2H_2	Slower cutting speed	Faster cutting speed
#2	3.2 to 4.8	42.0	5.0	12.7	38.1

formed. The acetylene pressure was 5 x 10^3 Pa and oxygen pressure was 42 x 10^3 Pa in this work. Correspondingly, the flow rates of oxygen and acetylene were 46.2 and 6.6 m^3/h, respectively.

Cutting Speed

It is important that the forward cutting speed of the torch be correct. It must be just fast enough so that the cutting oxygen jet passes completely through the plate thickness to make a clean cut on the top and the bottom of the steel. At the correct travel speed, the slag will be thrown out at the bottom of the plate in the same direction of the movement of the torch. For a 2.54-cm plate thickness, 38.1 cm/min is the correct flame-cutting speed. In this work, both 38.1- and 12.7-cm/min cutting speeds were used to cut the steel plates. Other cutting parameters were constant.

MICROHARDNESS TESTS

As the HAZ width is uniform only in the middle region along the thickness of the plate, as revealed by the macroprofile obtained by etching with Nital solution, the microhardness tests were carried out in the midthickness of the plate. The hardness traverse was thus taken across the midthickness as shown schematically in figure 3. This surface (A in figure 3(b)) is perpendicular to both the flame-cut surface and the top (rolling) surface. Hardness values were measured using a microhardness tester. This procedure was repeated for each steel and each cutting speed. Knoop hardness vs. distance from flame-cut edge plots were made for all the cases. Before each set of tests, the tester was calibrated using standard test blocks. The load used in these tests was 300 g, the same as the one used for tester calibration.

METALLOGRAPHY

Location Studied on HAZ

Metallographic examination of the HAZ was done across the midthickness of side A marked in figure 3(b). This was the region where HAZ width was uniform. Microstructure pictures were taken starting from the flame-cut edge, traveling through HAZ into the base metal.

Procedure

To retain the flame-cut edge during polishing, the specimen was nickel plated using Watts solution. First, the specimen was washed thoroughly with acetone and then it was kept immersed in hot NaOH solution. It was rinsed with water and then it was electroplated with nickel in the Watts solution. The specimen was mounted in bakelite and polished starting with coarse grinding papers (80 mesh) and ending with 0.05-um fine emery paper. It was then washed with water, etched with 2 percent Nital solution, washed with water and then

ethanol, and dried. The same procedure was repeated for each steel and for each cutting speed. The pictures were taken at X 1000 magnification using an oil immersion lens in a Nikon ephiphot microscope.

TENSION TESTS

Specimen Geometry

Two specimen types were used for the tension tests. Both were derived from ASTM standard A370 sheet-type specimen geometries, with some modifications. In the type 1 specimen, the width of the specimen was reduced at the middle region (38.1 mm in length) of the gauge length to 10.2 mm to facilitate necking and to ensure that fracture would occur within this region. The actual elongation was measured by marking a 2.54-cm gauge length within this region. This specimen geometry is given in figure 4 (a). In the type 2 specimen, along with reduction at the middle region of the gauge length, the thickness was increased to 6.4 mm to study the effect of thickness on tensile properties. It is shown in figure 4 (b).

Specimen Location in HAZ

The tensile specimens were taken from the HAZ through the plate midthickness as shown in figure 5. The type 1 specimen was entirely in the HAZ. Since the HAZ width was uniform in the midthickness of the plate, representative properties should be measured. Base metal specimens were taken from the same region with respect to rolling directions.

Tensile Test Variables

Temperature and strain rate were the two test variables studied. Specimens were tested at room temperature and one steel-specific low temperature. The AASHTO temperature for which the impact test results are reported for these steels was chosen as the low temperature. This is -34.4 °C for A514 steel and -12.2 °C for A572 and A588 steels. A low (quasi-static) strain rate and an intermediate strain rate were used to study strain-rate effects. Low strain rate required 30 s for failure and the intermediate strain rate required 1 s for failure.

Procedure

Low-temperature tension tests were done by keeping the specimen and grips immersed in methanol cooled by a low temperature bath (Endocal) recirculating coils assembly. The desired low temperature was controlled by the recirculating bath. Actual bath temperature was monitored by an immersion thermometer. Load vs. elongation was recorded during the test using an X-Y plotter. Elongation was measured from the change in length of the gauge length markings. For each steel, three conditions (base metal, flame cut at 12.7 cm/min, and
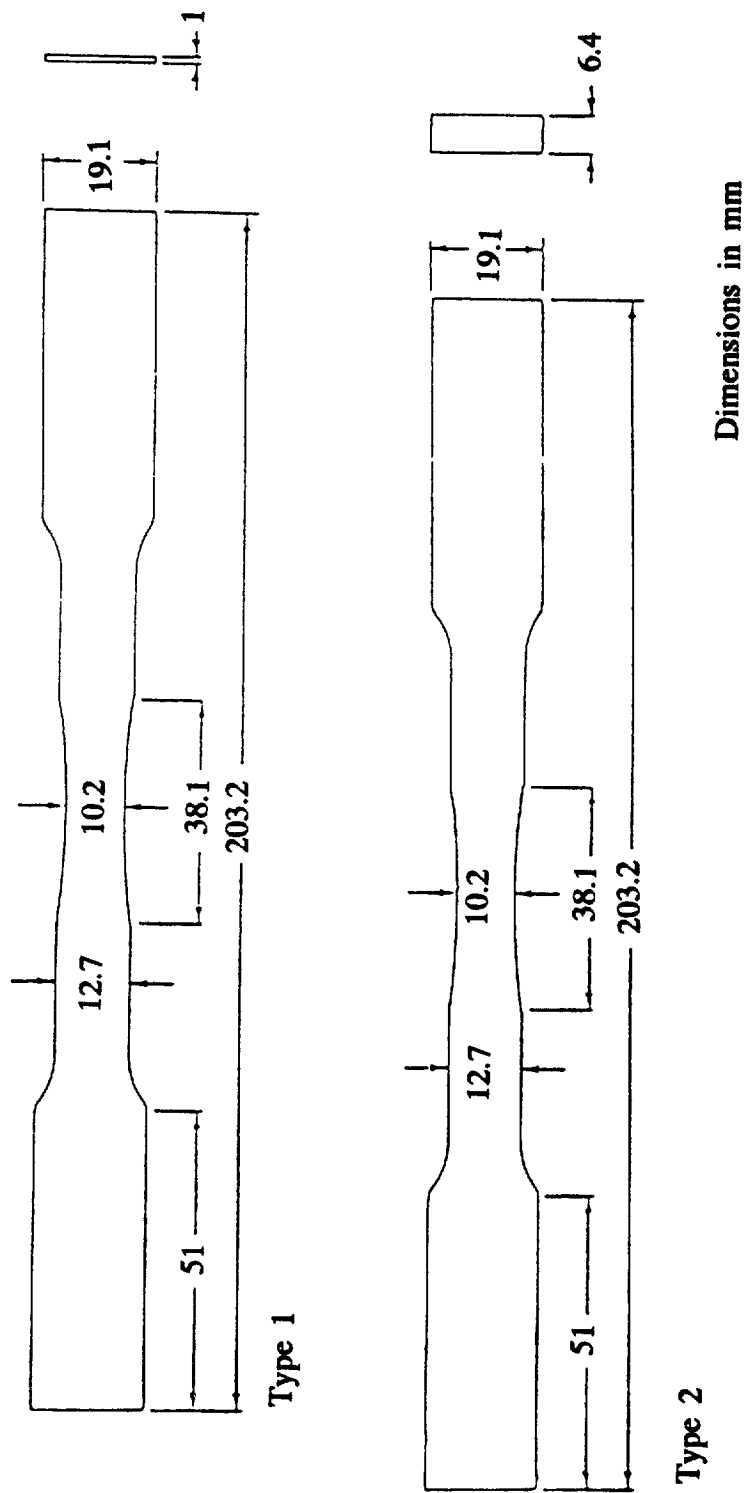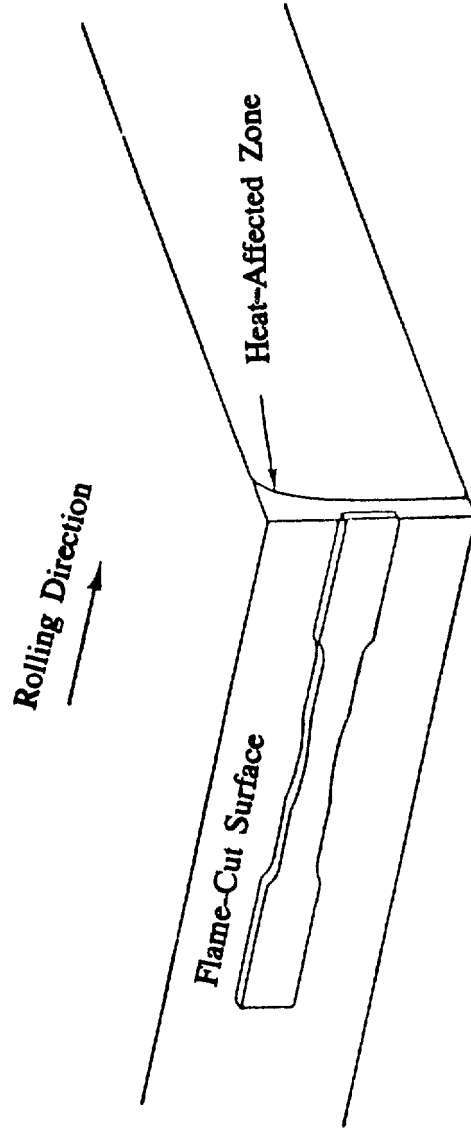
Figure 4. Tensile specimen geometry.

16

Figure 5.   Tensile specimen location in HAZ.

flame cut at 38.1 cm/min) were studied. For each test condition, three specimens were tested and the mean values of YS, UTS, and percentage elongation were taken. All three steels were tested using the same procedure.

Tension tests with type 2 specimens (6.4 mm thick) were done for A514 and A572 for both base metal and flame cut at 12.7-cm/min conditions at low temperature and intermediate strain rate.   The results were obtained in the same manner as in the case of the type 1 specimens.

CHARPY V-NOTCH IMPACT TESTS

Specimen Geometry, Location, and Notch Orientation

For Charpy impact toughness studies, specimens of three different geometries were used (figure 6). The notch angles for these specimens are shown in figure 7. The overall dimensions of the normal and subsize specimens conform to ASTM-E23 specifications. Based on the length along the notch direction with respect to the normal 10- x 10- x 55-mm specimens, the specimens are termed as full-size (normal-size), quarter-size (thickness), and half-size (subsize) specimens.   It was decided to test for two conditions in relation to the HAZ.

1. To test the impact toughness of the HAZ alone, the Charpy specimen should lie entirely in HAZ.   Since the HAZ width was small in thermal cutting, the quarter-size specimen geometry was suitable for carrying out this test. As the thermal cutting direction was along the rolling direction, the specimen was also extracted from the thermally cut plate such that its length was lying along the rolling direction and the notch was lying across the HAZ as shown in figure 6. The flame-cut surface of the specimen was left unmachined so that the specimen was completely in HAZ.

2. To test the impact toughness with the crack initiation in HAZ and the propagation in the base metal, the notch needs to be in HAZ with the rest of the specimens in the base metal.   As the HAZ width was uniform at the midthickness of the plate, the specimen needed to be taken from this region. Half-size specimens with 0.75-mm notch depth and 2" notch angle (figure 7) were suitable for this test, with the specimen length lying along rolling direction and the notch length lying along the HAZ.

Full-size specimens were made of base metal for all three steels, with the same specimen and notch location and orientation as that of the quarter-size specimens.   Quarter- and half-size specimens were made for the three steels for the base metal, flame cut at slower speed, and flame cut at faster speed conditions.
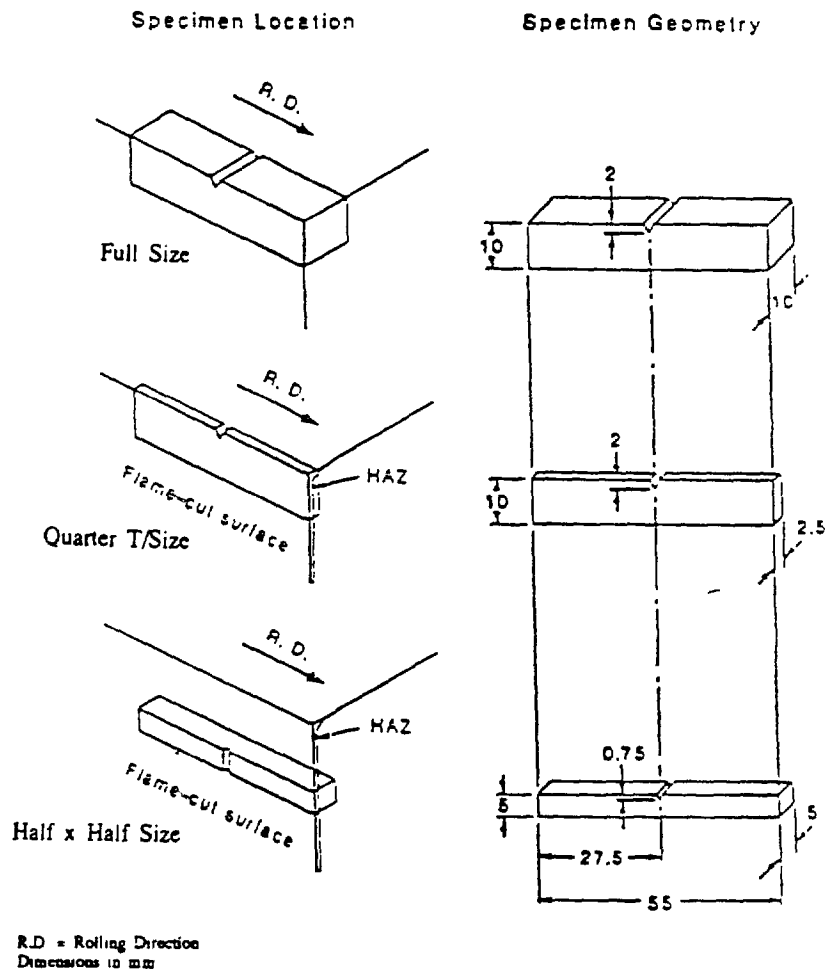
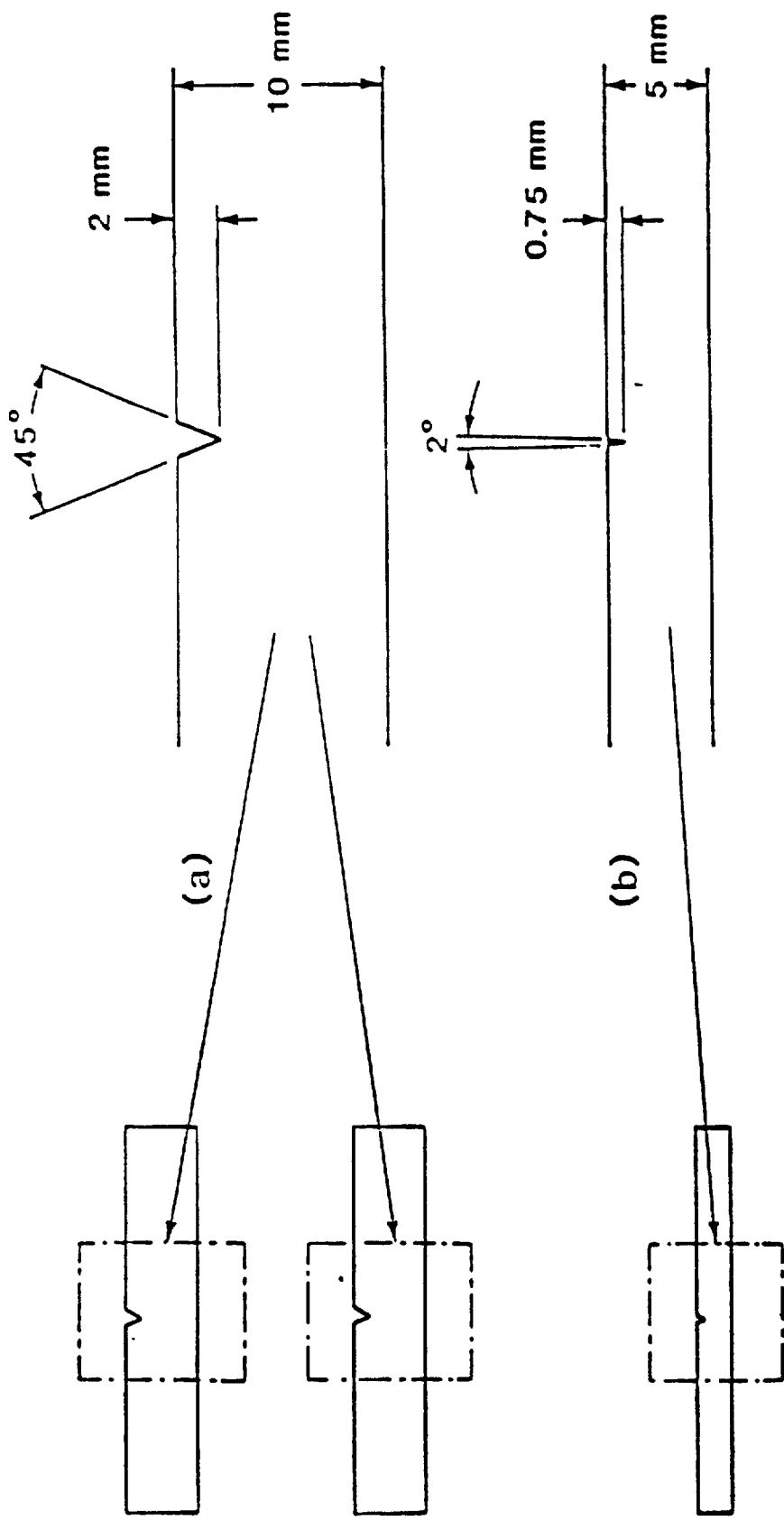Figure 6.   Charpy V-notch (CVN) specimen geometry and orientation.

Figure 7. Notch details for CVN specimens.

Impact Testing Procedure

A pendulum-type universal impact testing machine was used for testing the CVN specimens and an Endocal cooling tower unit was used for low-temperature tests in the range of 0 to -70 °C, using methanol as the liquid bath. Two walled cylindrical containers were used, with methanol or n-butane inside and pouring liquid nitrogen outside, to attain temperatures less than -70 °C.

Impact tests were conducted for each steel for the different geometries and metal conditions discussed earlier, and the dial energies were recorded manually. The impact energies were normalized by dividing them with the area below the notch (ligament area). As there was always a time lag between the specimen removal from the low-temperature bath and impact, the specimen temperature was higher at impact than that of the low-temperature bath. Hence, temperature corrections were given to get the actual test temperatures, based on the heating rate experiment results and the time between specimen removal and impact.[40]

FRACTOGRAPHY

Scanning Electron Microscope, operating at a secondary electron voltage of 25 kV, was used for studying the flame-cut surfaces and fractured surfaces. The general procedure followed for analyzing the surface was as follows.

The specimen surface was cleaned ultrasonically in acetone, mounted in the Scanning Electron Microscope (SEM), and the surface scanned at suitable magnification to study the features of interest. Representative pictures were taken after scanning the whole surface. Flame-cut surfaces of each steel (cut at two different speeds), tensile specimen fractured surfaces, and CVN impact test fractured surfaces were studied in SEM.

RESULTS AND DISCUSSION

EFFECT OF CUTTING SPEED ON HAZ APPEARANCE, HARDNESS, AND MICROSTRUCTURE

The effect of cutting speed on the HAZ appearance is shown in figure 8 for A5 14.   At the slow cutting speed, the heat input to the material was high and it resulted in wider HAZ as shown in figure 8 (a), whereas, at a faster cutting speed, the heat input was lower and a correspondingly narrower HAZ was obtained, which is shown in figure 8 (b). Since the cutting torch flame is in contact with the top surface, the HAZ is wider at the top surface and it narrows to a constant width away from the top at both speeds.   Similar effects of cutting speed on HAZ appearance were observed in both A572 and A588 steels.

Microhardness plots for the two cutting speeds for A514 steel are given in figures 9 and 10.   At both cutting speeds, the hardness was at a maximum point near the flame-cut edge and it decreased sharply moving towards the base metal. The HAZ hardness was higher for the faster cutting speed (figure 10), which can be explained by the respective HAZ microstructures. Figure 11 (a) and (b) illustrate schematically HA.2 microstructures for A5 14 at the two cutting speeds.   The A5 14 steel HAZ microstructures at three distances from the flame-cut edge for the two cutting speeds are given in figures 12 and 13. At the slow cutting speed, the structure observed, within 0.15 mm from the edge (figure 12 (a)), was identified as bainite from its appearance and hardness.[41]   As the distance from the cut edge was increased, tempered martensite (figure 12 (b) and (c)), which was the same as the base metal structure, was observed.   This explains the lower edge hardness for the slower cutting speed than for the faster cutting speed, where plate and lath martensite formed at distances less than 0.1 mm from the cut edge (figure 13) and the martensite was not auto-tempered to the extent of the base metal until reaching a distance of 0.8 mm from the edge.

Hardness profiles of A572 for the two cutting speeds are given in figures 14 and 15, and HAZ microstructures are shown in figures 18 and 19. Hardness profiles of A572 steel (figures 14 and 15) and A588 steel (figures 16 and 17) revealed that the material cut at a higher cutting speed had a higher hardness at distances less than 0.05 mm from the flame-cut edge.   This was due to the wider martensitic zone at the higher cutting speed and, conversely, increased auto-tempering of the martensite at the slow cutting speed, as illustrated in figure 11 (c) and (f).   For A588 cut at the slow speed, the structure changed from tempered martensite to bainite (figure 20) up to 4 mm from the flame-cut edge. The base metal structure of ferrite and pearlite was changed to auto-tempered (referred to as tempered from here on) martensite phase near the flame-cut edge for A588 at the faster cutting speed and for A572 at both cutting speeds (figures 18, 19, and 21). The cutting speed had little influence on microhardness values beyond a distance of 0.50 mm from the flame-cut edge for all steels. Within 0.50 mm from the flame-cut edge, the hardness decreased from the edge into the HAZ, except A588 steel flame cut at the slower speed, where it remained nearly constant, as the tempered martensite near the edge and the bainite had nearly the same hardness.

(a)
Flame cut at slower
cutting speed.
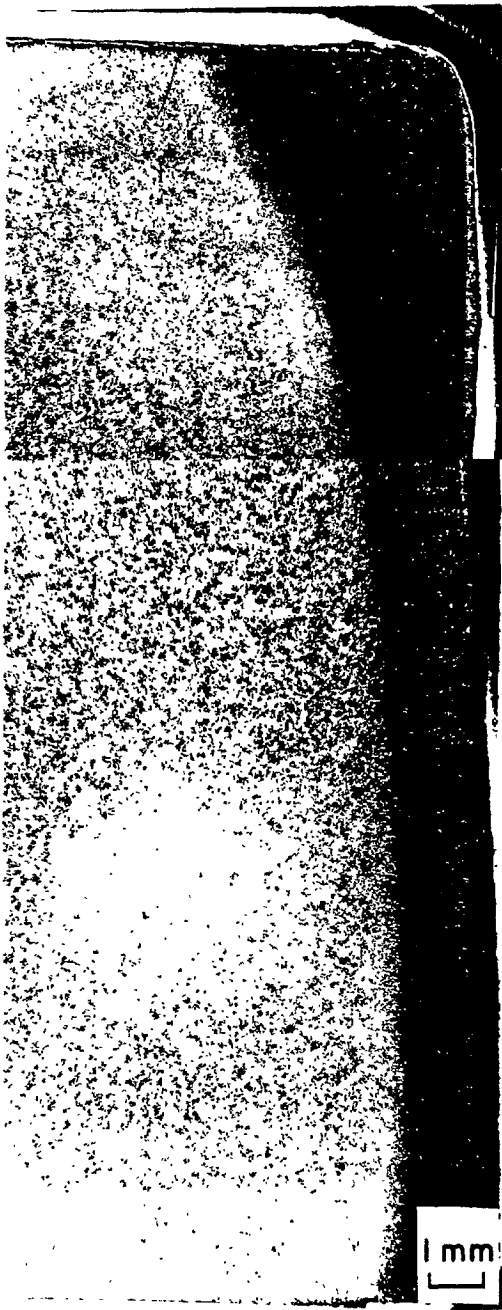
(b)
Flame cut at faster
cutting speed.

Figure 8.   Optical micrographs for A514 steel HAZ.
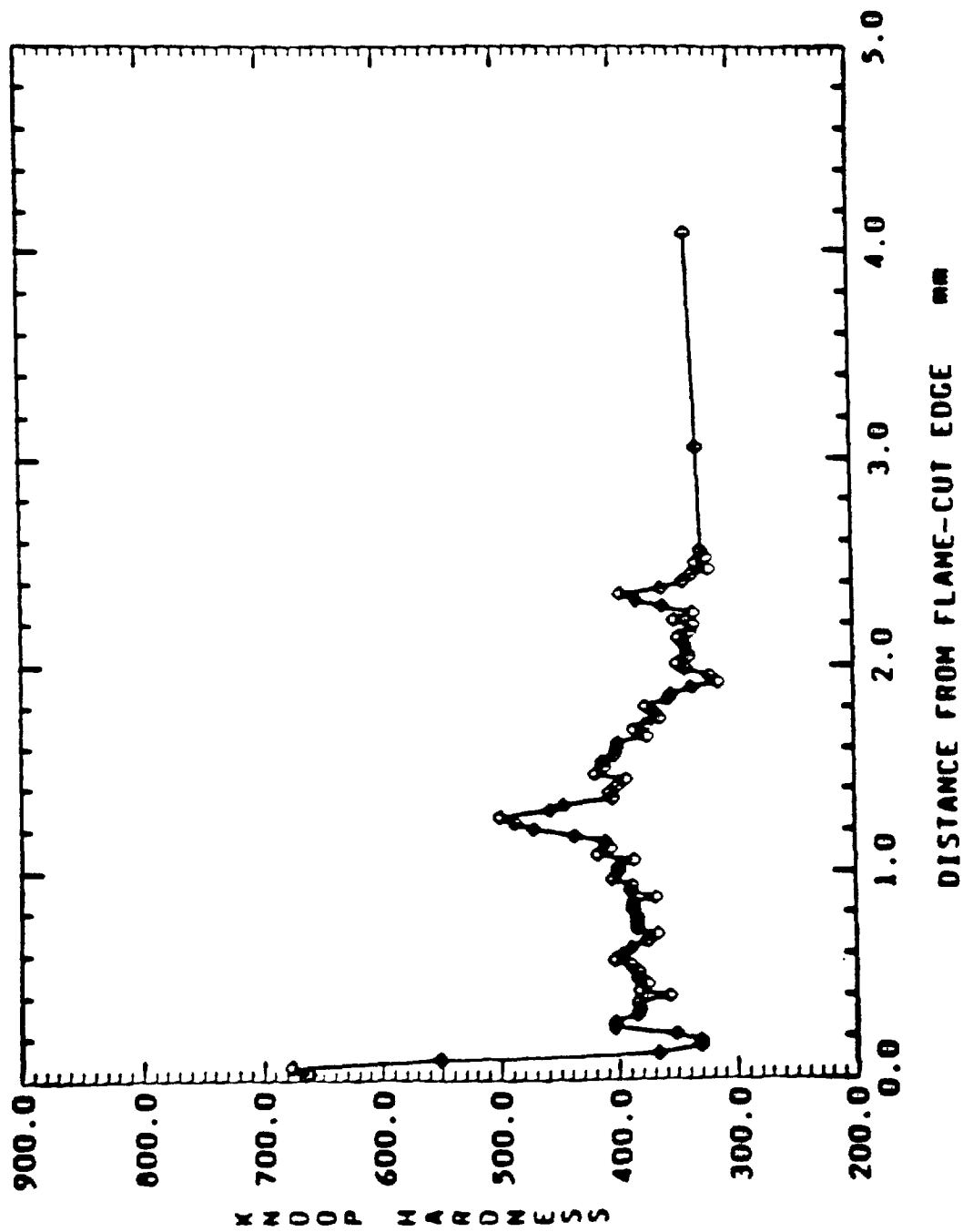
Figure 9.   Microhardness plot across HAZ for A514 steel flame cut at 127-mm/min cutting speed.
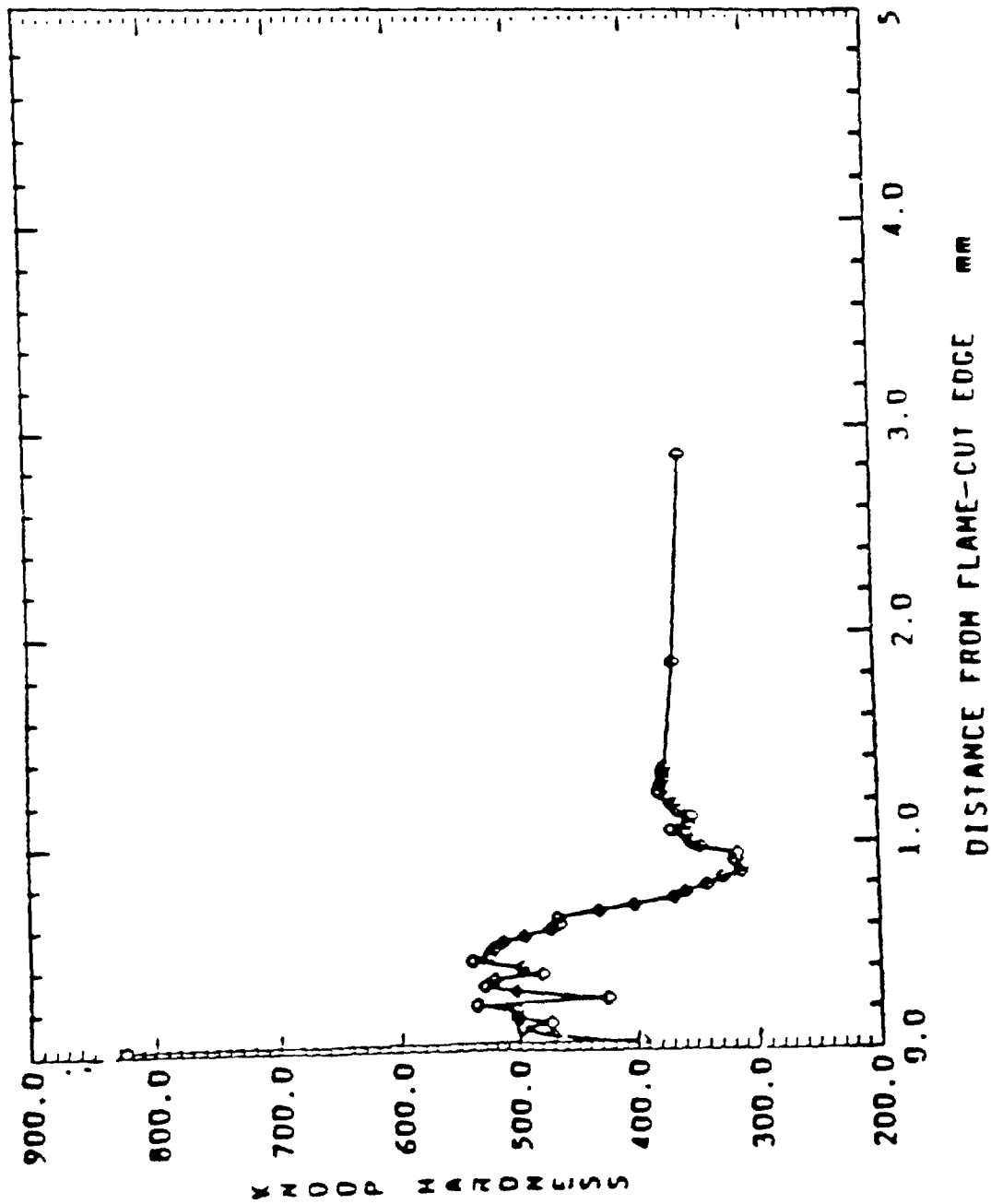
Figure 10.   Microhardness plot across HAZ for A514 steel flame cut at 381-mm/min cutting speed.
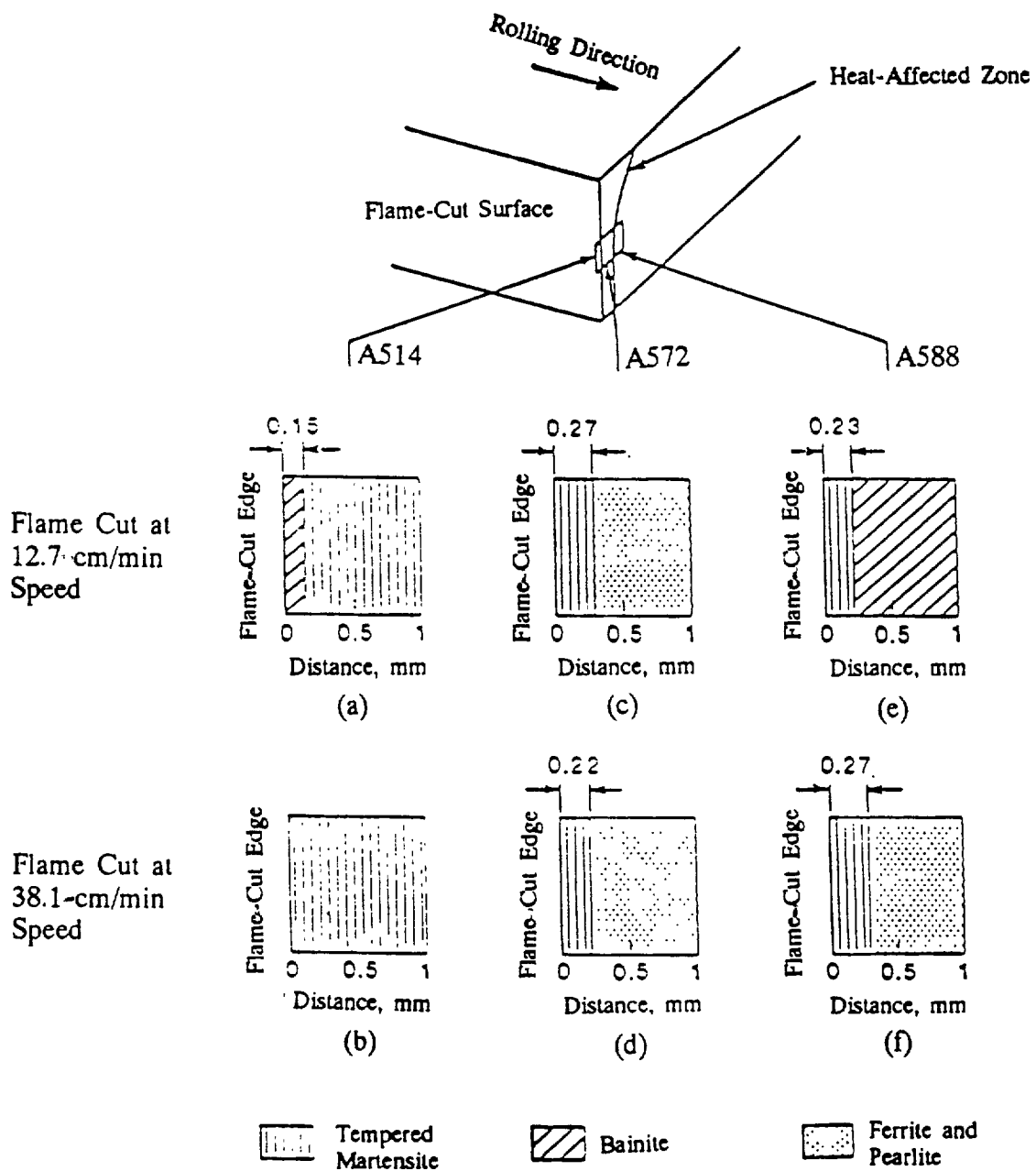
26

Rolling Direction

Heat-Affected Zone

Flame-Cut Surface

A514 A572 A588

Flame Cut at 12.7 cm/min Speed

0.15

Flame-Cut Edge

0   0.5   1
Distance, mm
(a)

0.27

Flame-Cut Edge

0   0.5   1
Distance, mm
(c)

0.23

Flame-Cut Edge

0   0.5   1
Distance, mm
(e)

Flame Cut at 38.1-cm/min Speed

Flame-Cut Edge

0   0.5   1
Distance, mm
(b)

0.22

Flame-Cut Edge

0   0.5   1
Distance, mm
(d)

0.27

Flame-Cut Edge

0   0.5   1
Distance, mm
(f)

Tempered Martensite   Bainite   Ferrite and Pearlite

Figure 11.   Schematic representation of flame-cut HAZ microstructures.
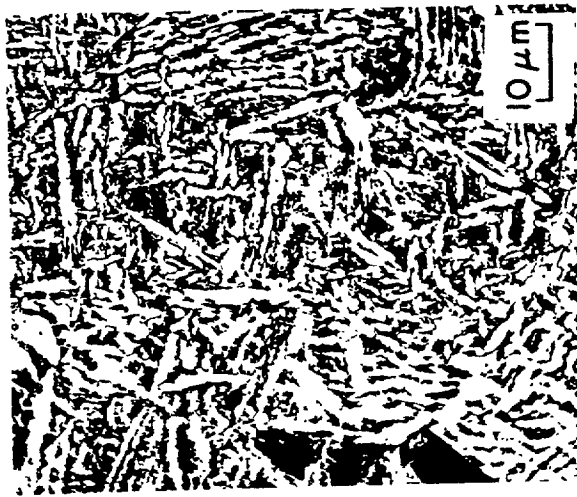
(a)
Bainite at 0.1-mm distance
(1000 X).
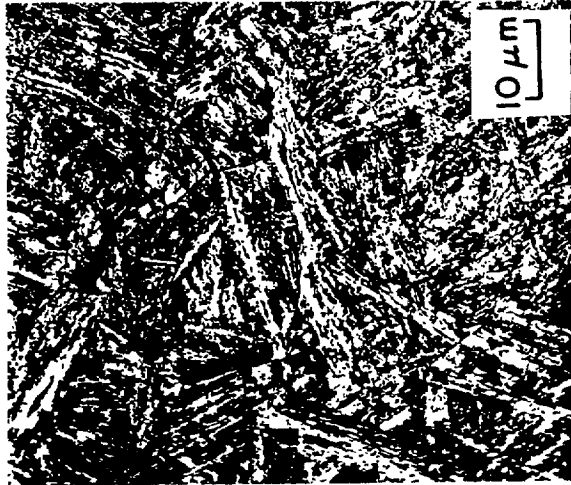
(b)
Tempered martensite
at 0.6-mm distance
(1000 X).
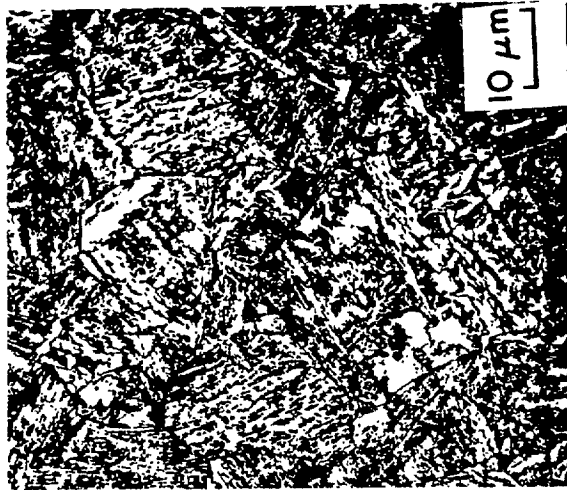
(c)
Tempered martensite
at 0.8-mm distance
(1000 X).

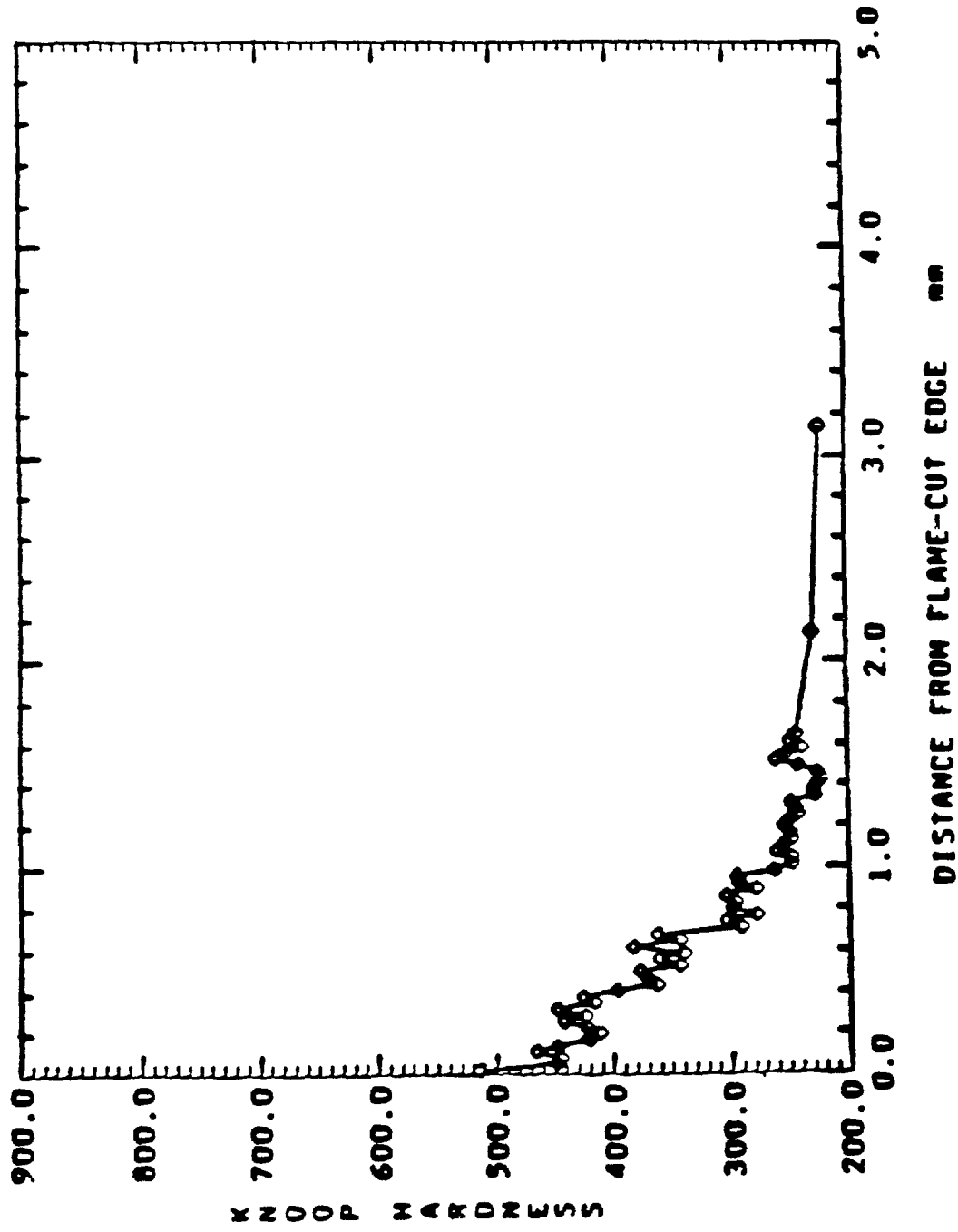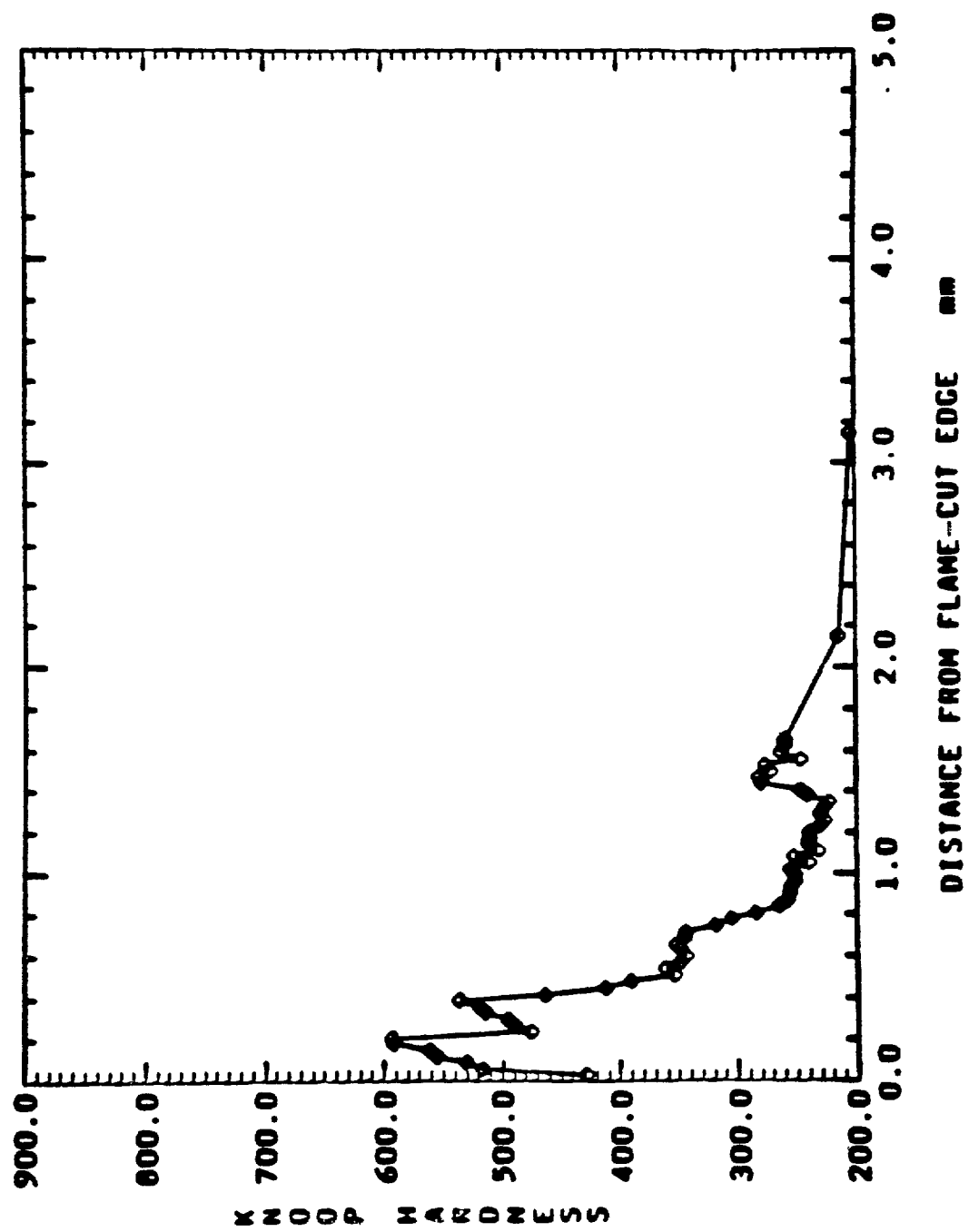Figure 12. HAZ microstructure for A514 steel flame cut at 127-mm/min cutting speed.

28
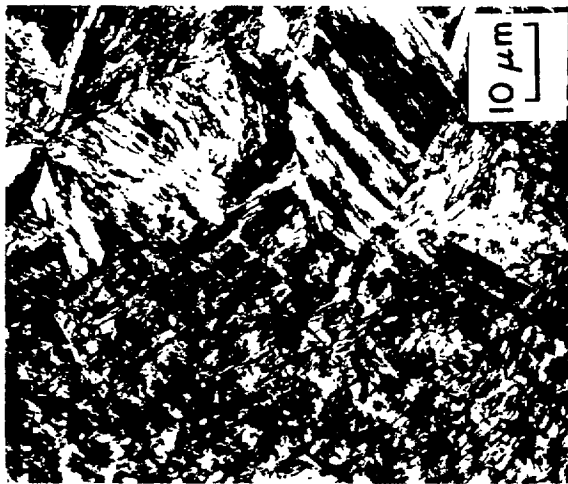
(a)
Lath and plate martensite
at 0.1-mm distance
(1000 X).
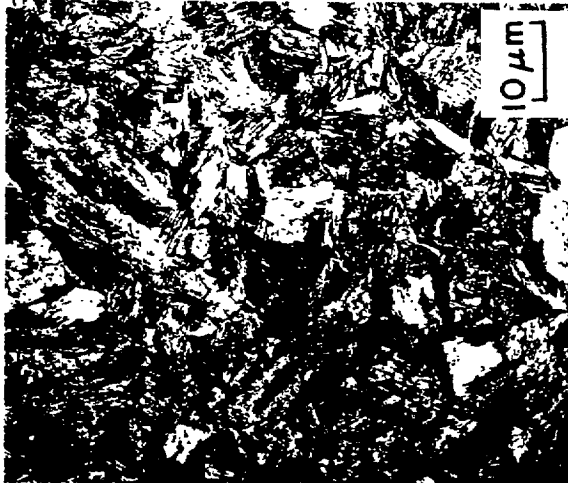
(b)
Tempered martensite
at 0.5-mm distance
(1000 X).
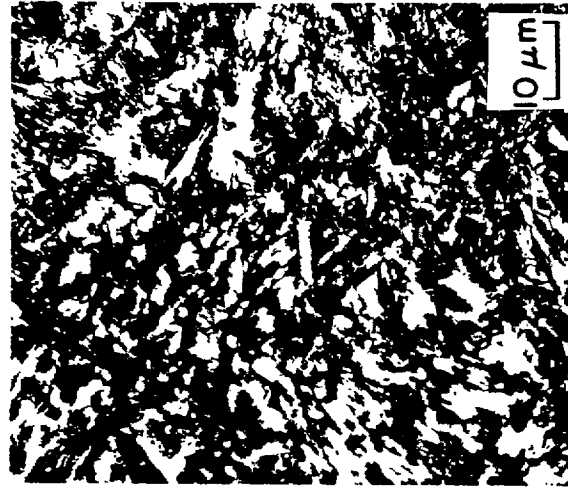
(c)
Tempered martensite
at 0.8-mm distance
(1000 X).

Figure 13.   HAZ microstructures for A514 steel flame cut at 381-mm/min cutting speed.

Figure 14.   Microhardness plot across HAZ for A572 steel flame cut at 127-mm/min cutting speed.

30

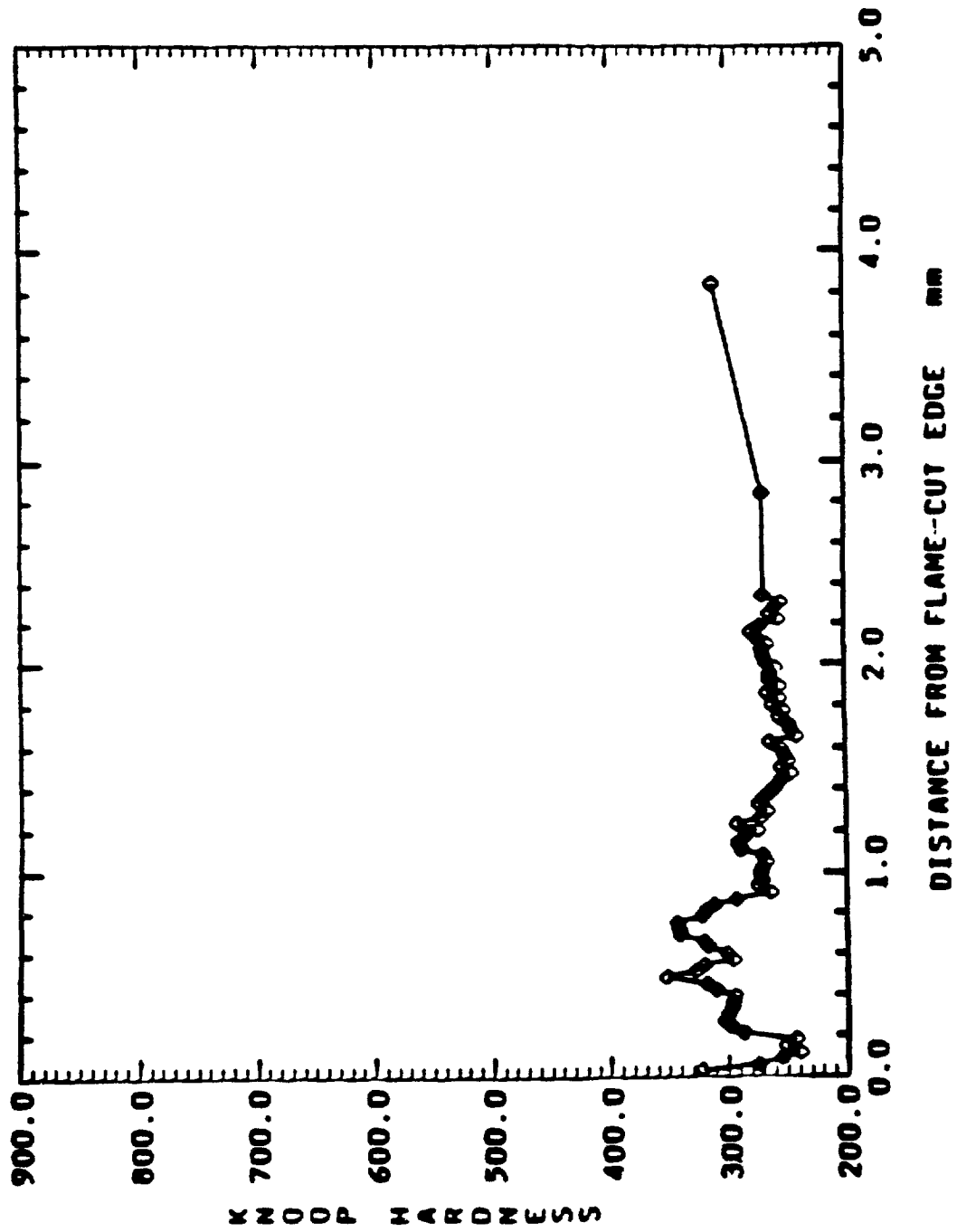Figure 15. Microhardness plot across HAZ for A572 steel flame cut at 381-mm/min cutting speed.

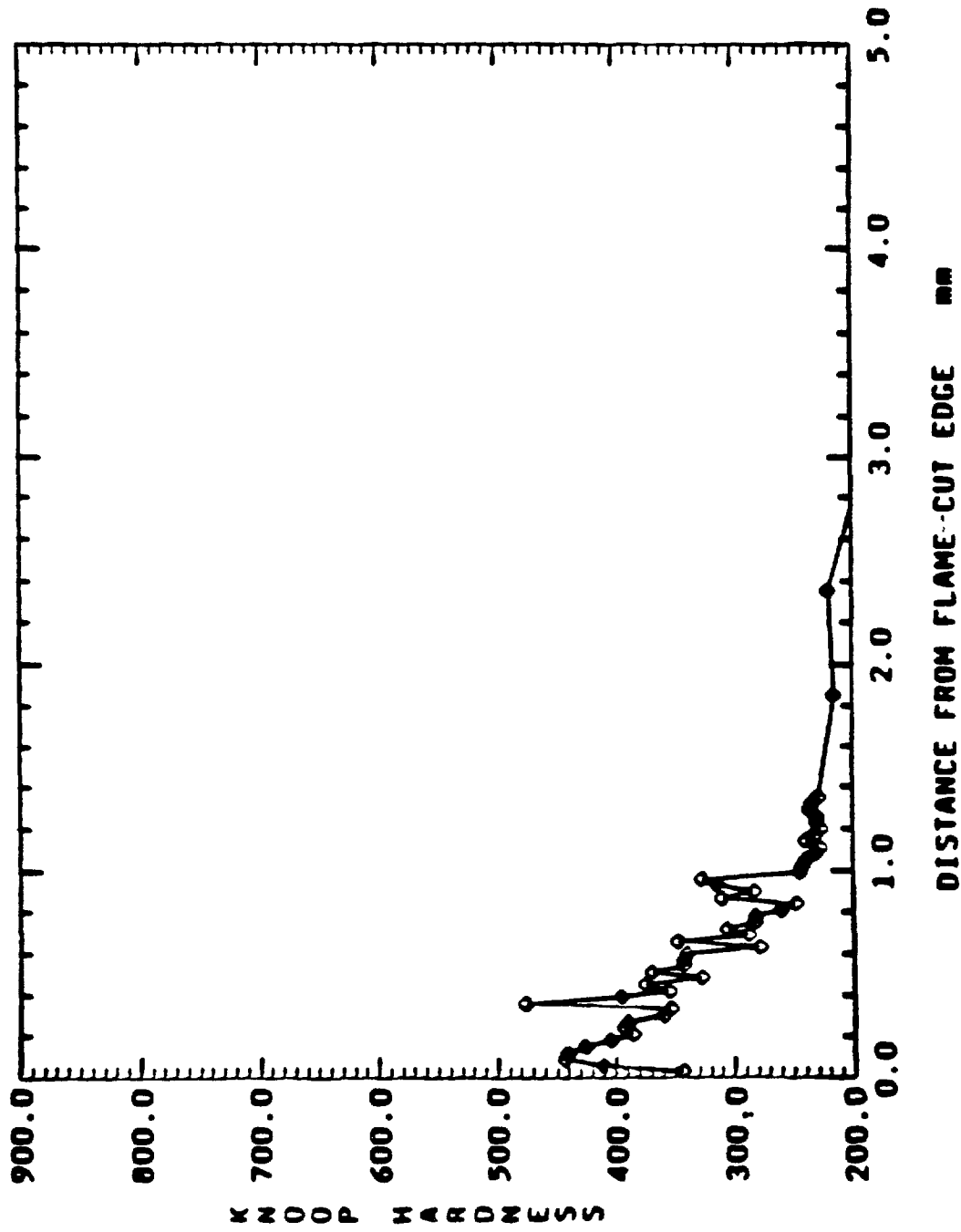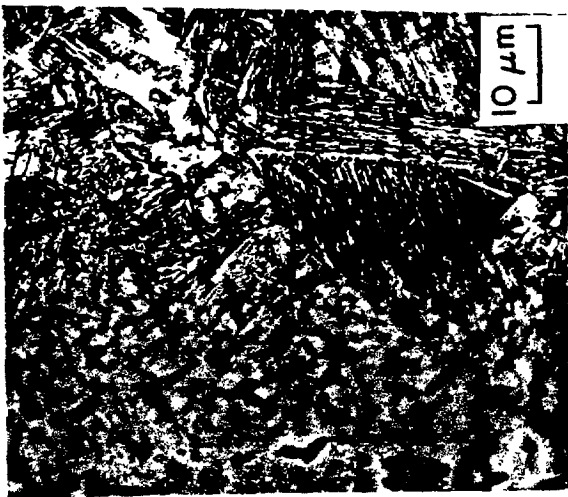Figure 16.   Microhardness plot across HAZ, A588 steel flame cut at 127-mm/min cutting speed.
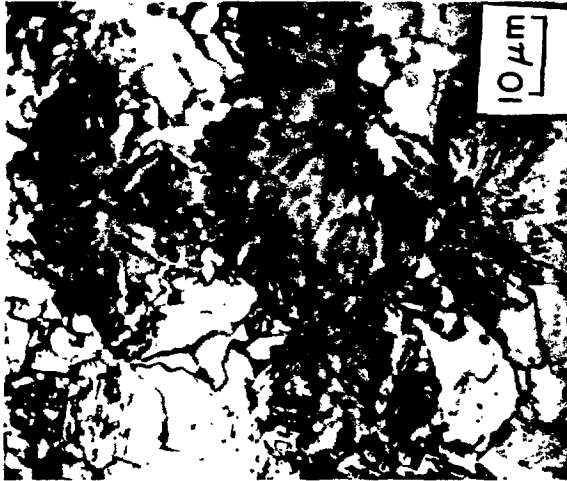
32

Figure 17. Microhardness plot across HAZ, A588 steel flame cut at 381-mm/min cutting speed.
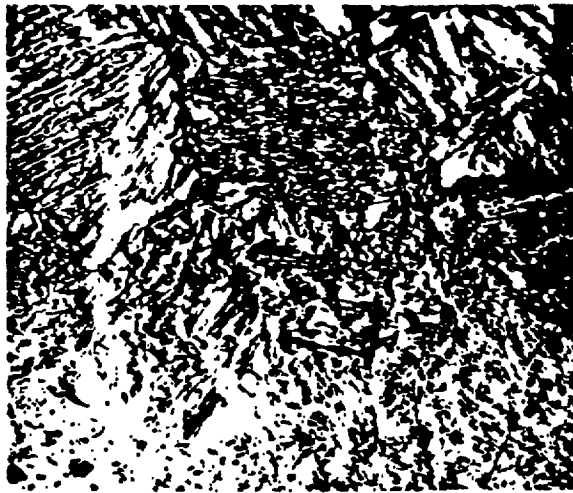
(a)
Lath martensite
at 0.5-mm distance.

(b)
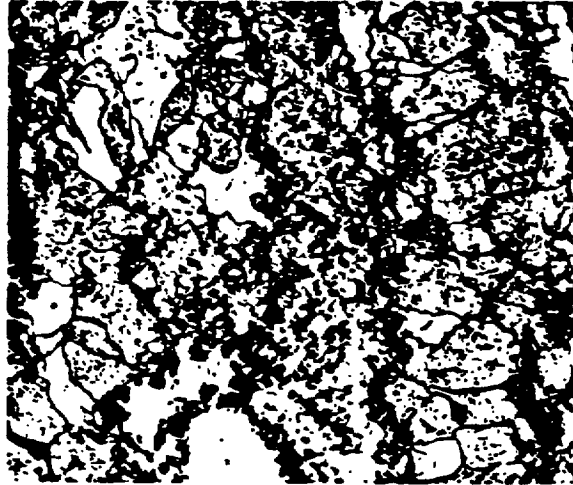Ferrite and Pearlite
at 0.6-mm distance.

(c)
Ferrite and Pearlite
at 3-mm distance.

Figure 18.   HAZ microstructures for A572 steel flame cut at 127-mm/min cutting speed.

(c)
Ferrite and Pearlite
at 1.2-mm distance.

(b)
Ferrite and Pearlite
at 0.6-mm distance.

(a)
Lath and plate martensite
at 0.05-mm distance.

Figure 19. HAZ microhardness, A572 steel flame cut at 381-mm/min cutting speed.
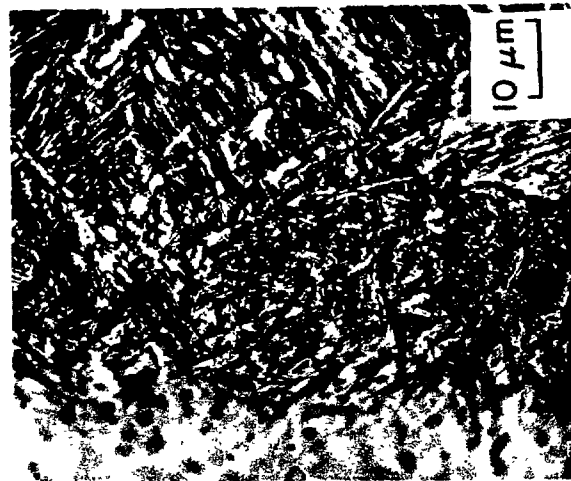
(a)
Lath and martensite
at 0.05-mm distance.

(b)
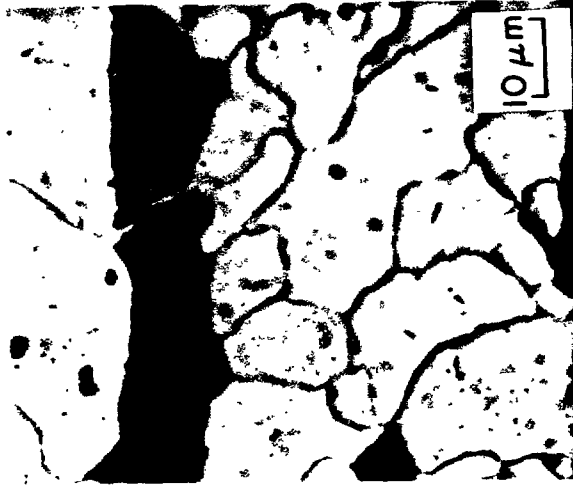Bainite at 0.5-mm distance.

(c)
Bainite at 4-mm distance.

Figure 20.   HAZ microstructures, A588 steel flame cut at 127-mm/min cutting speed.

(c)
Ferrite and Pearlite
at 2.5-mm distance.

(b)
Ferrite and Pearlite
at 0.6-mm distance.

(a)
Lath and martensite
at 0.05-mm distance.

Figure 21. HAZ microstructures for A588 steel flame cut at 381-mm/min cutting speed.

TENSION TEST RESULTS

The YS, UTS, and percentage elongation of l-mm-thick (type 1) specimens are listed in tables 3 through 5, respectively. The UTS and YS comparison for l-mm-thick (type 1) and 6.4-mm-thick (type 2) specimens, along with their percentage elongation values, are given in table 6.

Effect of Cutting Speed

All three steels, under all test conditions, had higher YS in the flame-cut HAZ than in the base metal, except for A5 14 tested at the high-strain rate. Generally, the HAZ yield strength was higher for steels flame cut at the faster speed than for those flame cut at the slower speed (for all three steels). The UTS also showed a similar trend.

The increased HAZ yield and ultimate strengths, as well as the increased strength with increased cutting speed, can be understood from the HAZ microstructures. Since the type 1 tensile specimens were 1 mm in thickness, the entire flame-cut tensile specimen was removed from inside the HAZ (figure 5). The tensile specimen properties thus depended on the microstructures contained in the l-mm distance from the HAZ flame-cut edge. From the schematic representation of the HAZ microstructures for the three steels, figure 11 (a) through (f), it can be seen that for A514, the HAZ within 1 mm from the flame-cut edge consisted of bainite and tempered martensite for the slower cutting speed (figure 11 (a)), and tempered martensite for the faster cutting speed case (figure 11 (b)). Microhardness analysis showed that the HAZ martensite was less tempered than the martensite in the base metal. Hence, the high-speed flame-cut HAZ had higher strength than the base metal. The flame-cut HAZ resulting from the slower cutting speed received more heat input than the faster cutting speed and, hence, more time for tempering the resulting martensite. The less-tempered martensite had higher strength than bainite formed at the slower cutting speed. Hence, the YS and UTS increased with increasing cutting speed. Due to the same reasons, a similar trend was observed for A5 14 tested at low temperature.

For both A572 and A588 steels, the presence of tempered martensite in the flame-cut HAZ increased the strength compared to the base metal. As the martensite was tempered less when cutting at a higher speed, it had higher strength.

The percentage elongation was less in the flame-cut HAZ than in the base metal for all steels (table 5). Also, the percentage elongation decreased with increased cutting speed. The A514 steel HAZ martensite was less tempered than the base metal. So its ductility was less than the base metal. As the martensite was less tempered with increased cutting speed, the ductility decreased with increasing cutting speed. As the base metal structure was ferrite and pearlite, while flame-cut HAZ had tempered martensite, the ductility of the base metal was higher than flame-cut HAZ for A572 and A588 steels. The amount of martensite was nearly the same at both cutting speeds for these steels, figure 11 (c) through (f). As the martensite was less tempered with increased cutting speed, the ductility decreased with increased cutting speed.

Table 3.   Tension test results: yield strength.

Yield Strength (MPa)

Room temperature (R.T.)   80.6F (27°C)
Low temperature (L.T.)   10F (-12.2°C) for A572 and A588 steels
                          -30F (-34.4°C) for A514 steel.

Metal condition	Temperature	A588		A572		A514	
		Low strain rate	Intermediate strain rate	Low strain rate	Intermediate strain rate	Low strain rate	Intermediate strain rate
Base metal	R.T.	335.8	376.5	401.3	408.9	837.1	897.1
	L.T.	328.9	363.4	415.8	495.1	934.9	915.7
Flame cut at slower cutting speed	R.T.	634.3	617.8	619.9	602.6	882.6	834.3
	L.T.	651.6	585.4	617.1	605.4	934.9	779.1
Flame cut at faster cutting speed	R.T.	686.7	544.1	666.1	585.4	1039.8	969.4
	L.T.	597.8	561.9	601.9	452.3	1029.4	1043.9

Table 4. Tension test results: ultimate tensile strength.

Ultimate tensile strength (MPa)

Room temperature (R.T.) 80.6F (27°C)
Low temperature (L.T.) 10F (-12.2°C) for A572 and A588 steels
-30F (-34.4°C) for A514 steel.

Metal condition	Temperature	A588		A572		A514	
		Low strain rate	Intermediate strain rate	Low strain rate	Intermediate strain rate	Low strain rate	Intermediate strain rate
Base metal	R.T.	519.2	545.4	566.8	581.9	897.1	928.1
	L.T.	506.1	537.8	601.2	641.9	1001.8	1005.9
Flame cut at slower cutting speed	R.T.	813.6	823.3	763.9	776.4	1043.4	1001.2
	L.T.	865.3	795.7	804.7	781.2	1074.2	957.1
Flame cut at faster cutting speed	R.T.	856.4	774.9	899.8	841.2	1227.3	1170.8
	L.T.	770.9	735.7	815.7	712.3	1232.8	1305.2

Table 5.   Tension test results: percentage elongation.

Percentage elongation (2.54-cm gage length)

Room temperature (R.T.)   80.6F (27°C)
Low temperature (L.T)   10F (-12.2°C) for A572 and A588 steels
  -30F (-34.4°C) for A514 steel.

Metal condition	Temperature	A588		A572		A514	
		Low strain rate	Intermediate strain rate	Low strain rate	Intermediate strain rate	Low strain rate	Intermediate strain rate
Base metal	R.T.	20.3	17.9	20.9	17.7	8.5	7.8
	L.T.	19.6	11.3	19.0	19.1	6.5	6.1
Flame cut at slower cutting speed	R.T.	9.2	8.3	7.2	6.9	4.7	4.7
	L.T.	7.2	6.4	7.5	5.9	3.8	4.1
Flame cut at faster cutting speed	R.T.	7.9	6.9	5.5	2.2	3.1	3.0
	L.T.	5.4	5.2	4.6	4.1	2.8	2.6

Table 6.   Tension test results: effect of specimen thickness.

Tested at low temperature and intermediate strain rate for base metal and flame-cut metal at slower speed. L.T. : 10F (-12.2°C) for A572 and -30F (-34.4°C) for A514.						
Steel	Thickness (mm)	Metal	UTS MPa	YS ⁻ MPa	Percentage elongation (2.54 cm)	Normalized percentage elongation
A514	1.0	Base metal	1006	916	6	6
		Flame cut metal	957	779	4	4
	6.4	Base metal	1056	985	20	8
		Flame cut metal	1052	896	19	7
A572	1.0	Base metal	642	495	19	19
		Flame cut metal	781	605	6	6
	6.4	Base metal	656	461	27	11
		Flame cut metal	725	504	24	10

Effect of Strain Rate and Temperature

Generally, base metal yield strength and ultimate tensile strength increased with increasing strain rate and decreasing test temperature (tables 3 and 4) for all three steels. The flow stress is related to strain rate (ε) and test temperature (T) as given in the following equation:[42]

$$\sigma = f[\dot{\varepsilon} \exp(\Delta H/Rt)] \qquad (1)$$

where ΔH is the activation energy and R is the gas constant.[42] Since the flow stress σ, is related to nominal stress S by the relation,

$$\sigma = S(1+e) \qquad (2)$$

where e is the elongation, both the YS and UTS increased with increased strain rate and decreased temperature. Equation 1 has been applied only to metals with homogeneous microstructure throughout the test specimen.[42] As the flow properties depend on a material's dislocation structure, such a simple equation of state as equation 1 cannot be applied to a flame-cut HAZ due to its non-uniform microstructure. The overall effect of strain rate and temperature on the flame-cut-induced HAZ tensile properties was less than the effect of cutting speed.

Effect of Specimen Thickness

Increasing the base metal tensile specimen thickness slightly increased both the UTS and YS values (table 6) for A514 base metal and flame-cut HAZ and A572 base metal, but did not increase the YS of A572 base metal. The increase in strength with increase in specimen thickness was due to increased specimen thickness constraint with increasing thickness. But in the case of A572, the YS and UTS values for the flame-cut condition decreased with increased specimen thickness. As the HAZ was very narrow compared to the gauge thickness in the thicker specimen, HAZ contribution to tensile properties was less and so there was little difference in YS and UTS values between the base metal and the flame-cut metal. Since the specimen sizes had different cross-sectional areas, their elongations cannot be directly compared since elongation is directly proportional to the square root of the tensile specimen cross-sectional area.[43] Area normalization of the thicker specimen elongation data was done relative to the thinner specimen (table 6). The normalized percentage elongation for the specimen flame cut at the slower speed increased with increasing thickness for both steels, due to the increased amount of more ductile base metal in the thicker specimen. The percentage elongation for the base metal increased slightly with increasing specimen thickness for A514 steel, but for A572 steel, there was a decrease in normalized percentage elongation. Since elongation depends on the microstructure of the material, base metal elongation was nearly the same with increasing thickness. Additional specimens would need to be tested to confirm the anomalous decrease of elongation for the base metal of A572 steel with increasing tensile specimen thickness.

43

CHARPY V-NOTCH IMPACT TEST RESULTS

Effect of Specimen Size

Area normalized CVN energy vs. test temperature plots were made for each steel (base metal) for the three different specimen sizes to study the effect of specimen size on the impact properties.   Results for the three steels are presented in figures 22 through 24.   The lower-shelf energy values were the same, but the upper-shelf energy values varied for the three sizes in all the steels.   This is because normalizing the energy values based on the specimen cross-sectional area (A), is applicable only when the fracture mode is fully cleavage, which was the case only at the lower shelf.   Better correlation of upper-shelf energy data was obtained for the three sizes by applying volume $(A^{3/2})$ normalization.[38] The volume normalized plots are shown in figures 25 through 26.   Lower upper-shelf energies were obtained for full-size specimens than for subsize specimens, due to the increased constraint present in the thicker specimen.[44]

The transition temperature for quarter-size specimens was less than for the full-size specimen since the plastic constraint at the notch was reduced with the reduced width (figures 22 through 24).   However, the half-size specimen had a higher transition temperature than both the other sizes, since the plastic constraint at the notch was much higher due to a higher flank angle of the notch in this case (figure 7).   Plastic constraint factor at the notch produces a triaxial state of stress, and from the relation

$$K_\sigma(1 + \frac{\Pi}{2} - \frac{\omega}{2})$$

where K_0 is the maximum plastic stress concentration and wis the included flank angle of the notch, K_O values for full-, quarter-, and half-size specimens were obtained as 1.79, 1.79, and 2.54, respectively. The increased plastic stress concentration of the half-size specimen explains the higher transition temperature of these specimens compared to the full-size and quarter-size specimens.

Effect of the Notch Location in HAZ

The effect of the notch location in HAZ was studied by plotting area normalized energy values vs. temperature for each specimen size for three test conditions (figures 28 through 33).

The trend of these plots can be understood by schematic diagrams (figures 34 through 36) of notch orientation in relation to the microstructure of the HAZ.   In quarter-size specimens, most of the notch root structure was tempered martensite for A514 steel (figure 34 (a) and (c)), and tempered martensite and fine pearlite for A572 and A588 steels (figures 35 through 36), except for A588 flame cut at the slower cutting speed where most of the notch root microstructure was tempered martensite and bainite (figure 36 (a)). But in the case of half-size specimens, due to the orientation and since the notch depth was 0.75 mm,
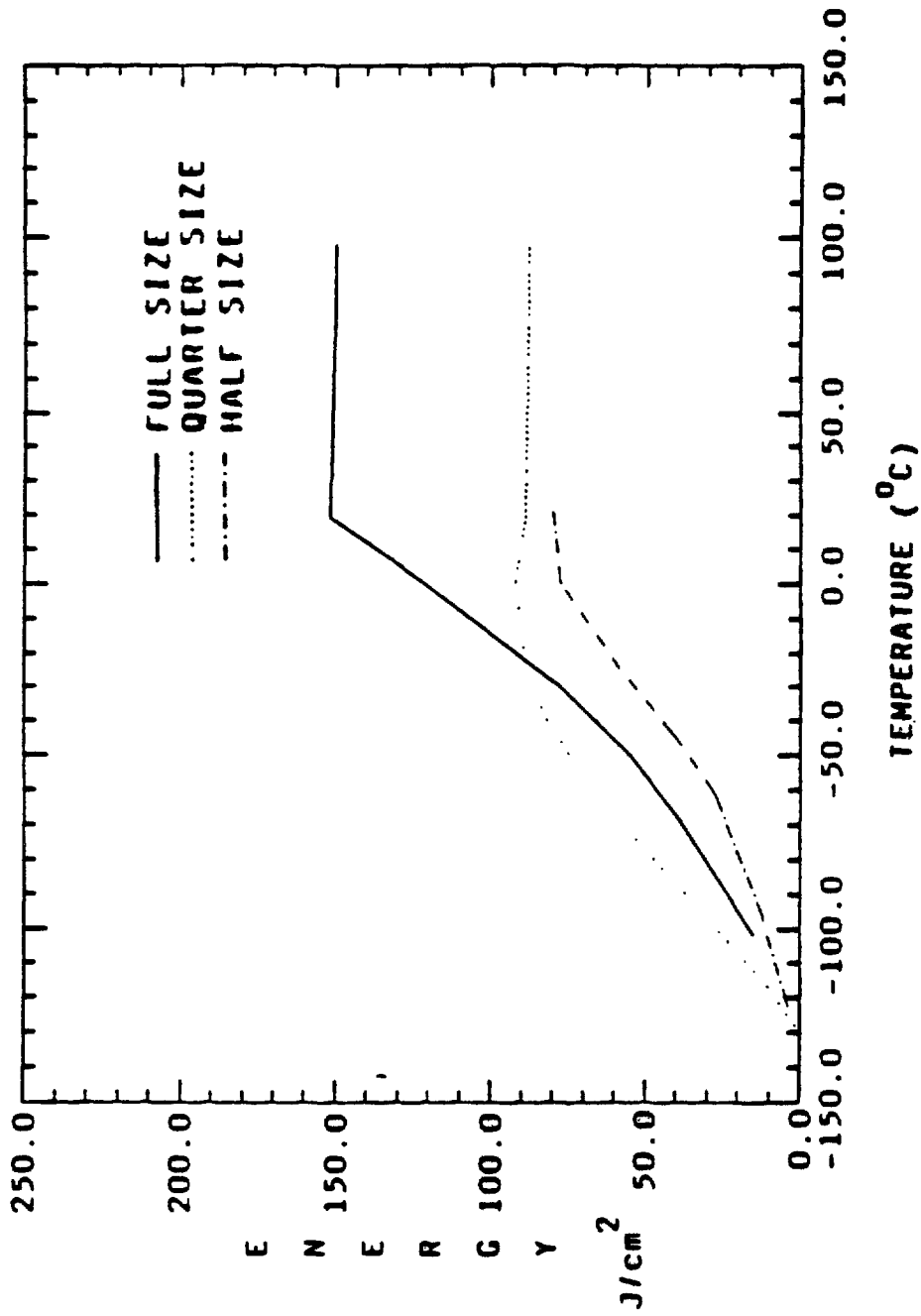
Figure 22.   Area normalized CVN energy vs. test temperature, A514 steel, base metal.
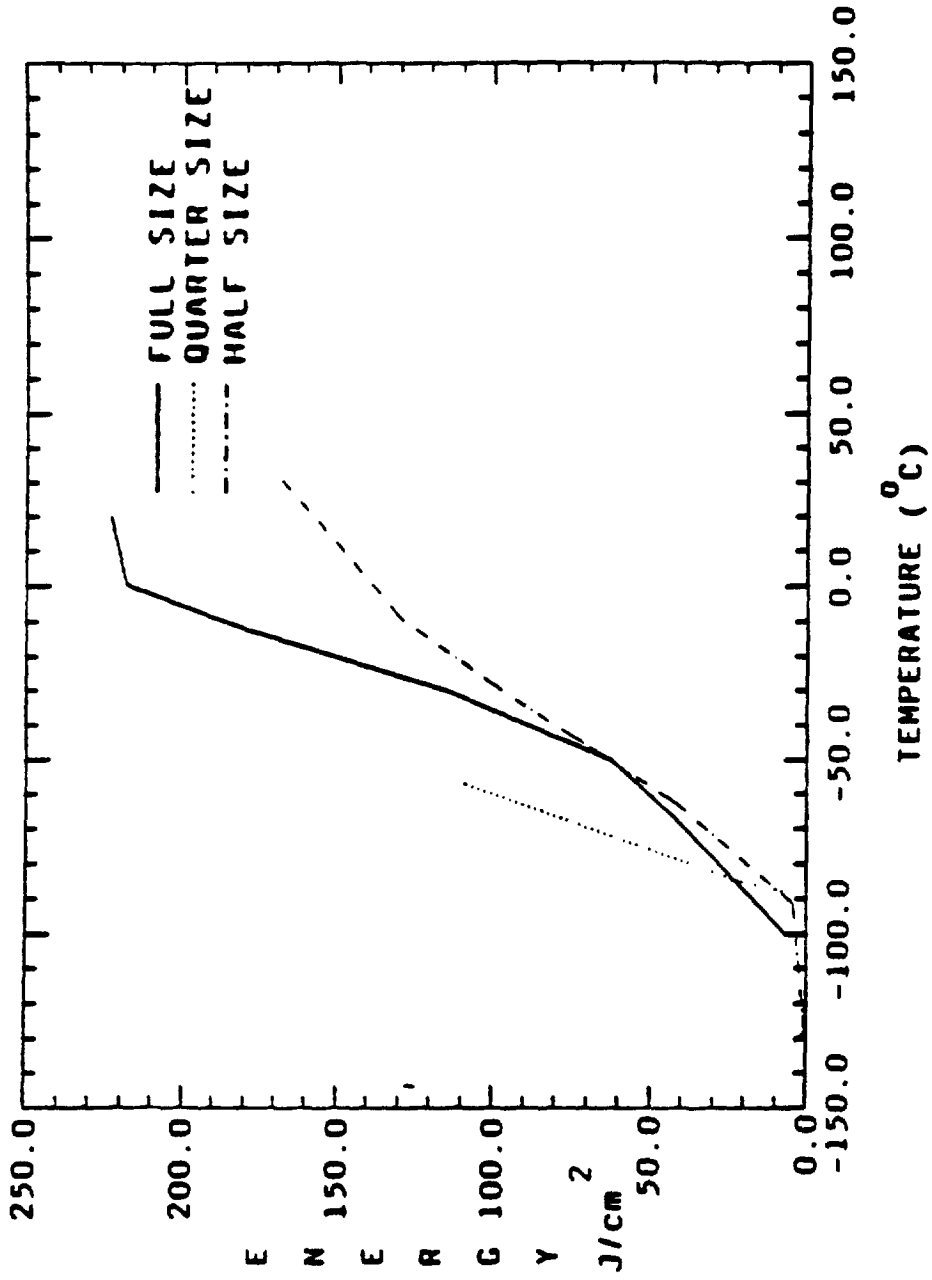
Figure 23.   Area normalized CVN energy vs. test temperature, A572 steel, base metal.
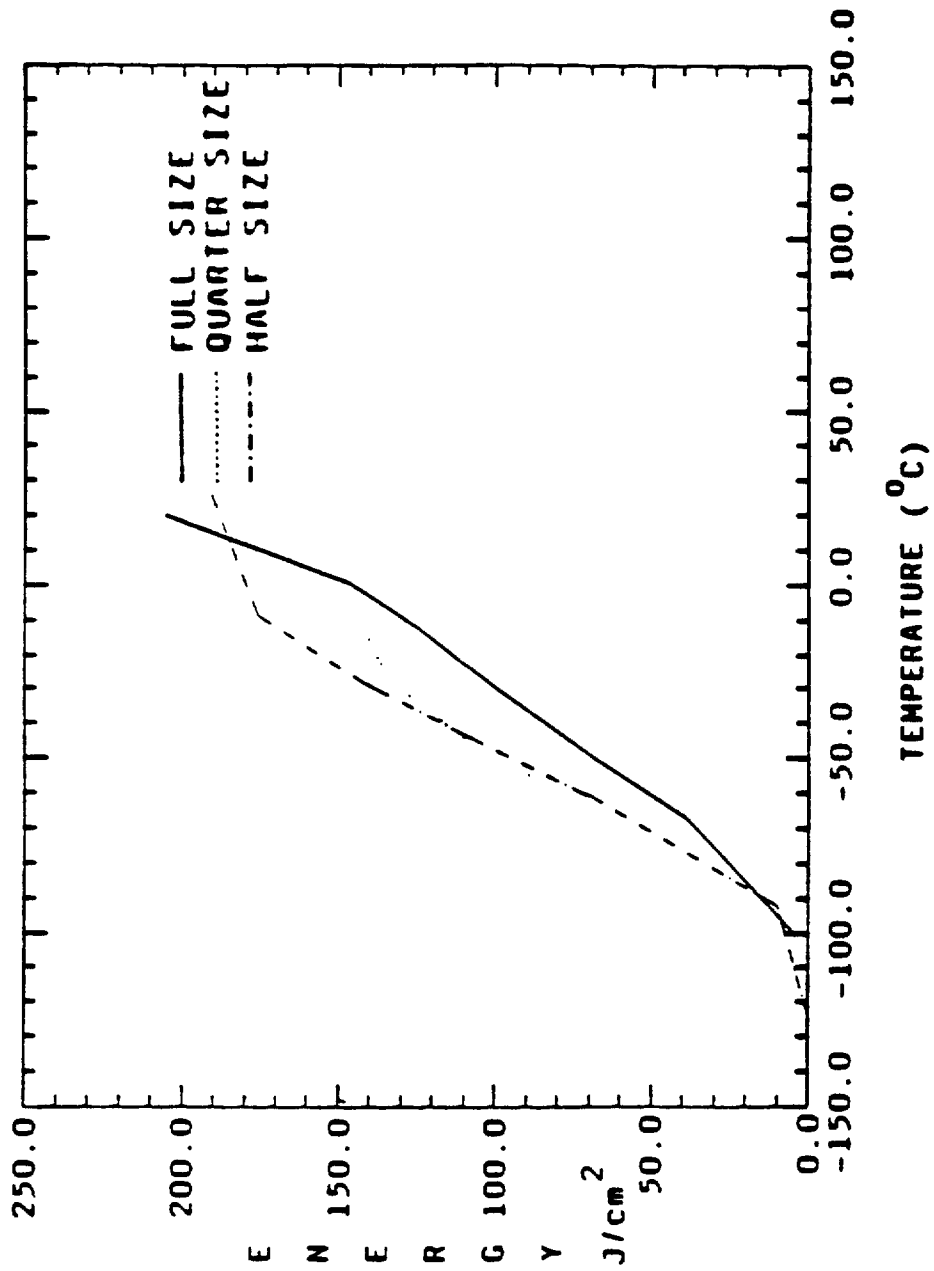
46

Figure 24. Area normalized CVN energy vs. test temperature, A588 steel, base metal.
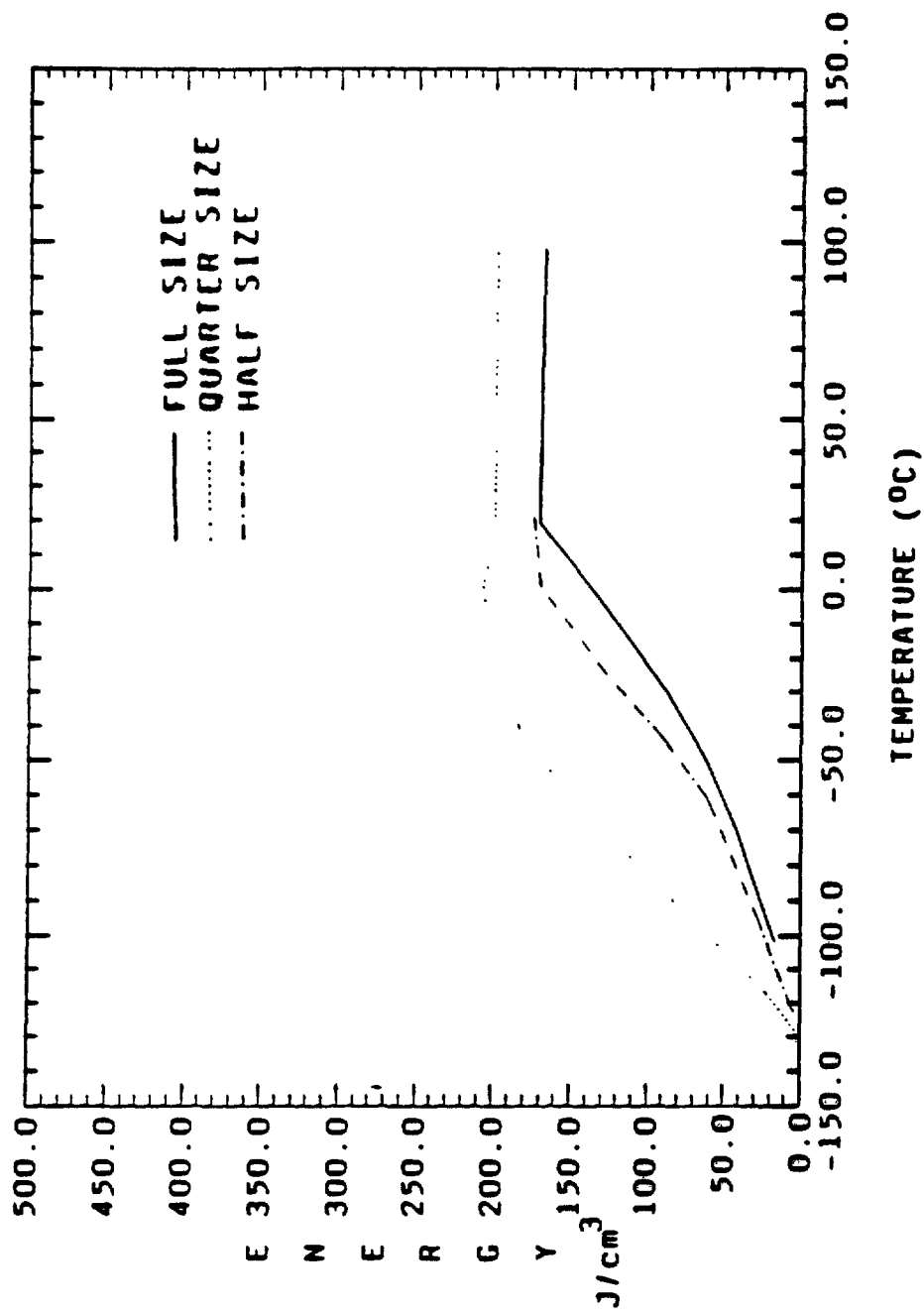
47

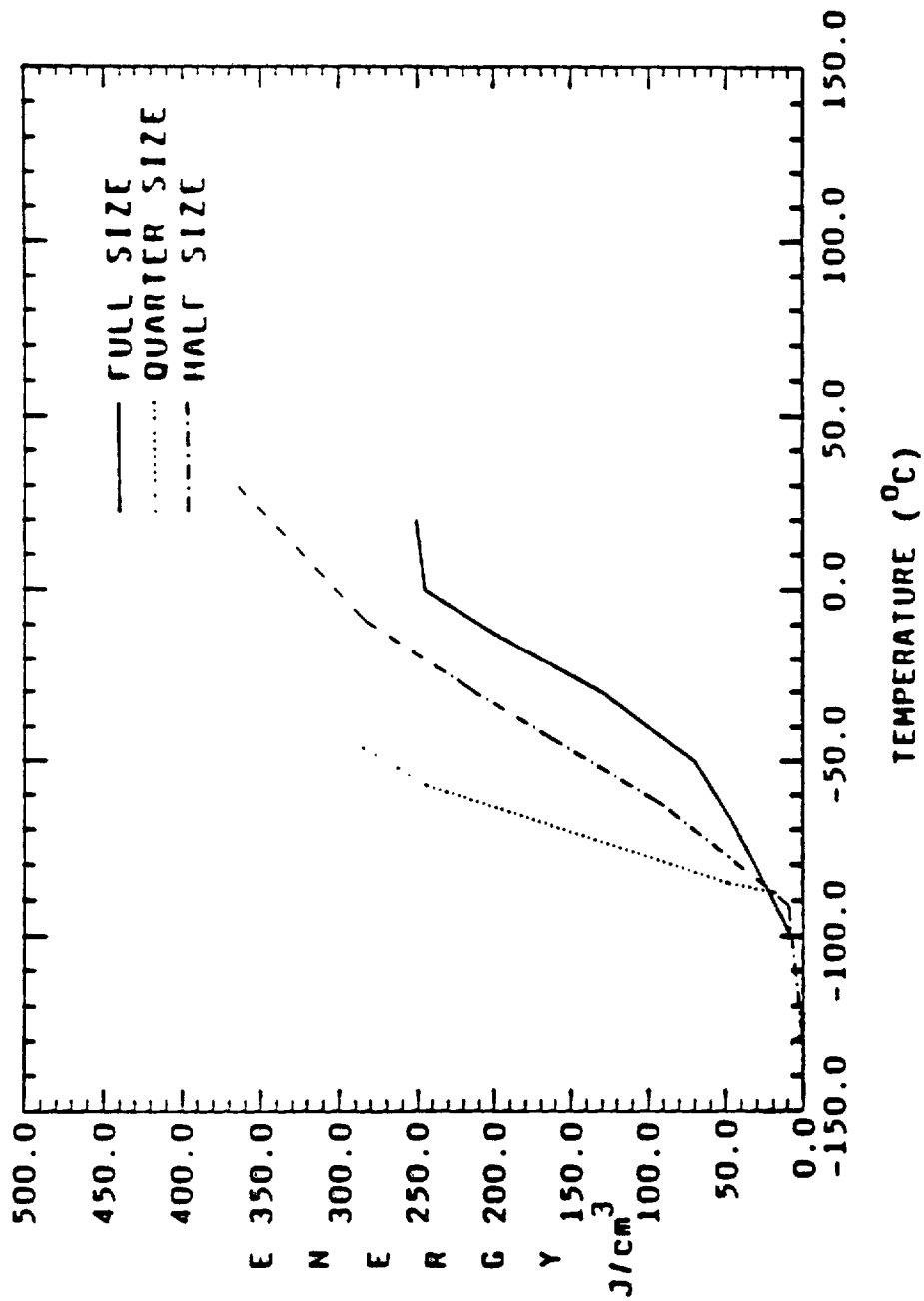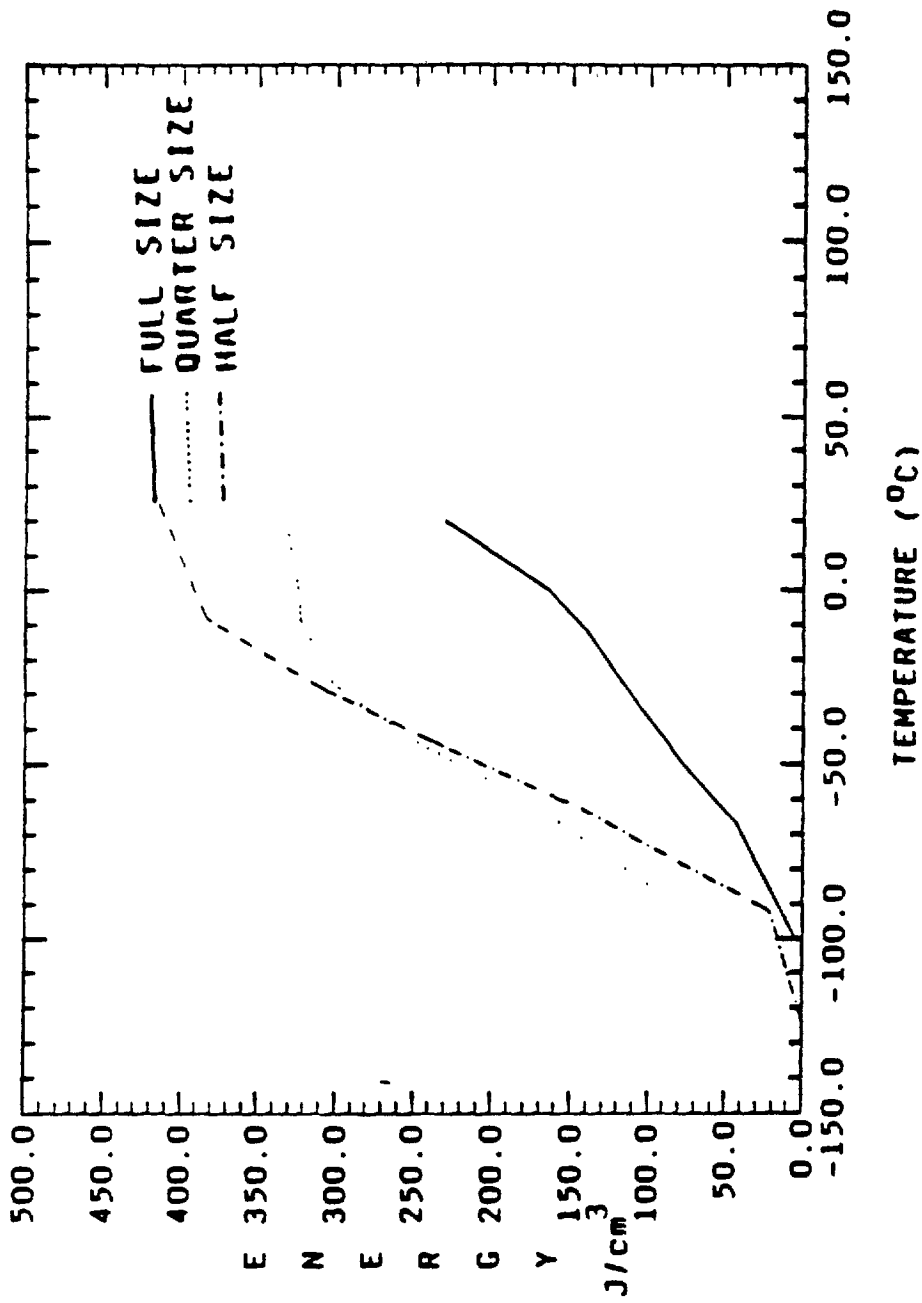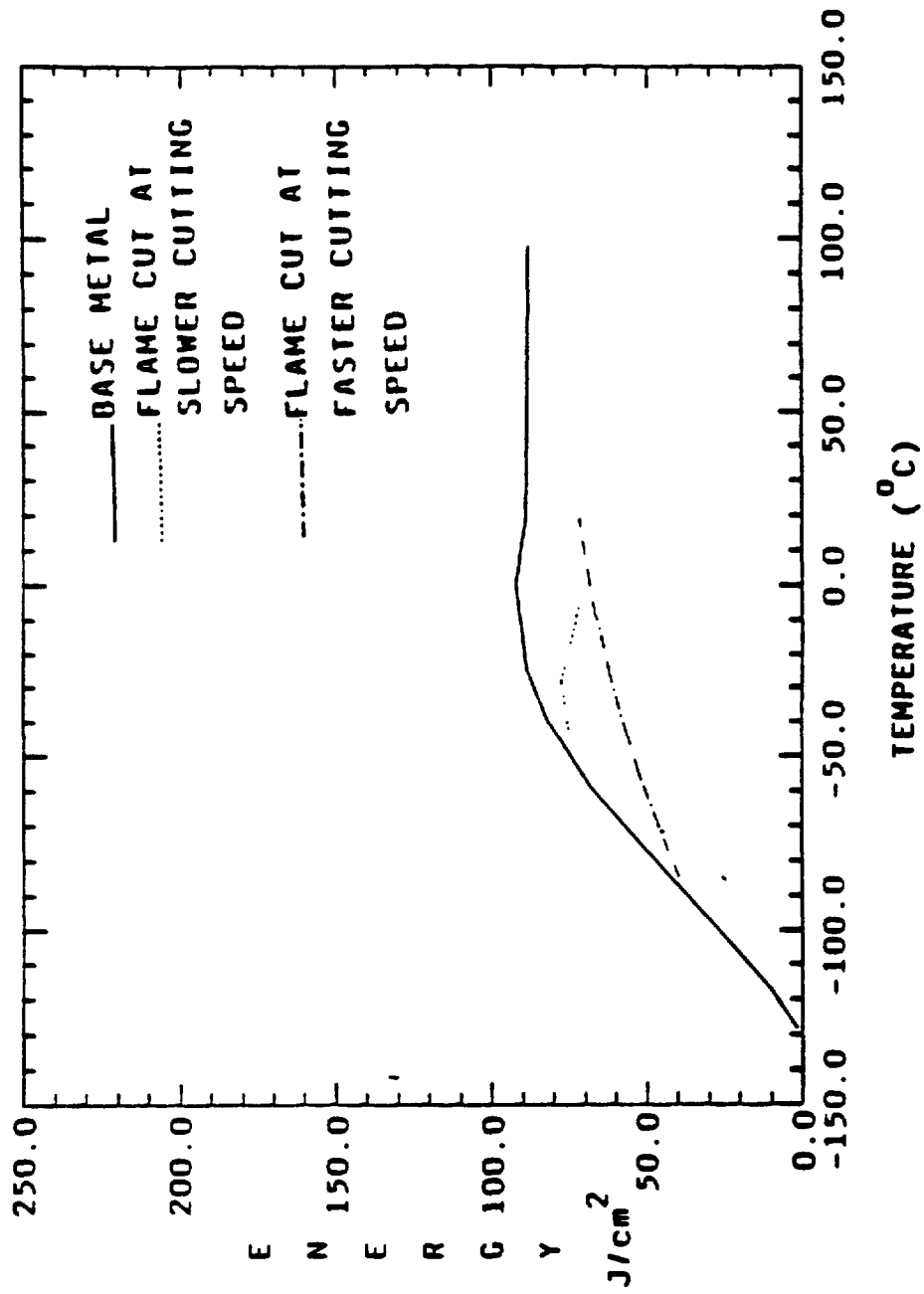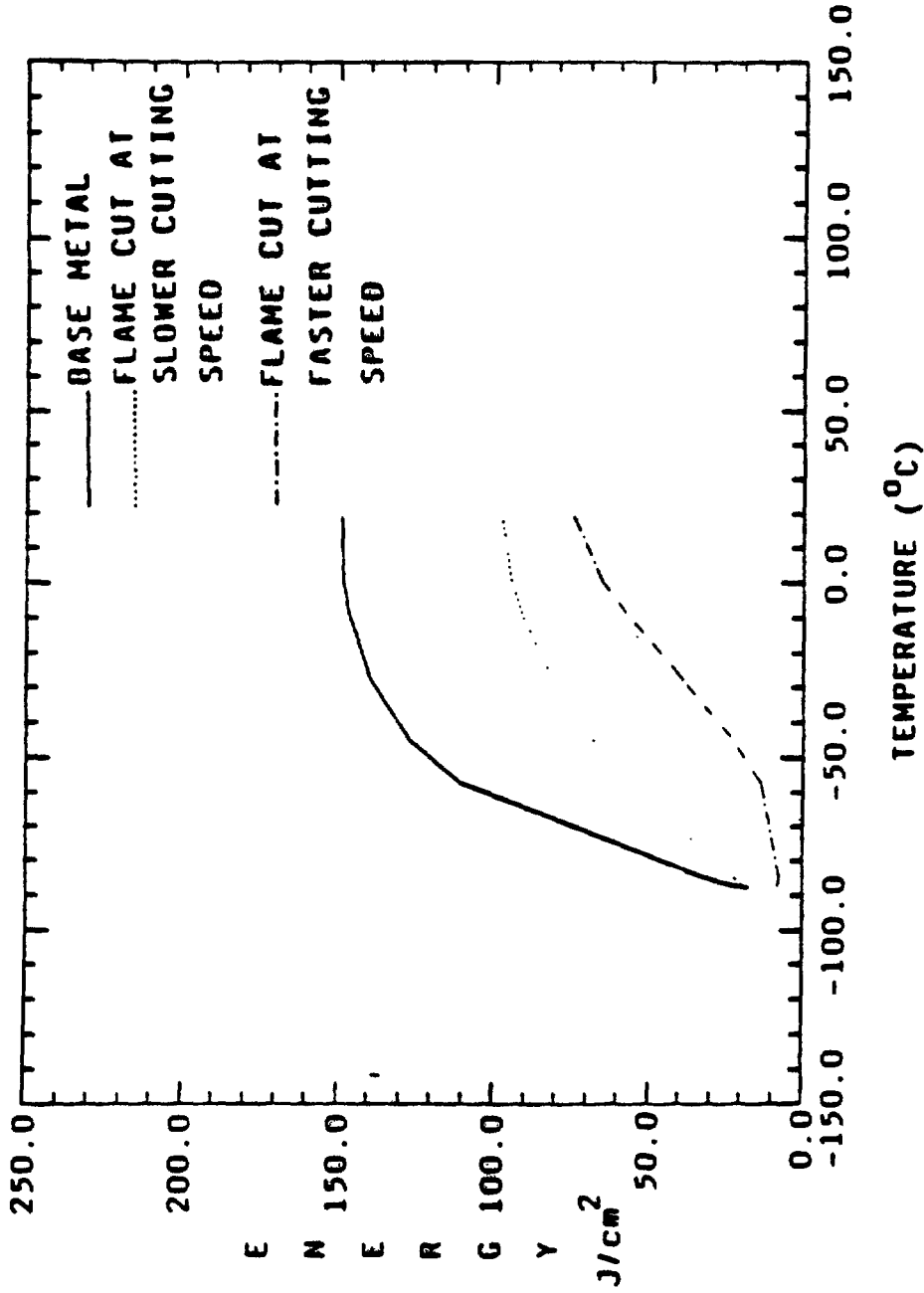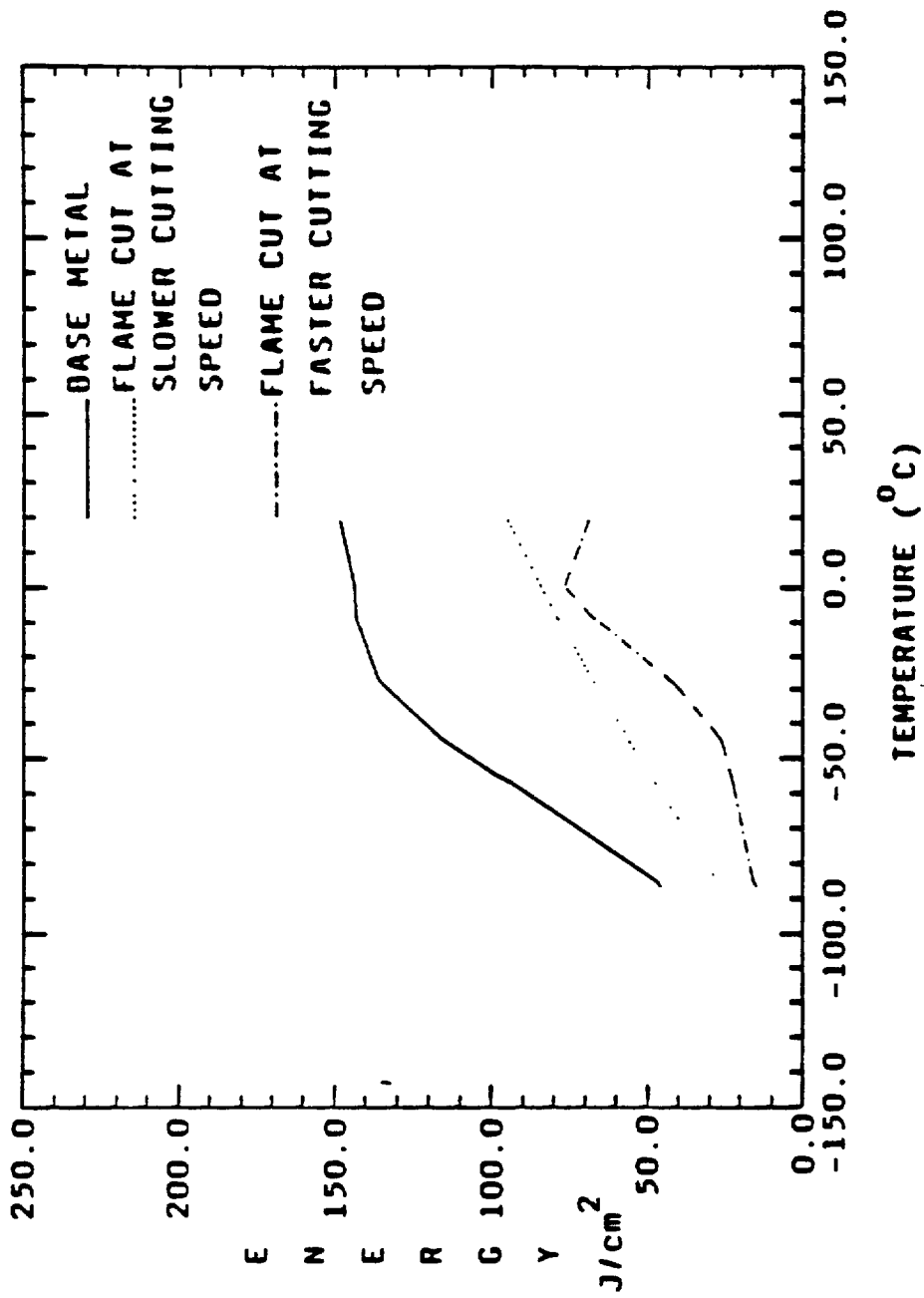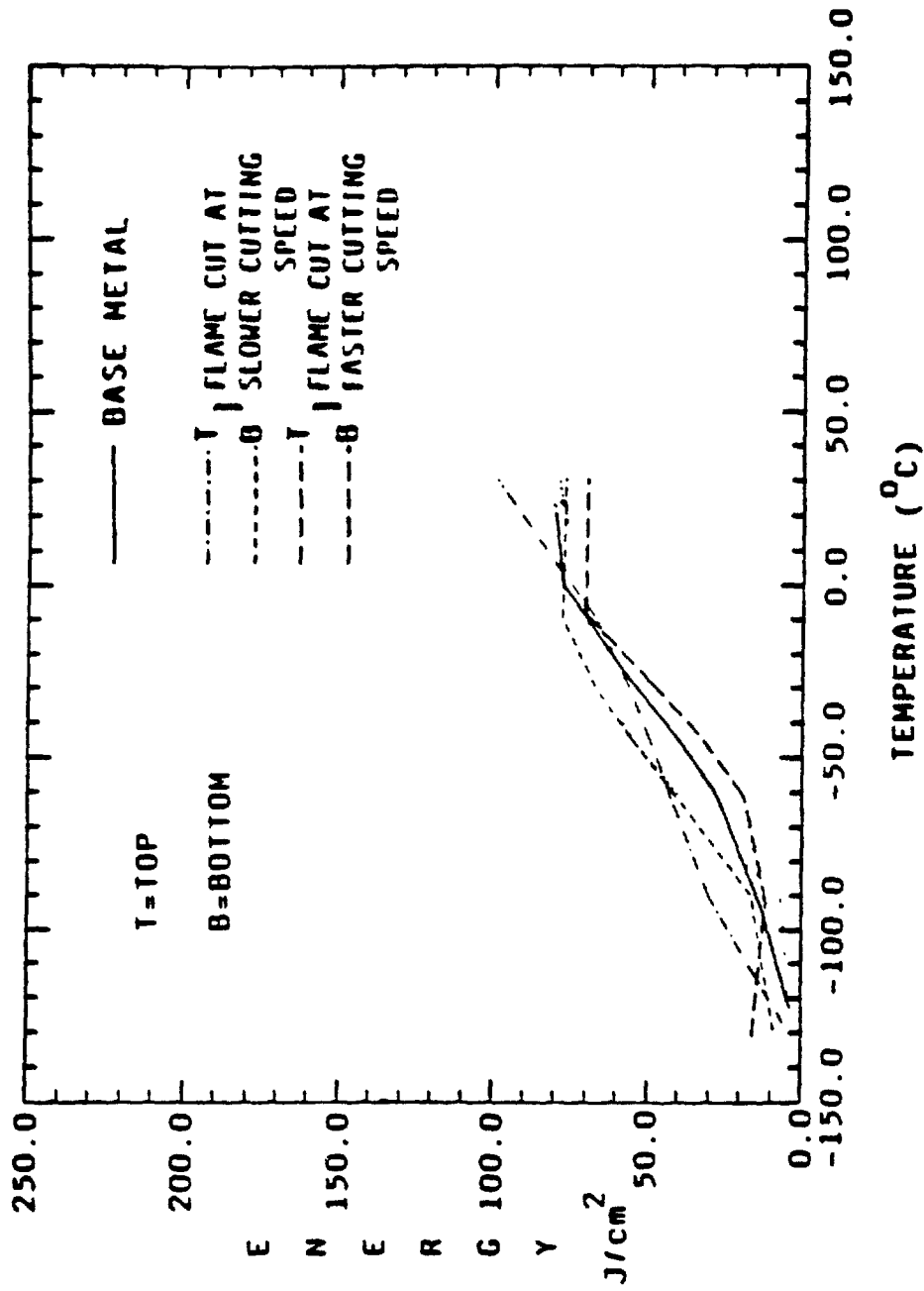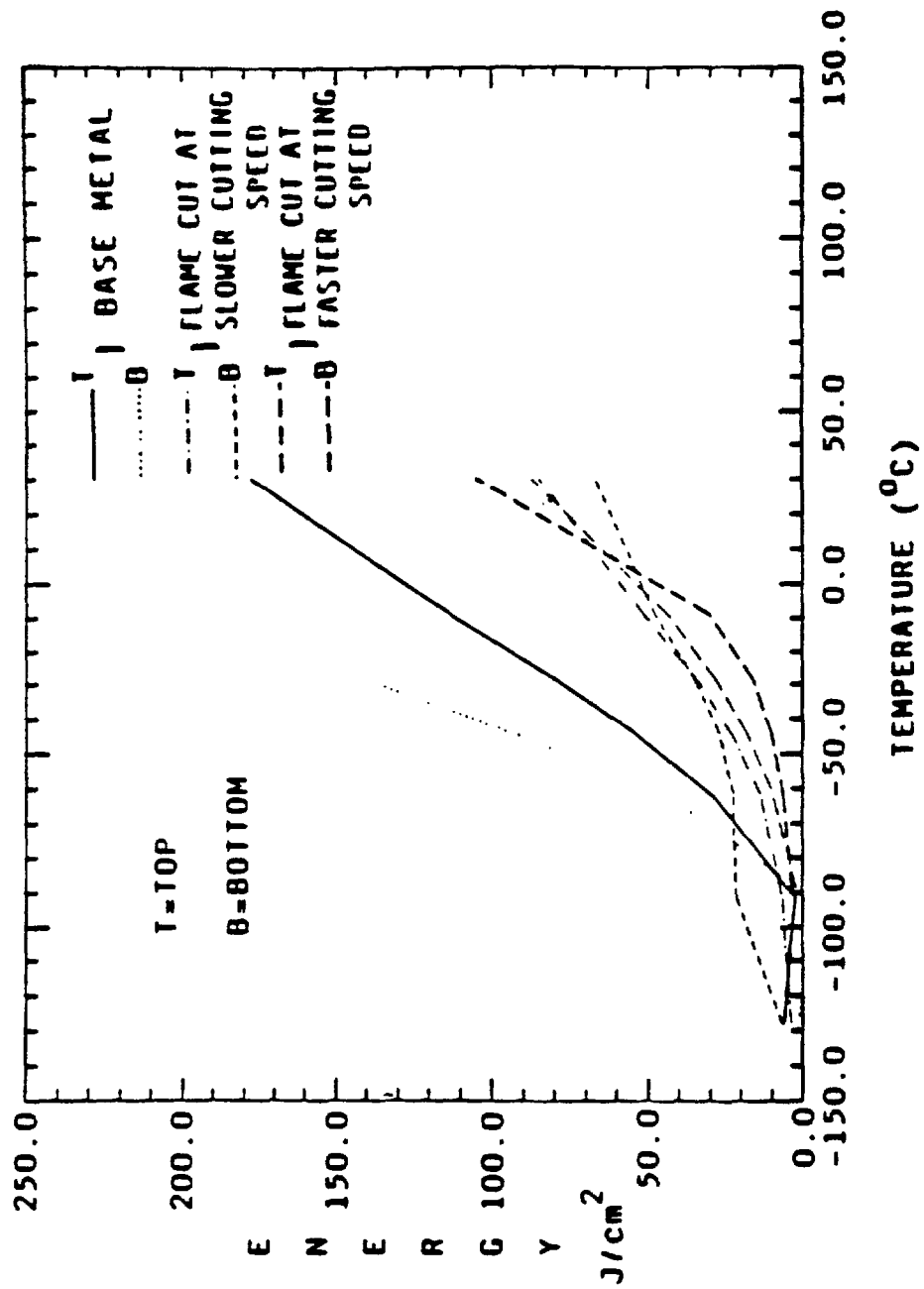Figure 25. Volume normalized CVN energy vs. test temperature, A514 steel, base metal.

48

Figure 26.   Volume normalized CVN energy vs. test temperature, A572 steel, base metal.

49

Figure 27.   Volume normalized CVN energy vs. test temperature, A588 steel, base metal.

Figure 28.   Area normalized quarter-size CVN energy vs. test temperature, A514 steel.

51

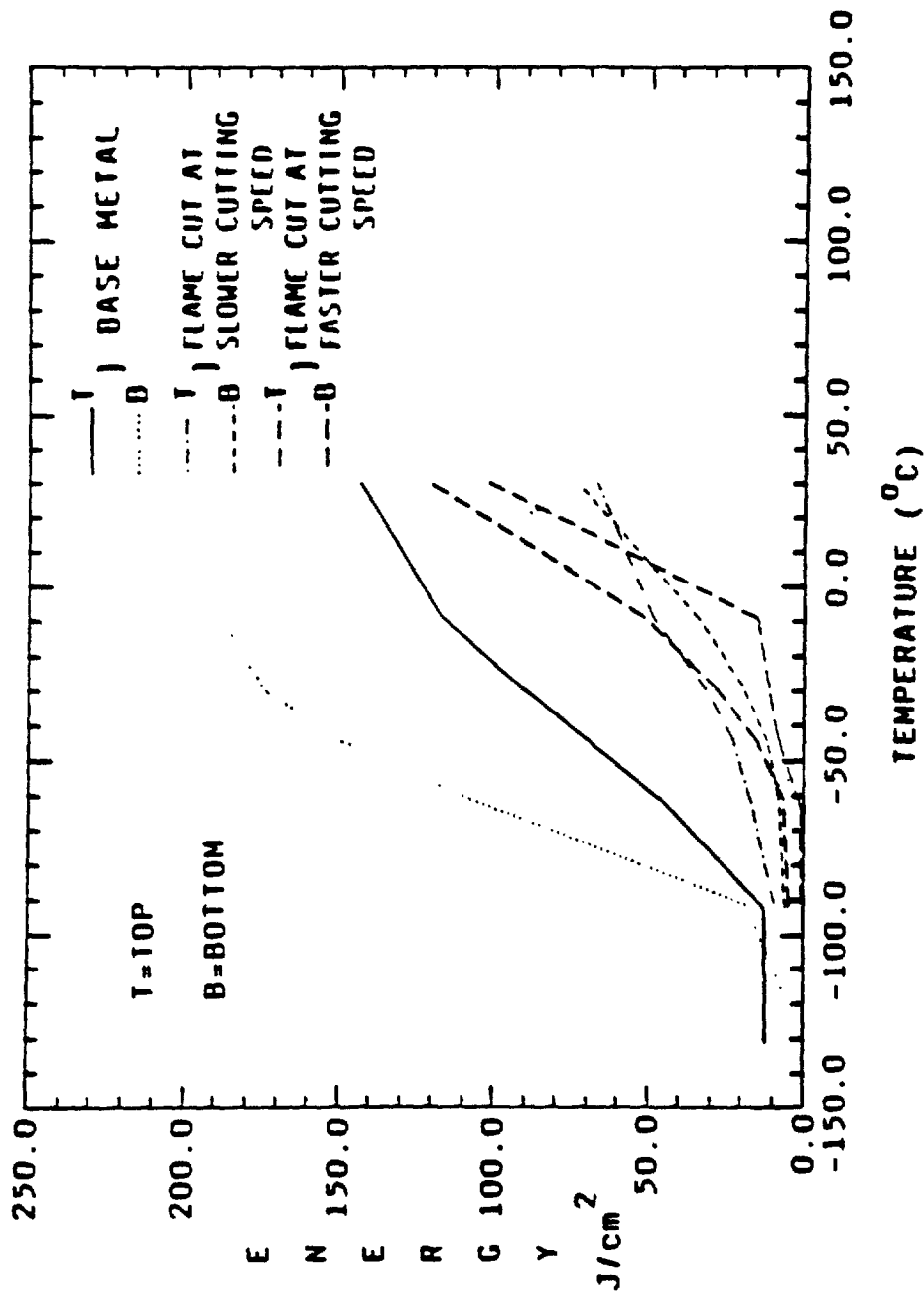Figure 29.   Area normalized quarter-size CVN energy vs. test temperature, A572 steel.

Figure 30.   Area normalized quarter-size CVN energy vs. test temperature, A588 steel.

53

Figure 31.   Area normalized half-size CVN energy vs. test temperature, A514 steel.

54

Figure 32.   Area normalized half-size CVN energy vs. test temperature, A572 steel.

55

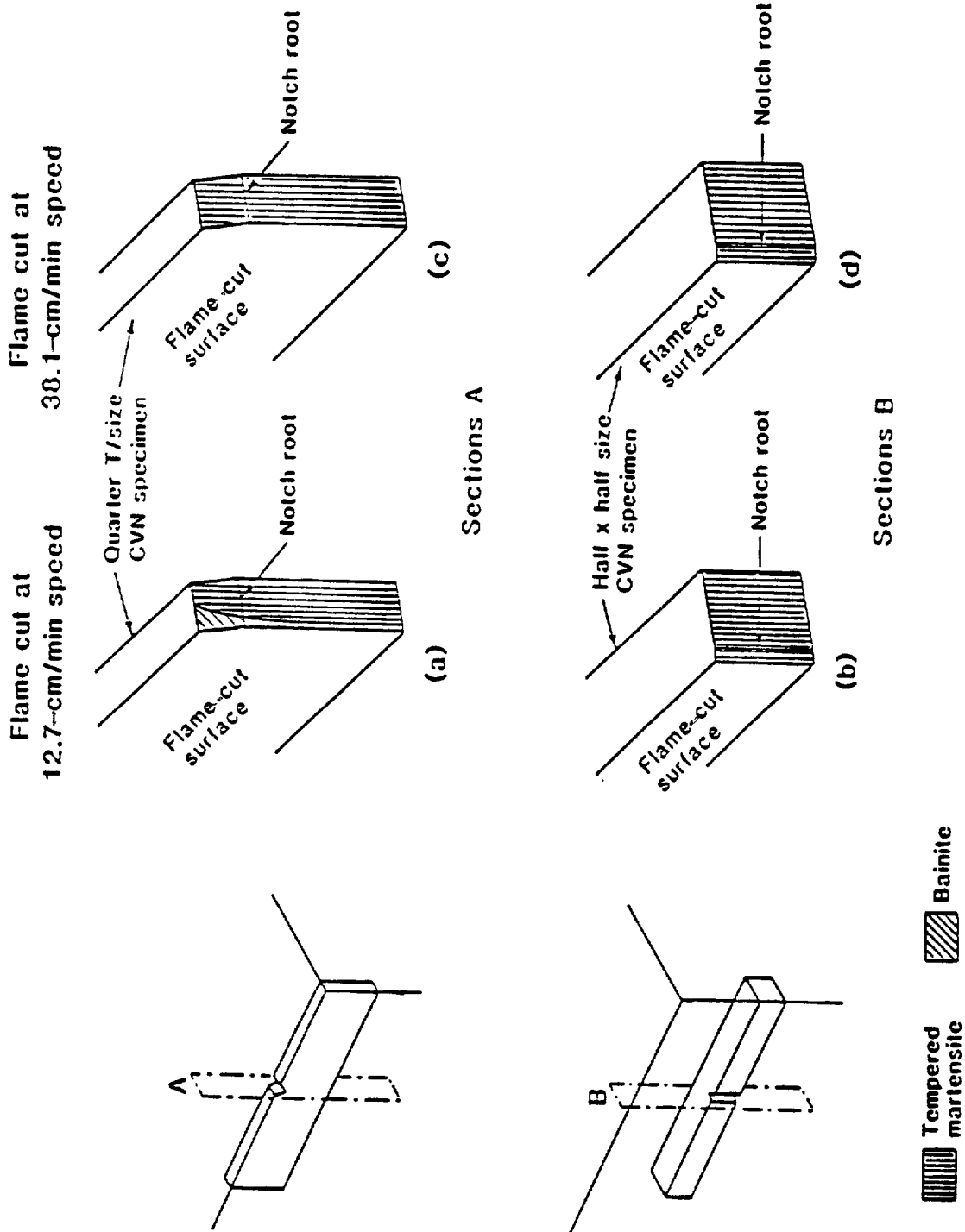Figure 33.   Area normalized half-size CVN energy vs. test temperature, A588 steel.

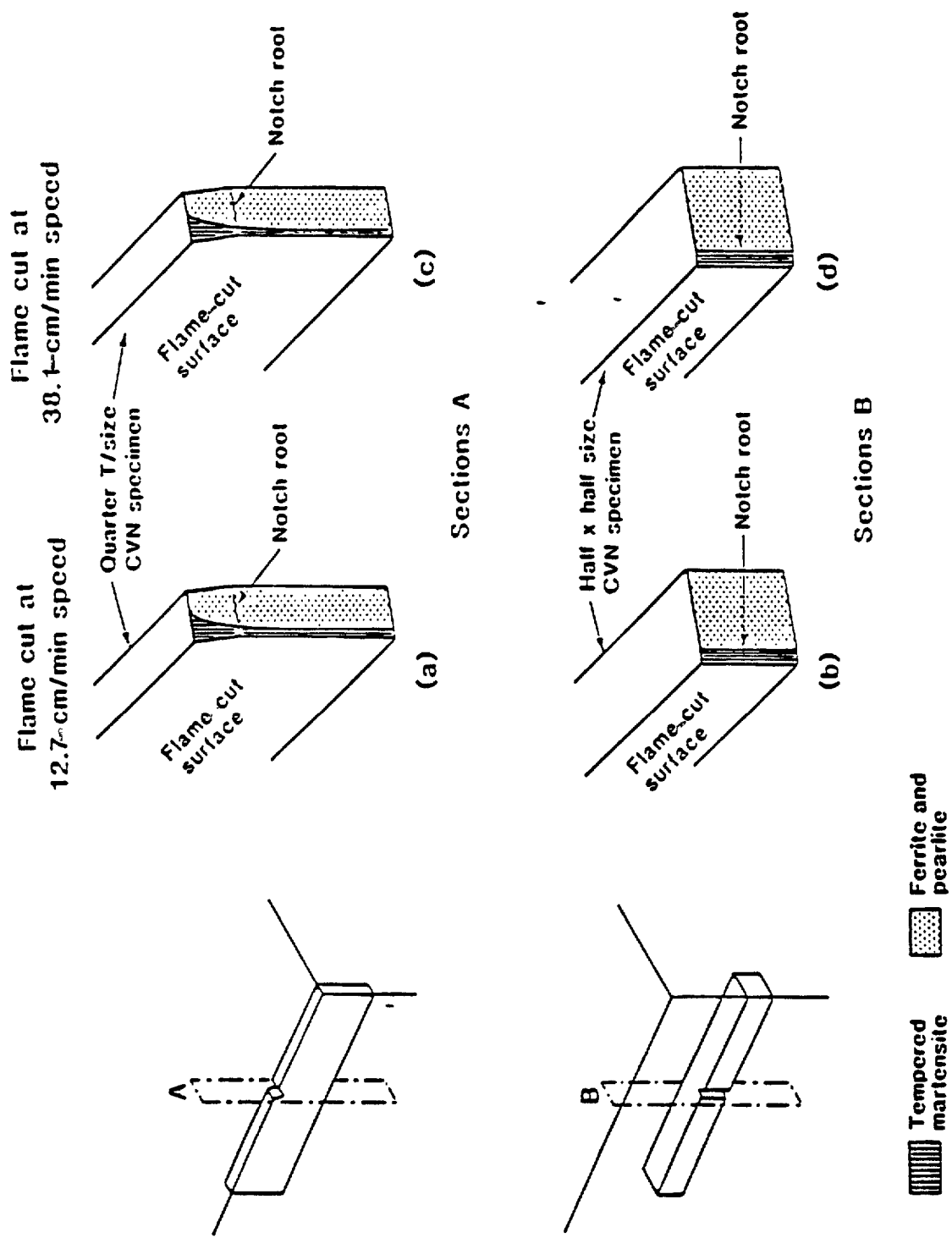Figure 34. Schematic of flame-cut HAZ microstructures at CVN root, A514 steel.

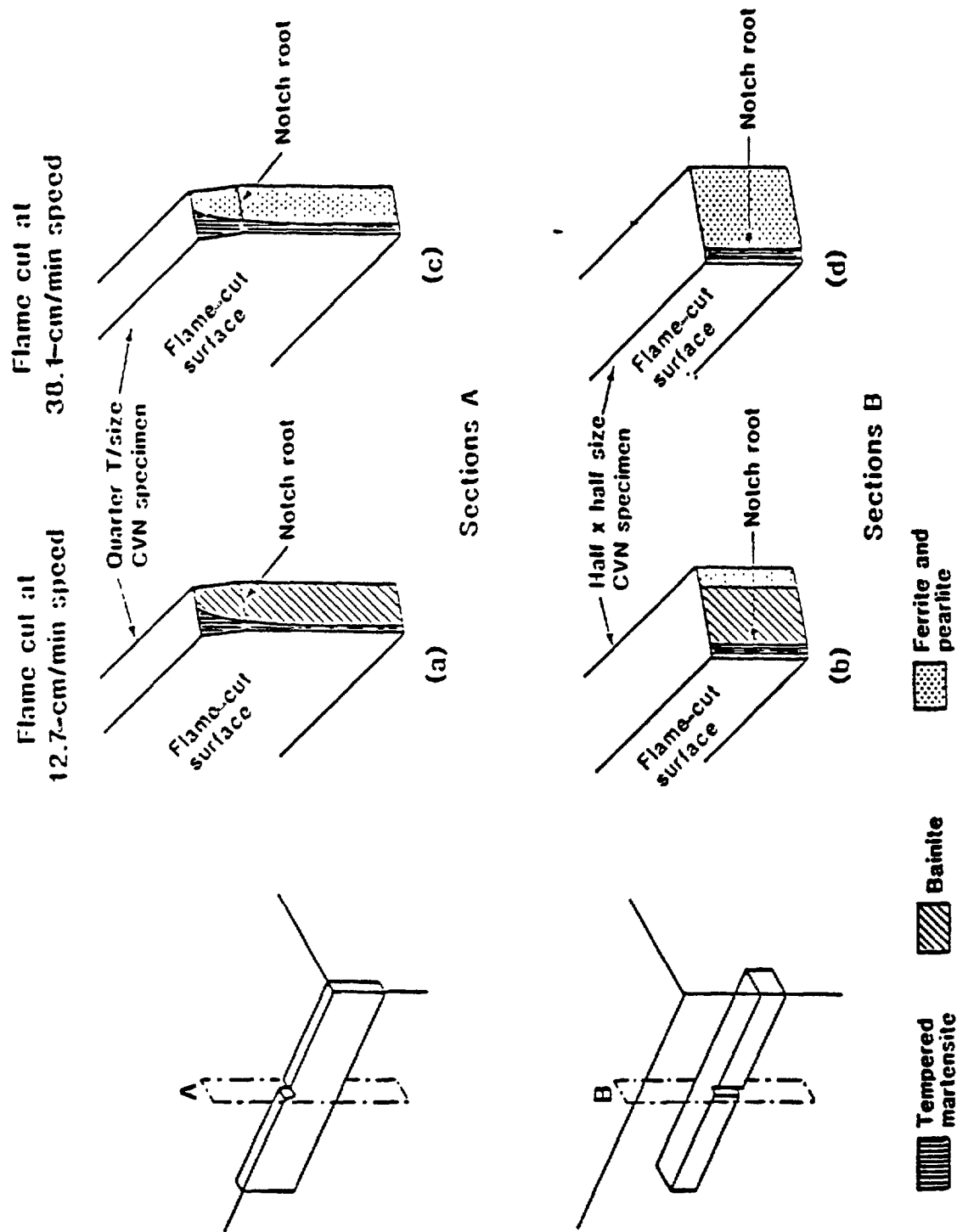Figure 35. Schematic of flame-cut HAZ microstructures at CVN root, A572 steel.

Flame cut at
12.7-cm/min speed

Flame cut at
30.1-cm/min speed

Notch root

Notch root

Flame-cut
surface

Flame-cut
surface

Quarter T/size
CVN specimen

(a)

(c)

Sections A

Notch root

Notch root

Flame-cut
surface

Flame-cut
surface

Half x half size
CVN specimen

(b)

(d)

Sections B

Tempered
martensite

Bainite

Ferrite and
pearlite

Figure 36.   Schematic of flame-cut HAZ microstructures at CVN root, A588 steel.

59

the notch was entirely in tempered martensite for A514 steel (figure 34 (b) and (d)), and was entirely in fine pearlite for A572 and A588 steels (figures 35 and 36), except A588 flame cut at a slower speed where the notch root was entirely in bainite (figure 36 (c)).


Effect of Cutting Speed

The A514 steel impact toughness values in both quarter-size (figure 28) and half-size specimens (figure 31) were nearly identical, because A514 steel is quenched and tempered and flame cutting did not change the microstructure very much.   The flame-cut HAZ microstructures were tempered martensite and bainite for the slower cutting speed, and tempered martensite for the faster cutting speed.   In quarter-size A514 specimens, the metal had slightly more impact toughness than A514 flame cut at the faster speed.   This small difference was due both to the presence of bainite in samples cut at the slower cutting speed and to more tempering of the martensite at slower speed.   For flame-cut half-size specimens, the impact energy values were close to one another as the notch was entirely in tempered martensite.   In half-size specimens, the specimens taken from the top of midthickness had higher impact toughness than those taken from the bottom of the midthickness.   As the top of the plate was in contact with the cutting torch, there was more tempering of the HAZ microstructure at the top of the midthickness than at the bottom.   This explains the higher toughness of the specimens taken from the top of the midthickness than those taken from the bottom.

Both A572 and A588 steels showed decreased impact toughness and increased transition temperature with increasing cutting speed.   This was due to the tempered martensite present in flame-cut HAZ, while the base metal consisted of ferrite and pearlite, and more tempering of martensite in the case of specimens cut at slower cutting speed.   Again, in the case of half-size specimens, for each flame-cut steel, the impact toughness values were similar since the notch was entirely in the ferrite and pearlite region.


FRACTOGRAPHY

The appearance of flame-cut surfaces for A514, A572, and A588 steels at the two cutting speeds are given in figures 37 through 39. The scanning electron micrographs of fractured surfaces of tension tests and impact tests are given in figures 41 through 53.   A514 steel had very few cracks (figure 37 (a) and (b)) on the flame-cut surface, while A572 (figure 38 (a) and (b)) and A588 (figure 39 (a) and (b)) had cracks all over the surface with A572 having more cracks than A588 steel.

The fracture surfaces in tension tests for A572 steel base metal at room temperature are shown in figure 41.   The dimples at both the low strain rate (figure 41 (a)) and the intermediate strain rate (figure 41 (b)) show ductile mode of failure.   The flame-cut steel at faster cutting speed also shows ductile dimple failure (figure 43 (a) and (b)) on the fractured surfaces at both strain rates.   The large pits might have been caused by inclusions being pulled out during fracture.   Even though the fractured surfaces were flat in low temperature
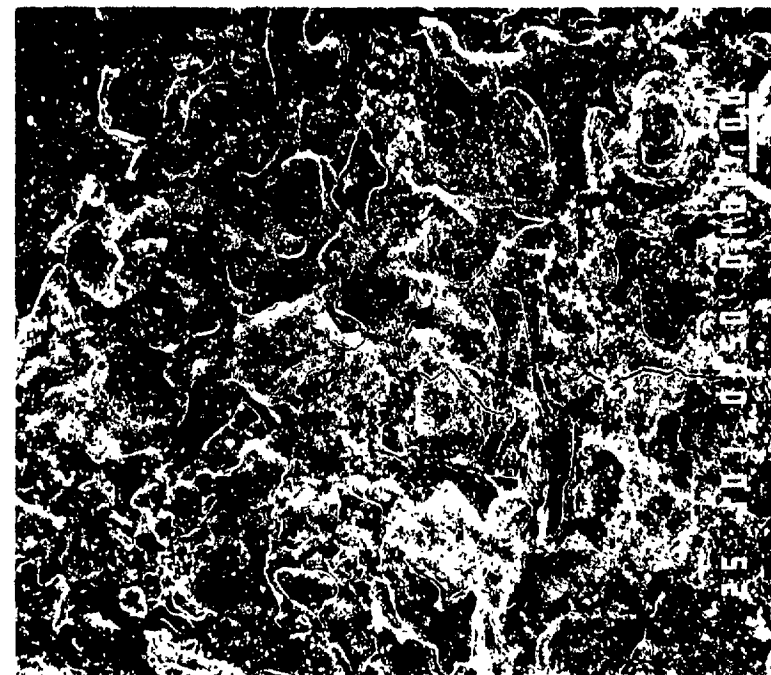
(a)
Flame cut at slower cutting speed.
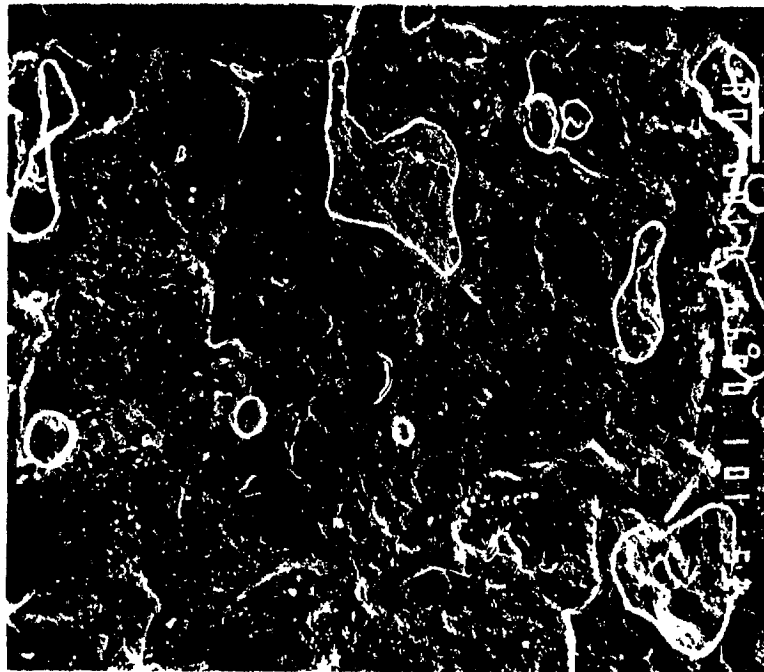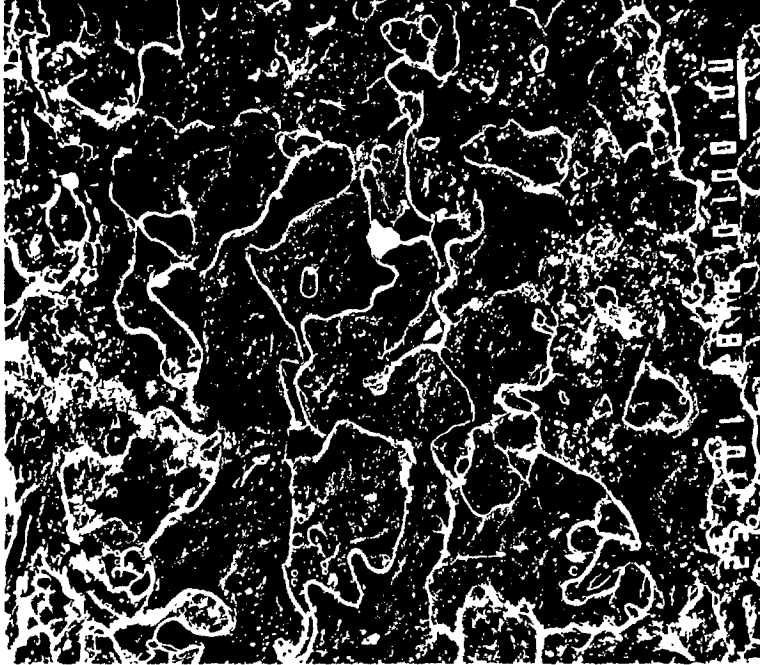
(b)
Flame cut at faster cutting speed.

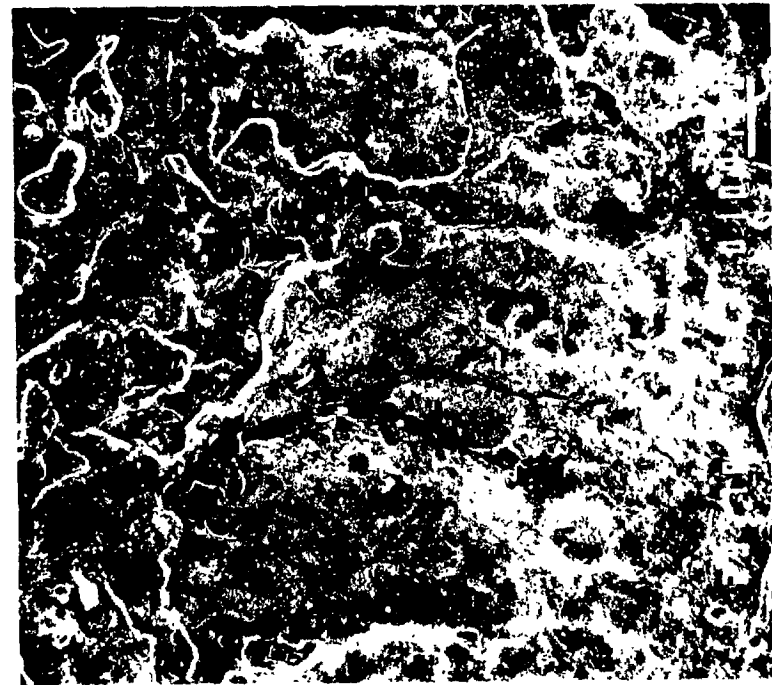Figure 37.   A514 steel flame-cut surfaces.
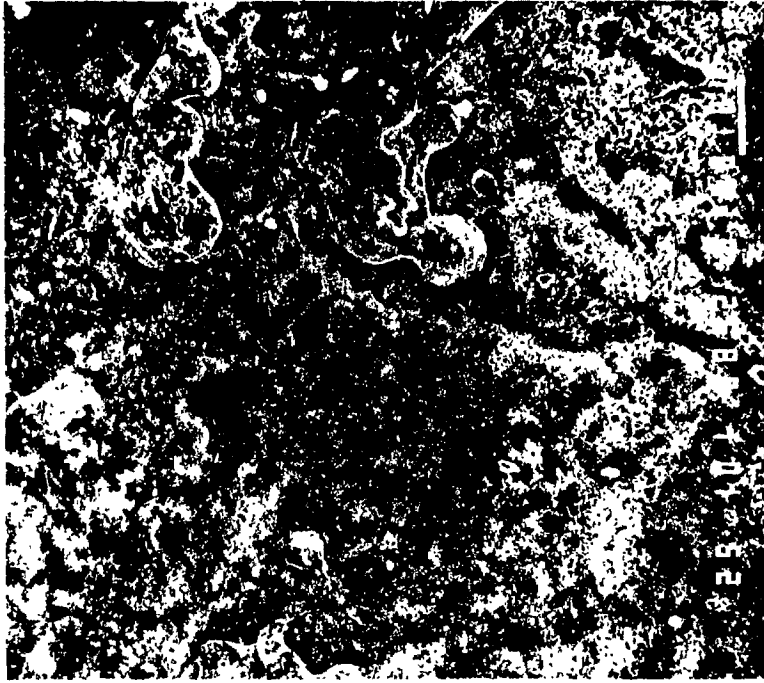
(a)
Flame cut at slower cutting speed.

(b)
Flame cut at faster cutting speed.
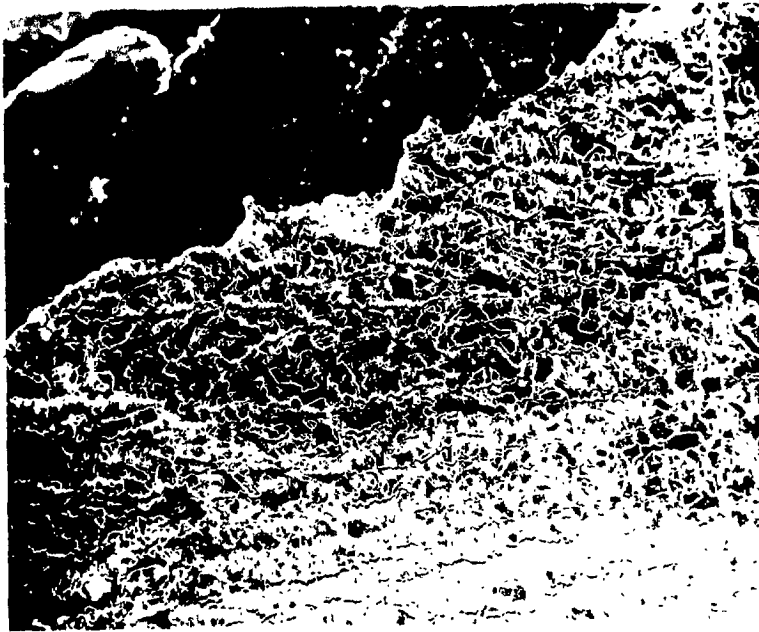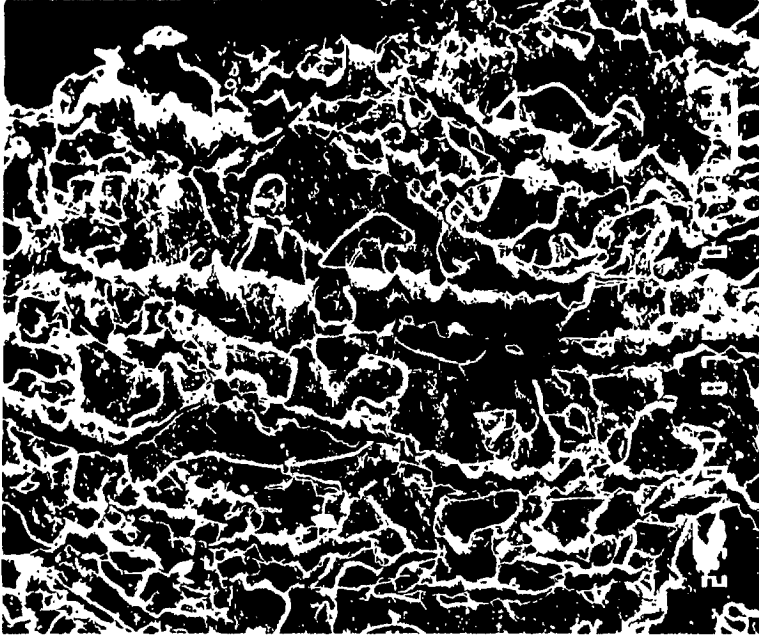
Figure 38.   A572 steel flame-cut surfaces.

62

(b)

Flame cut at faster cutting speed.

(a)

Flame cut at slower cutting speed.

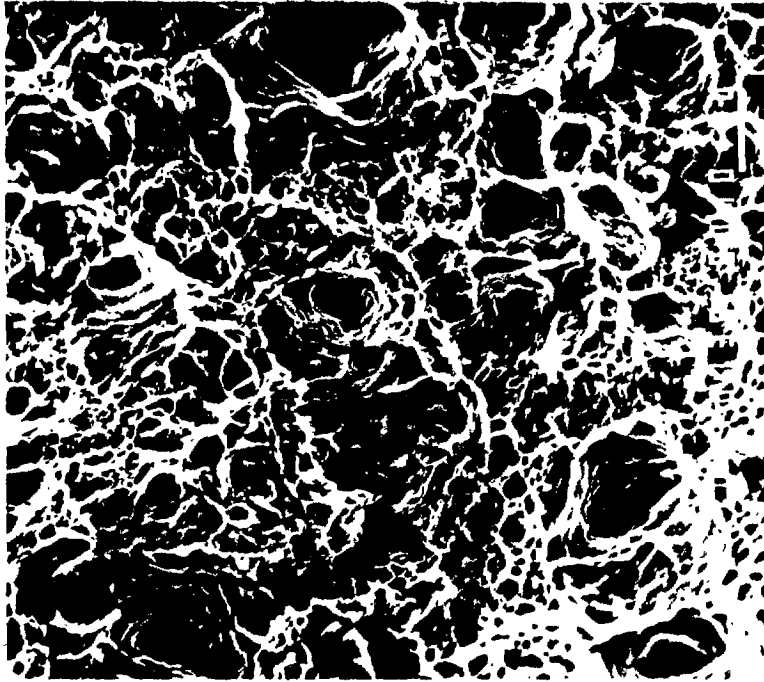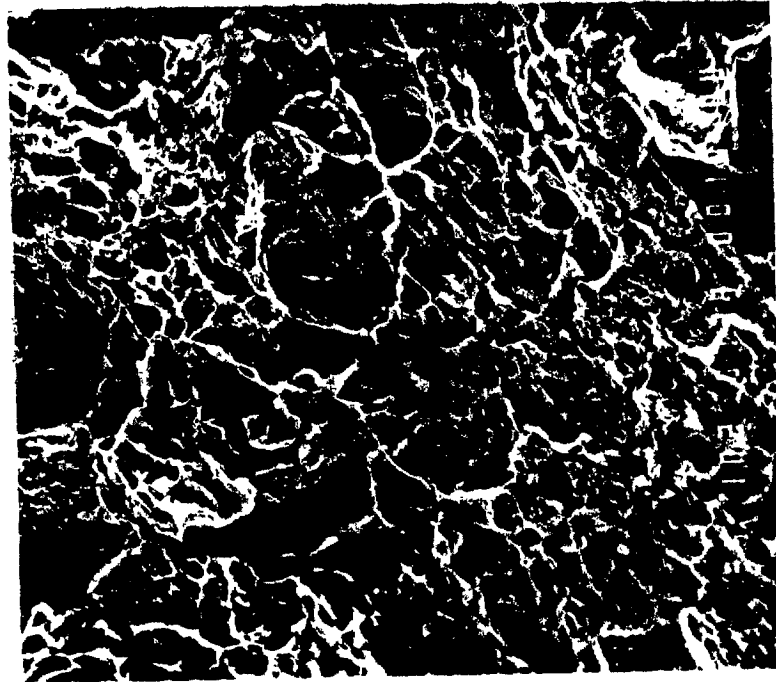Figure 39.   A588 steel flame-cut surfaces.

(b) X 100

(a) X 50

Figure 40.   Flame-cut surface of fractured tensile specimen, A572 steel flame cut at 381-mm/min cutting speed.

(b)

At room temperature and intermediate strain rate.

(a)

At room temperature and low strain rate.

Figure 41. Fractured surfaces of tensile specimen, A572 steel, base metal.
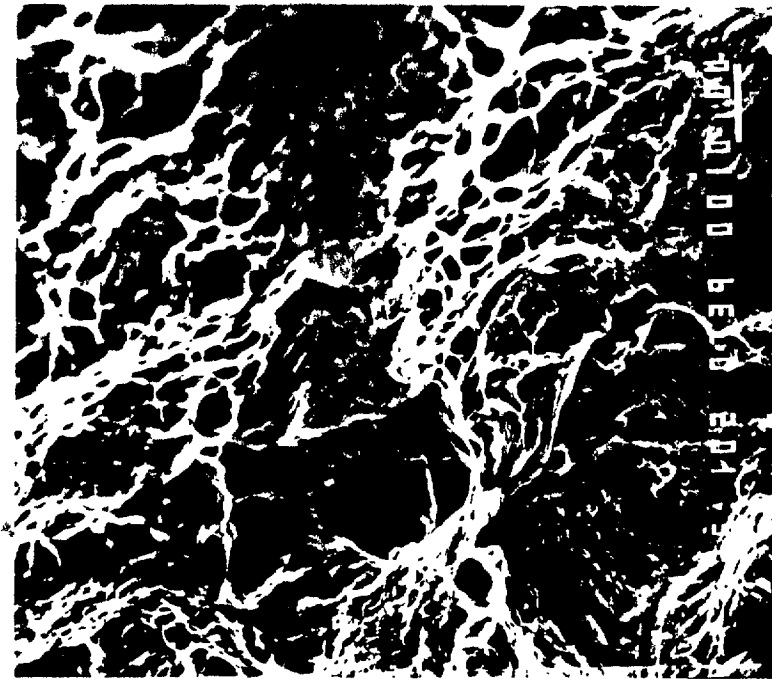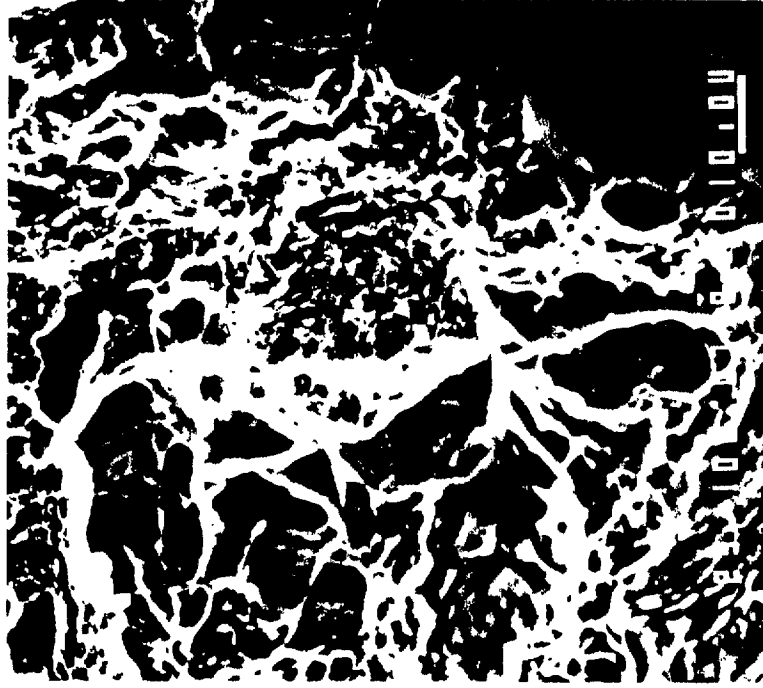
65

(a)

At room temperature and intermediate strain rate.

(b)

At room temperature and low strain rate.

Figure 42.   Fractured surfaces of tensile specimen, A572 steel flame cut at 381-mm/min cutting speed(room temperature).

(a)
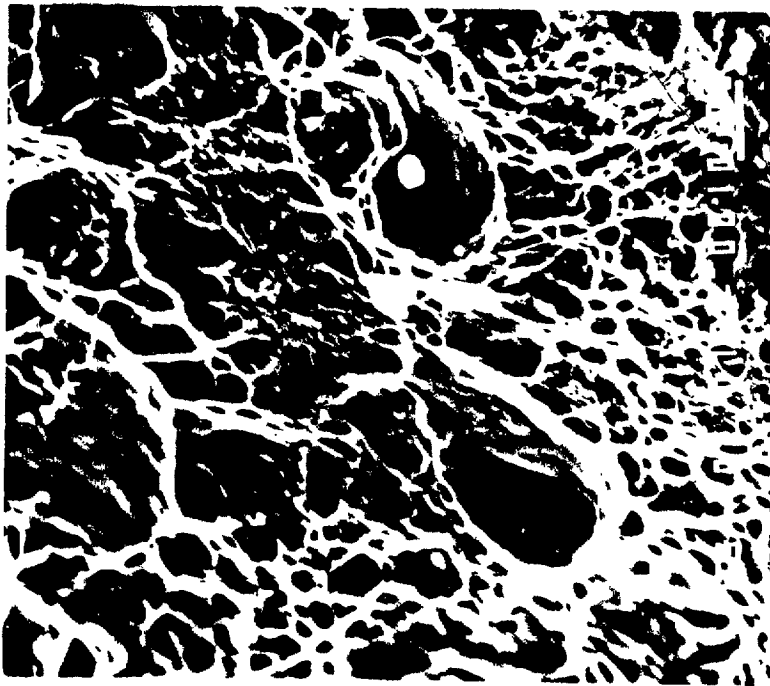
At low temperature and intermediate strain rate.

(b)
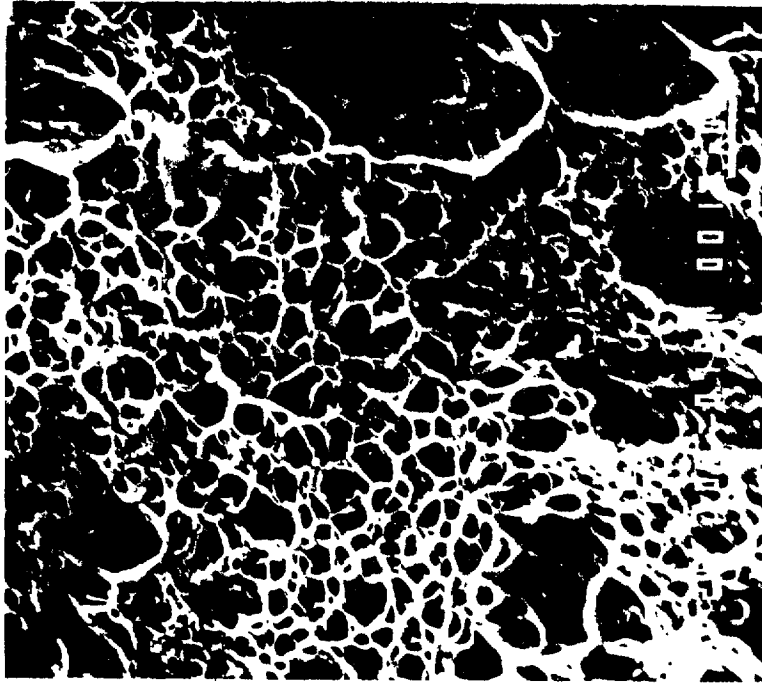
At low temperature and low strain rate.

Figure 43. Fractured surfaces of tensile specimen, A572 steel flame cut at 381-mm/min cutting speed (low temperature).

tests, the fracture appearance (figure 43 (a) and (b)) always exhibited a ductile failure mode. Thus, the flame-cut surface cracks did not induce brittle failure.

A similar trend was seen in both A514 and A588 steels.   Figure 44 shows fracture surfaces for A514 steel for two extreme cases, one for base metal tested at room temperature and low strain rate (figure 44 (a)), and the other for faster cutting speed flame-cut condition at low temperature and intermediate strain rate (figure 44 (b)). Both show ductile mode of failure.   Increasing the specimen thickness to 6.4 mm did not produce brittle failure (figures 45 and 46).

The fractured surfaces for A572 steel in CVN impact tests, for full-, quarter-, and half-size specimens, are revealed for the lower-shelf energy value (a), for the transition temperature region (b), and for the upper-shelf energy value (c), in figures 47 through 53.

Room temperature tests (upper shelf) for A572 base metal (full size) produced dimple fractured surfaces, as seen in figure 47 (c) showing ductile fracture. At the transition temperature region (figure 47 (b)) and at low temperature (figure 47 (a)), fracture occurred by quasi-cleavage mode.   For quarter-size A572 steel base metal, both at room temperature and transition temperature region, figure 48 (b) and (c) respectively, ductile fracture mode was observed and at low temperature, quasi-cleavage fracture (figure 48 (a)) was observed. For the flame-cut steel, at slower cutting speed, (quarter-size specimen) the fracture was ductile at room temperature and quasi-cleavage type at transition temperature region and lower-shelf temperature (figure 49) and for the flame-cut steel at faster cutting speed, the fracture was ductile at room temperature and transition temperature, but quasi-cleavage at lower-shelf temperature as shown in figure 51.   Similar fracture appearance trends were seen in half-size CVN specimens for both base metal and flame-cut conditions, the fracture mode varying between ductile and quasi-cleavage at the transition temperature, ductile at high temperature and quasi-cleavage type at low temperature.   These are shown in figures 52 through 53.

Similar fracture appearances were seen for both A514 and A588 steels in impact tests.   From the presence of flame-cut surface cracks, brittle cleavage failure was expected to occur in Charpy impact tests at low temperature.   Though the test conditions, like low temperature and high strain rate of impact tests, were favorable for brittle fracture, fully cleavage facets, as would be seen in failure entirely by brittle mode, did not occur in any of these steels. These results show that even in impact tests, the flame-cut surface cracks did not produce brittle failure in the temperature range studied.   These results also show that none of the constituents of the HAZ, like martensite, result in brittle fracture.
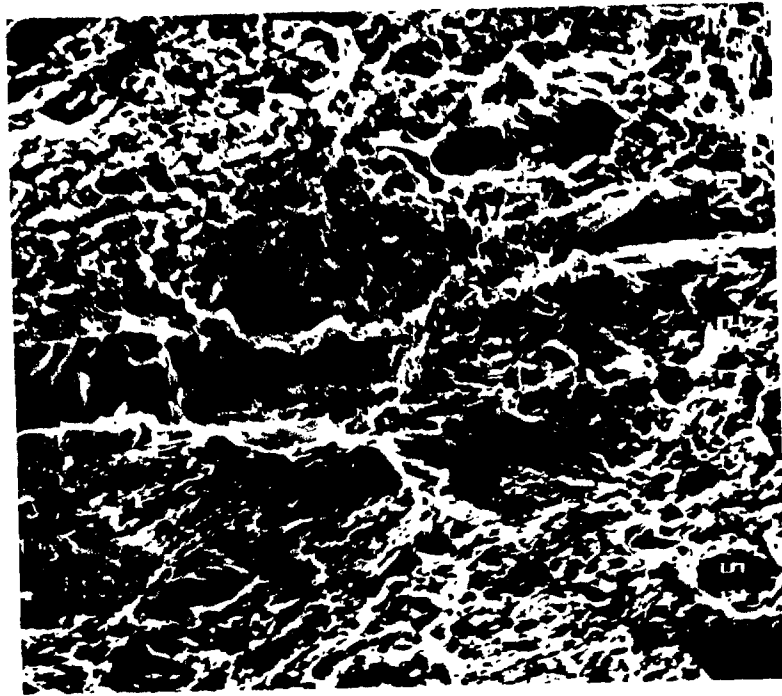
(a)

Flame cut at faster cutting speed.

At low temperature and intermediate strain rate.
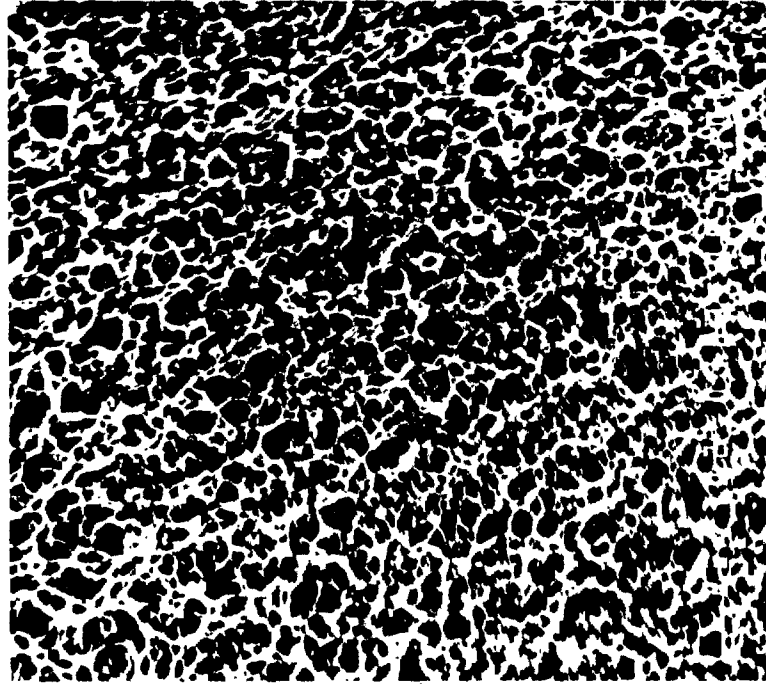
(b)

Base Metal

At low temperature and low strain rate.

Figure 44.   A514 steel tensile specimen fractured surfaces.

(b)

Flame cut at 12.7-cm/min cutting speed.

(a)
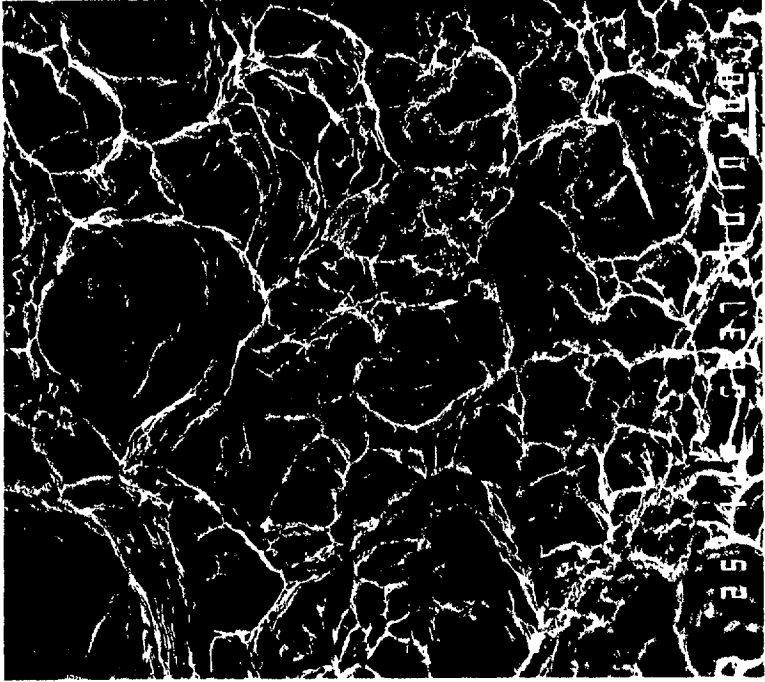
Base Metal

Figure 45.   A514 steel fractured surfaces of tensile specimen of 6.4-mm-thick tensile specimens, tested at low temperature and intermediate strain rate.

70
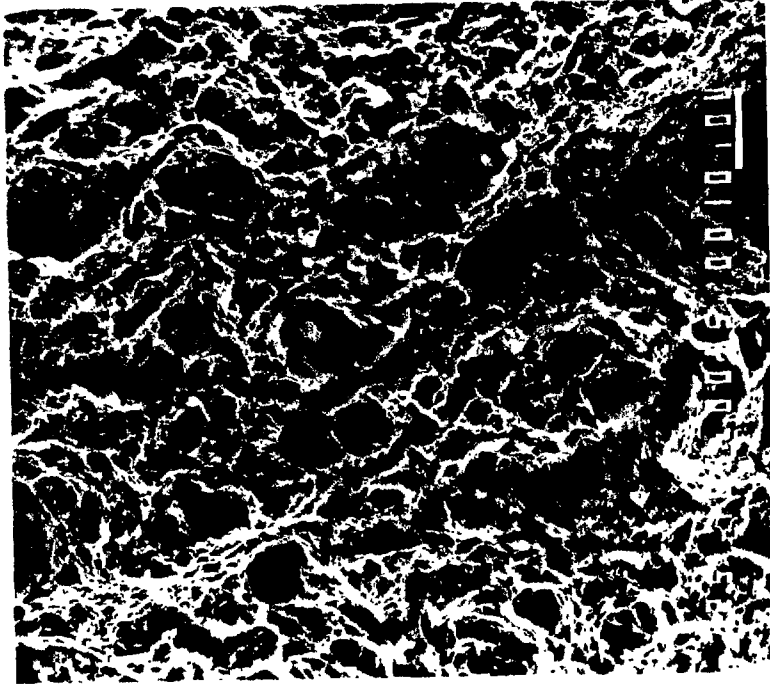
(a)
Base Metal
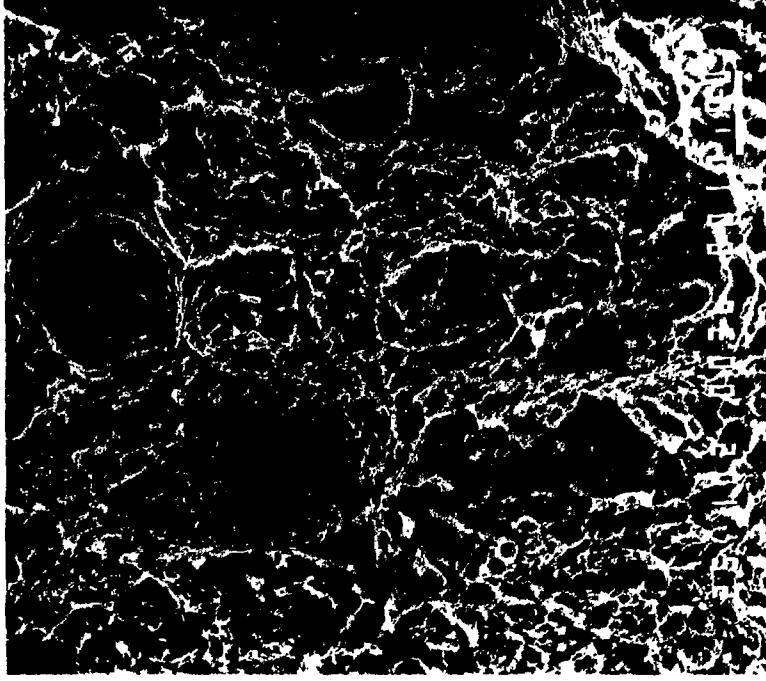
(b)
Flame cut at 12.7-cm/min cutting speed.

Figure 46.   A514 steel fractured surfaces of 6.4-mm-thick tensile specimens, tested at low temperature and intermediate strain rate.

(a) At -100 °C.

(b) At -30 °C.

(c) At +20 °C.

Figure 47.   Fractured surfaces of full-size CVN impact specimens, A572 steel, base metal.
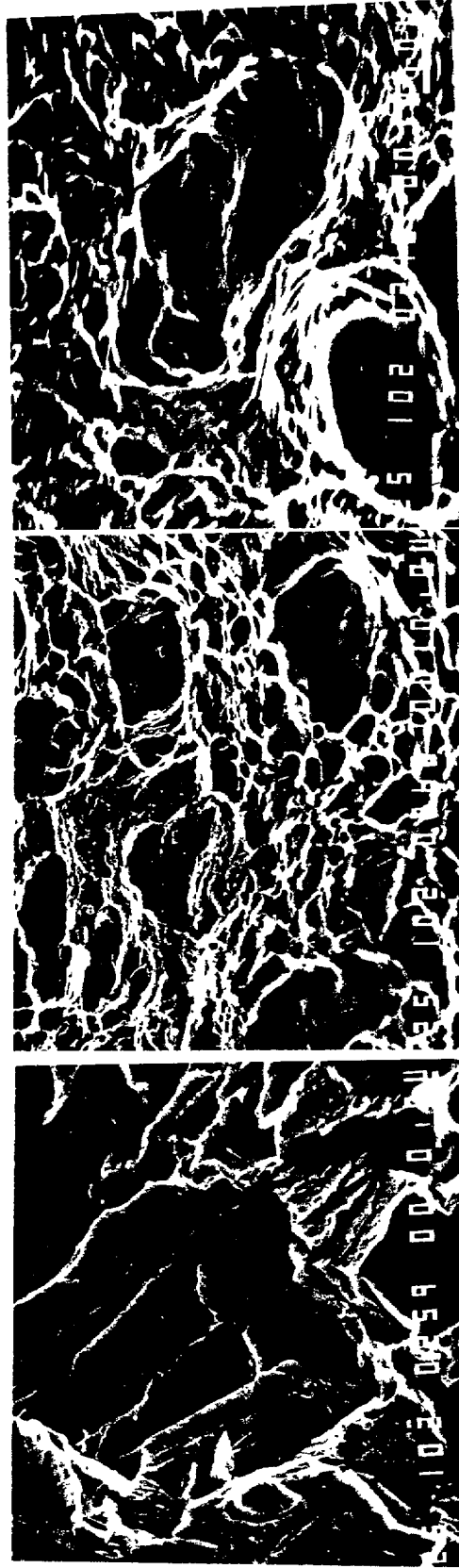
(a) At -85 °C.　　　　　(b) At -57 °C.　　　　　(c) At +19 °C.

Figure 48.　Fractured surfaces of quarter-size CVN impact specimens, A572 steel, base metal.

(a) At -87 °C.   (b) At -45 °C.   (c) At +19 °C.

Figure 49.   Fractured surfaces of quarter-size CVN impact specimens, A572 steel, flame cut at 127-mm/min cutting speed.

(a) At -85 °C. (b) At -21 °C. (c) At +19 °C.

Figure 50.   Fractured surfaces of quarter-size CVN impact specimens, A572 steel, flame cut at 381-mm/min cutting speed.

75

(a) At -131 °C.　　(b) At -62 °C.　　(c) At +31 °C.

Figure 51.　Fractured surfaces of half-size CVN impact specimens, A572 steel, base metal.

(a) At -128 °C.   (b) At -30 °C.   (c) At +31 °C.

Figure 52.   Fractured surfaces of half-size CVN impact specimens, A572 steel, flame cut at 127-mm/min cutting speed.
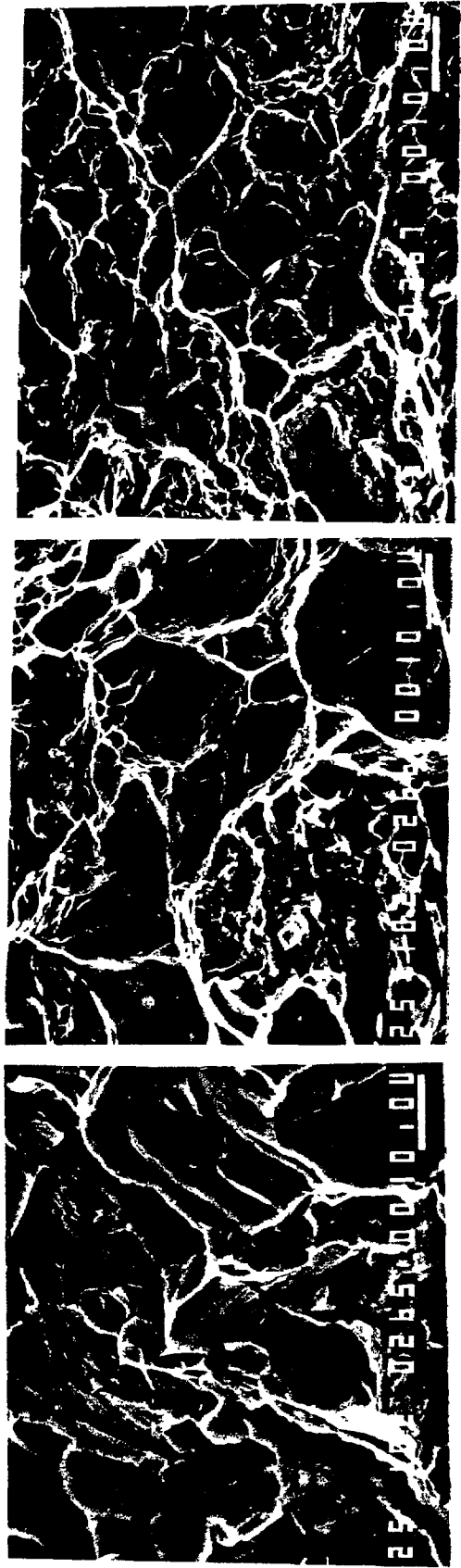
(a) At -128 °C.   (b) At -9 °C.   (c) At +31 °C.

Figure 53.   Fractured surfaces of half-size CVN impact specimens for A572 steel, flame cut at 127-mm/min cutting speed.
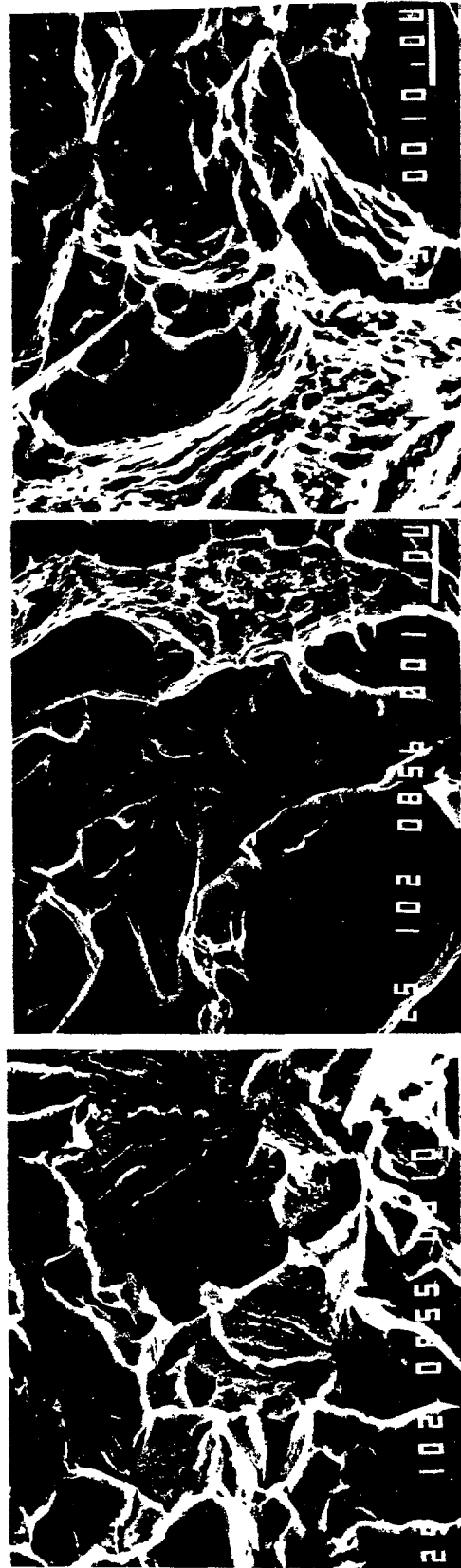
78

SUMMARY OF RESULTS

1. The HAZ of each alloy was wider at the top of the plate, decreasing to a narrower, essentially constant width away from the top.   The width decreased with an increase in cutting speed.

2. The microhardness values were maximum at/near the flame-cut edge and decreased towards the base metal in all the steels.   The maximum hardness increased with an increase in cutting speed.

3. The HAZ consists of mostly tempered martensite in the case of all the steels with the presence of bainite in the case of A514 steel flame-cut at slower cutting speed and fine ferrite and pearlite in the case of A572 and A588 steels.

4. The YS and UTS values increased and percentage elongation decreased from base metal to flame-cut metal and with increase in cutting speed in all three steels.   A change in strain rate, temperature, and specimen size had little if any effect on the tensile properties.

5. Generally, impact toughness decreased and transition temperature increased with increase in cutting speed in the three steels.   Decrease in specimen size decreased the transition temperature.

6. Flame-cut surface cracks did not induce brittle fracture in either tension and CVN impact test, at all test conditions, in all three steels.

CONCLUSIONS AND SUGGESTIONS FOR FURTHER WORK

CONCLUSIONS

1. The flame-cut HAZ's of the three steels had higher strength, lower ductility, and lower impact toughness values than the base metal.

2. Brittle cleavage fracture was not produced in the temperature and strain rate regime tested by flame-cut HAZ in all three steels in tensile and CVN impact tests.

SUGGESTIONS FOR FURTHER WORK

1. It is recommended that the various HAZ structure properties of these steels can be studied individually by knowing the heating and cooling cycles during flame cutting and simulating the same on individual test specimens.

2. Conduct surface chemical analysis to explain the change in hardness near the flame-cut surface.

3. Conduct fatigue tests of the flame-cut steels to test the resistance of the HAZ structure to the flame-cut surface crack propagation.

REFERENCES

1. Alexander D. Wilson, Ed., "Thermal Cutting of HSLA Bridge Steels," Final Report, American Iron and Steel Institute Sponsored Project, August 1987, p. 2 and appendix A.

2. Rosalie Brosilow, "Thermal Cutting," *Metals Handbook,* vol. 6, pp. 896-925.

3. Nicolai Manfred, Griesheim Gmblt. Darmstadt and A. Graham, "Flame Cutting in Modern Industrial Production," *Welding Review, Nov.* 1983, pp. 297-300.

4. W.C. Brayton and J.A. Hogen "Shipyard Welding & Cutting, Plasma Processes of Cutting and Welding," Final Report Sponsor United Carbide Corp., Forensa, SC; Maritime Administration, Washington, DC; Bethlehem Steel Corp., Sparrows Pt., MD, Report No. MA-RD-77039, Feb. 1976, p. 85.

5. D. Geary, *The Welder's Bible: A Hands-On Guide to All Kinds of Oxy-Acetylene Welding and Cutting,* TAB Books Inc., Blue Ridge Summit, PA, 1980, p. 416.

6. W.H. Kearns, Ed., "Welding Processes-Arc and Gas Welding and Cutting Brazing and Soldering," *Welding Handbook,* vol. 2, 7th ed., American Welding Society, Miami, FL, 1978.

7. D. Smith, "Flame-Cutting Shapes, Edges, and Holes," Chapter *5, Welding Skills and Technology,* W.H. Mercer and R.E. Barnett, Eds., McGraw Hill, NY, 1984, pp. 99-137.

8. *The Oxy-Acetylene Handbook,* Union Carbide Corporation, Linde Division, New York, NY, April 1972.

9. K. Nishiguchi and K. Matsuyama, "Kerf Formation and Slag Adhesion in Plasma Jet Cutting with Arc Transfer," *Soudage Tech Connexes,* 34, (Y2), Jan.-Feb. 1980, pp. 49-54.

10. V.L. Shukhmaister and V.T. Kotik, "Improving the Quality of Edges in Air Plasma Cutting," *Svar. Proiz,* no. 3, Moscow, U.S.S.R., 1981, p. 28.

11. H. Thomas and F. Goldberg, "Recommendations Concerning the Quality of Thermal Cut Surfaces in Steel Structures Subjected to Fatigue Loading," *Welding in The World,* vol. 17, no. 7/8, International Institute of Welding, 1979, pp. 192-195.

12. A. N. Kugler, *Oxy-Acetylene Welding and Oxygen-Cutting Instruction Course,* Air Reduction Company, Inc., New York, NY, June 1966.

13. R. Baus and W. Chapeau, "Application du Soundage aux Constructions," Sciences et Letters, Liege, France, 1981.

14. Netherlands Institute of Welding-Working Group 1913, "The Properties of Flame-Cut Edges," Final Report, Denhaag, the Netherlands, May 1973.

15. E. Piraprez, "Fatigue Strength of Flame-Cut Plates," *Fatigue of Steel and Concrete Structures, Proceedings IABSE Colloquium Lausanne,* March 1982, IABSE Reports, vol. 37, Publ. International Association for Bridge and Structural Engineering, Zurich, Switzerland, 1982, pp. 23-26.

16. Von Kurlagunda N. Rao, Jurgen Ruge, and Heinz Schimmoller, "Determination des Contraintes Residuelles dues a l' Oxy Coupage des Toles," For Schunng n^0, 36, Belgium, 1970.

17. B. W. Young and J.B. Dwight, *Residual Stresses Due to Longitudinal Welds and Flame Cutting,* University of Cambridge, Department of Engineering, Cambridge, England, 1971, 12 pp.

18. Jurgen Ruge and Alfred Krahl, "Etude dela Capacite au formage a Froid des Zones Thermiquement Influencees des Toles Oxycoupees," Schweissen und Schneider, n^0, 19, Germany, 1967.

19. J.J.W. Nibbeing, H. Thomas, and T.J. Bos, "The Properties of Plasma-Cut Edges," *Welding in the World,* vol. 18, nos. 9 and 10, 1980, pp. 182-195.

20. H. Honda, S . Kitamure, and T. Yamada, "On the Strength of Racks for Jack-Up Units," no. 1, Report: Fatigue Behavior of Large-Scale, Torch-Cut, and Machined High Tensile Strength Steel Racks, *Bulletin of the JSME,* vol. 27, no. 234, Dec. 1984, pp. 2879-2888.

21. N-J Ho, F.V. Lawrence, and C. J. Alstetter, "The Fatigue Resistance of Plasma- and Oxygen-Cut Steel," *Welding Research Supplement," Nov.* 1981, pp. 231-236.

22. E.P. Kharitonov, et al., "The Surface Plasma-Arc Cutting of Low-Alloy Steels 10Kh SND and 10Kh N1M," *Svar. Proiz,* no. 11, Moscow, U.S.S.R., 1980, pp. 33-34.

23. F. Goldberg, "Influence of Thermal Cutting and Its Quality on the Fatigue Strength of Steel," *Welding Journal, 52 (9),* 1973, pp. 392s-404s.

24. F. Koenigsberger and Z. Farcia-Margin, "Fatigue Strength of Flame-Cut Specimens of Bright Mild Steel," *British Welding Journal,* Jan. 1965, pp. 37-41.

25. F. Koenigsberger and H. W. Green, "Fatigue Strength of Flame-Cut Specimens in Block Mild Steel," *British Welding Journal,* July 1955, pp. 313-321.

26. R. Plecki, R. Yeske, C. Alstetter, and F.V. Lawrence, Jr., "Fatigue Resistance of Oxygen-Cut Steel," *Welding Journal, 56 (8),* 1977, pp. 225s-230s.

27. J.H. Gross, "Transition Temperature Data for Five Structural Steels," Weld Research Council Bulletin, no. 147, Jan. 1970.

28. R.C. McNicol, "Correlation of Charpy Test Results for Standard- and Nonstandard-Size Specimens," *Welding Journal, 44 (9),* 1965, pp. 3855-3935.

29. B. Hogen and B. Cottrell, "Behavior of Sub-Standard Charpy V-Notch Impact Specimens for Mild Steel," *British Welding Journal,* 15 (12), 1968, pp. 584-589.

30. R.S. Zeno, "Effect of Specimen Width on the Notch Bar Impact Properties of Quenched and Tempered and Normalized Steels, " *ASTM Special Technical Publication,* 176, 1955, pp. 59-69.

31. A. Cracknell, "Comments Submitted by the United Kingdom on the Subject of Subsidiary Standard Test Pieces, " Submitted to ISO/TC 17/WG15, document (United Kingdom-l), N30, Jan. 1978, pp. 1-7.

32. J.D. Embury, N.J. Petch, A.E. Wraith, and E.S. Wright, "The Fracture of Mild Steel Laminates," *Trans Metallurgical Soc. of AIME,* 239 (l), 1967, pp. 114-118.

33. B. L. Fergusen, "The Relationship Between Splitting Phenomena and Sample Thickness in Charpy V-Notch Impact Testing," *Proceedings Symposium, What Does the Charpy Test Really Tell* Us?, Publ. American Soc. for Metals, 1978, pp. 99-107.

34. W. Hussmann and A. Krisch, "Effect of Test Bar Width and Structure on the Notched Bar Impact Strength of Structural Steels for General Use," *Archir fur das Eisenhuttenwesen, 43 (9),* 1972, pp. *675-679* (in German); *Welding Institute Trans.* 586, Jan. 1982 (in English).

35. J. Kuvera, I. Talpa, and V. Smid, "On the Fracture of Laminated Charpy Specimens," *Proceedings of Conference, Analytical and Experimental Fracture Mechanics,* Publ. Sijthoff and Noordhoff, Brussels, Belgium, 1981, pp. 515-525.

36. O.L. Towers, "Testing Sub-Size Charpy Specimens; Part l- The Influence of Thickness on the Ductile/Brittle Transition," *Metal Construction,* March 1986, pp. 171R-176R.

37. O.L. Towers, "Testing Sub-Size Charpy Specimens; Part 3- The Adequacy of Current Code Requirements, " *Metal Construction,* May 1986, pp. 319B-325B.

38. W.R. Corwin and A.M. Hougland, "Effect of Specimen Size and Material Condition on the Charpy Impact Properties of 9 Cr-lMo-V-Nb Steel, " *The Use of Small-Scale Specimen for Testing Irradiated Material,* ASTM STP 888, W.R. Corwin and G.E.

Lucas, Eds., American Society for Testing and Materials, Philadelphia, PA 1986, pp. 325-338.

39. G.E. Lucas, G.R. Odette, J.W. She&herd, P. M°Connell, and J. Perrin, "Sub-Size Bend and Charpy V-Notch Specimens for Irradiated Testing, " The Use of *Small Scale Specimen for Testing Irradiated Material,* ASTM STP 888, W.R. Corwin and G.E. Lucas, Eds., American Society for Testing and Materials, Philadelphia, PA, 1986, pp. 305-324.

40. Department of Materials Science and Engineering, "Heating Rate Experiments on CVN Impact Specimens, " Oregon Graduate Center, Beaverton, OR, (Unpublished), 1988.

41. R.F. Hehemann, "Ferrous and Non-Ferrous Bainitic Structures," *Metals Handbook,* vol. 8, pp. 194-196.

42. C. Zener and J.H. Hollomon, "Effect of Strain Rate Upon Plastic Flow of Steel," *Journal of Applied Physics,* vol. 18, 1944, pp. 22-23.

43. M.J. Barba, *Mem. Soc. Ing. Civils,* pt. 1, 1980, p. 682.

44. O.L. Towers, "Testing Sub-Size Charpy Specimens, Part 2- The Influence of Specimen Thickness on Upper-Shelf Behavior, " *Metal Construction,* April 1986, pp. 258R,